APOLLO HEAT SHIELD
MONTHLY PROGRESS REPORT

Prepared by

RESEARCH AND ADVANCED DEVELOPMENT DIVISION
AVCO CORPORATION
Wilmington, Massachusetts

RAD-SR-65-27
Contract M3J3XA-406012
Avco Report Series 201

THIS REPORT WAS PREPARED IN ACCORDANCE WITH NAA/S&ID CONTRACT M3J3XA-406012. IT IS SUBMITTED IN PARTIAL FULFILLMENT OF THE CONTRACT AND IN ACCORDANCE WITH NAA/S&ID PROCUREMENT SPECIFICATION MC999-0025.

9 February 1965

SCD No. ME364-0001, Ablative Panel Shield

APPROVED

W. Zeh
Project Manager
Apollo Vehicle Design

C. L. Huffine
Project Manager
Materials Development and Fabrication

E. Offenhartz
Project Director
Manned Space Systems

Prepared for

NORTH AMERICAN AVIATION, INC.
SPACE AND INFORMATION SYSTEMS DIVISION
Downey, California

[redacted]

CONFIDENTIAL

[redacted]

(UNCLASSIFIED TITLE)

APOLLO HEAT SHIELD MONTHLY PROGRESS REPORT

Prepared by

RESEARCH AND ADVANCED DEVELOPMENT DIVISION
AVCO CORPORATION
Wilmington, Massachusetts

RAD-SR-65-27
Contract M3J3XA-406012
Avco Report Series 201

SCD No. ME364-0001, Ablative Panel Shield

THIS REPORT WAS PREPARED IN ACCORDANCE WITH NAA/S&ID CONTRACT M3J3XA-406012. IT IS SUBMITTED IN PARTIAL FULFILLMENT OF THE CONTRACT AND IN ACCORDANCE WITH NAA/S&ID PROCUREMENT SPECIFICATION MC999-0025.

9 February 1965

Prepared for

NORTH AMERICAN AVIATION, INC.
SPACE AND INFORMATION SYSTEMS DIVISION
Downey, California

[redacted]

[redacted]

CONTENTS

[redacted]

[redacted]

ILLUSTRATIONS

[redacted]

[redacted]

ILLUSTRATIONS (Cont'd)

[redacted]

[redacted]

ILLUSTRATIONS (Concl'd)

[redacted]

[redacted]

I. VEHICLE DESIGN

A. AEROTHERMODYNAMICS

1.0 Thermal Design

1.1 Main Ablator

1.1.1 Main Ablator Thickness Definition

Ablator thicknesses for airframes 006, 009, and 008 remain unchanged. Thickness definition and vehicle effectivity are as specified by the Monthly Progress Report, dated 9 December 1964.

1.1.2 Main Ablator Thickness Verification Studies

A comparison of the revised IBM fairing for airframe 009 (401098 Rev H) to thermal design requirements was initiated during this report period. A cursory review of Revision H indicated that the inadequacies of Revision G were corrected. A complete check of Revision H will be conducted, however, to ensure the thermal adequacy of the fairing for vehicle 009. This study will include plots of thickness distributions in both the circumferential and the longitudinal directions.

1.1.3 Analysis of Ablator Defects

Two-dimensional analyses of ablator voids were continued. In addition, data from OVERS test samples containing voids are being compared to analytical results to verify the calculation approach. Program 1327 was utilized to predict temperature responses and amount of ablation for the test samples. This information will be used in two-dimensional analyses which account for radiation and conduction across the void. The experimental data include single cell surface and backface voids and multiple cell backface voids.

1.1.4 Thermal Conductivity Studies

Analysis of the Thermatest conductivity data continues. Ablation characteristics were changed in the analytical model in an attempt to match OVERS test data. The cases under consideration were run with new transpiration factors and were found to match closely the corresponding OVERS ablation rates. Justification for using a larger or variable transpiration factor to compensate for the higher Thermatest conductivity is being investigated. Simultaneously, temperature comparisons are being completed for the analyses which have been performed thus far.

[redacted]

1.1.5 Forward Pitch-Panel Bolt-Plug Analysis

A proposed configuration of the forward pitch-panel bolt plug (revised to provide accessibility to the support nuts) is shown in figure 1. Two one-dimensional heat transfer cases were analyzed in order to determine the effects of the proposed change on backface temperatures. The first case considered heat transfer down the centerline of the fiberglass dutchman, while the second case considered heat transfer down the centerline of the cavity (filled with RTV-560) with the bolt removed.

Figure 2 shows the results obtained at the locations indicated in figure 1. It is seen that the maximum substructure temperature at point "A" on the revised configuration, with bolt removed, does not exceed the 600°F design limit. Point "B" on the revised configuration shows the substructure exceeding the 600°F design limit (621°F). This apparent over-temperature can be compensated for by introducing the heat sink characteristics of the steel bolt and steel close-out in the substructure, both of which were neglected in the current study. Histories C and D are included from the previous analysis and show the large temperature depressing effects that the bolt will have.

It is concluded, therefore, that the revised configuration is thermally adequate only when the attachment bolts are in place. Overheating will occur at the interface of the fiberglass dutchman and substructure when these conditions do not exist.

1.1.6 Compression Pad Thicknesses

As a sequel to the compression pad analyses presented in the Monthly Progress Report dated 9 January 1965 calculations were performed to define theoretical fiberglass thicknesses (T_{struct} = 600°F). These thicknesses were determined since previous analysis showed that these regions are fiberglass-thickness controlled. Thus in order to maintain thermal adequacy it is necessary to size the pads and fair the main ablator up to the pads.

Results for the three compression pads, based upon nominal heating and a dense substructure beneath each pad, are tabulated below:

Pad No.	F/G Thickness, inches
2	2.20
4	1.83
6	1.88

OLD CONFIGURATION

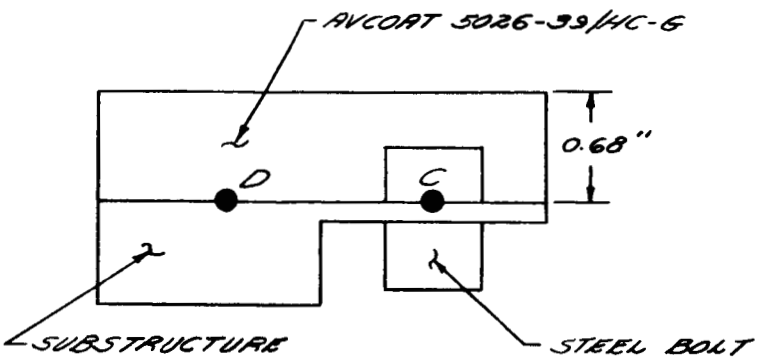

REVISED CONFIGURATION

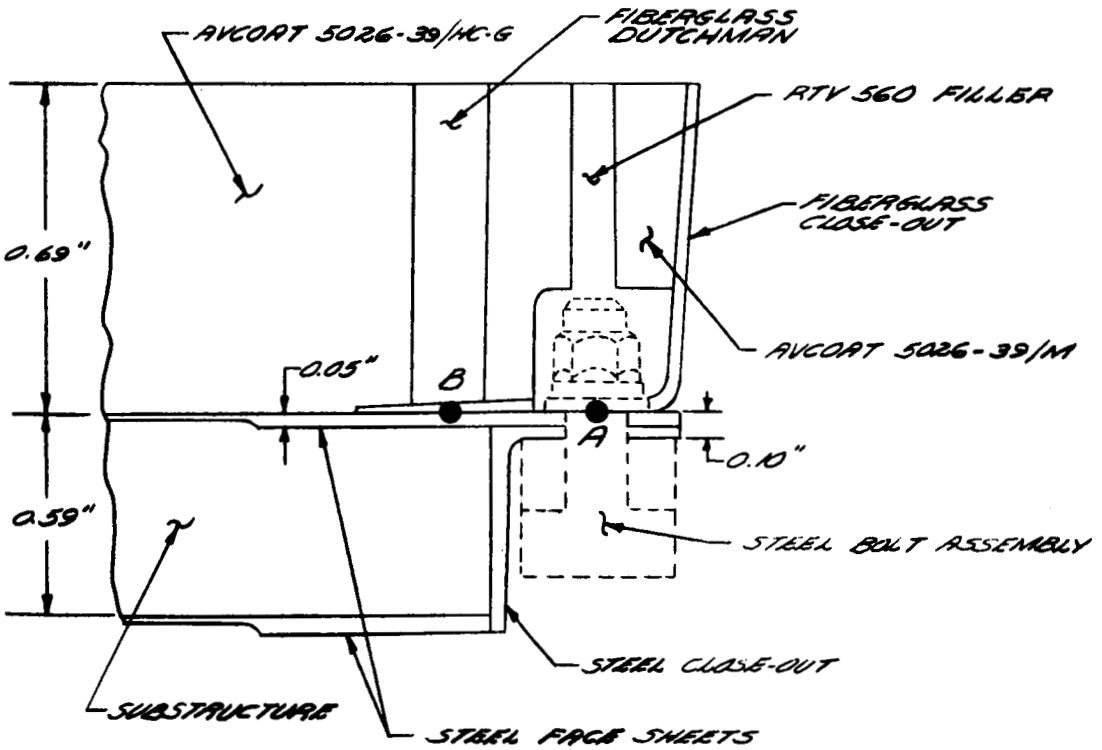

Figure 1 DESIGN CONFIGURATION FOR THE FORWARD PITCH PANEL ATTACHMENT BOLTS

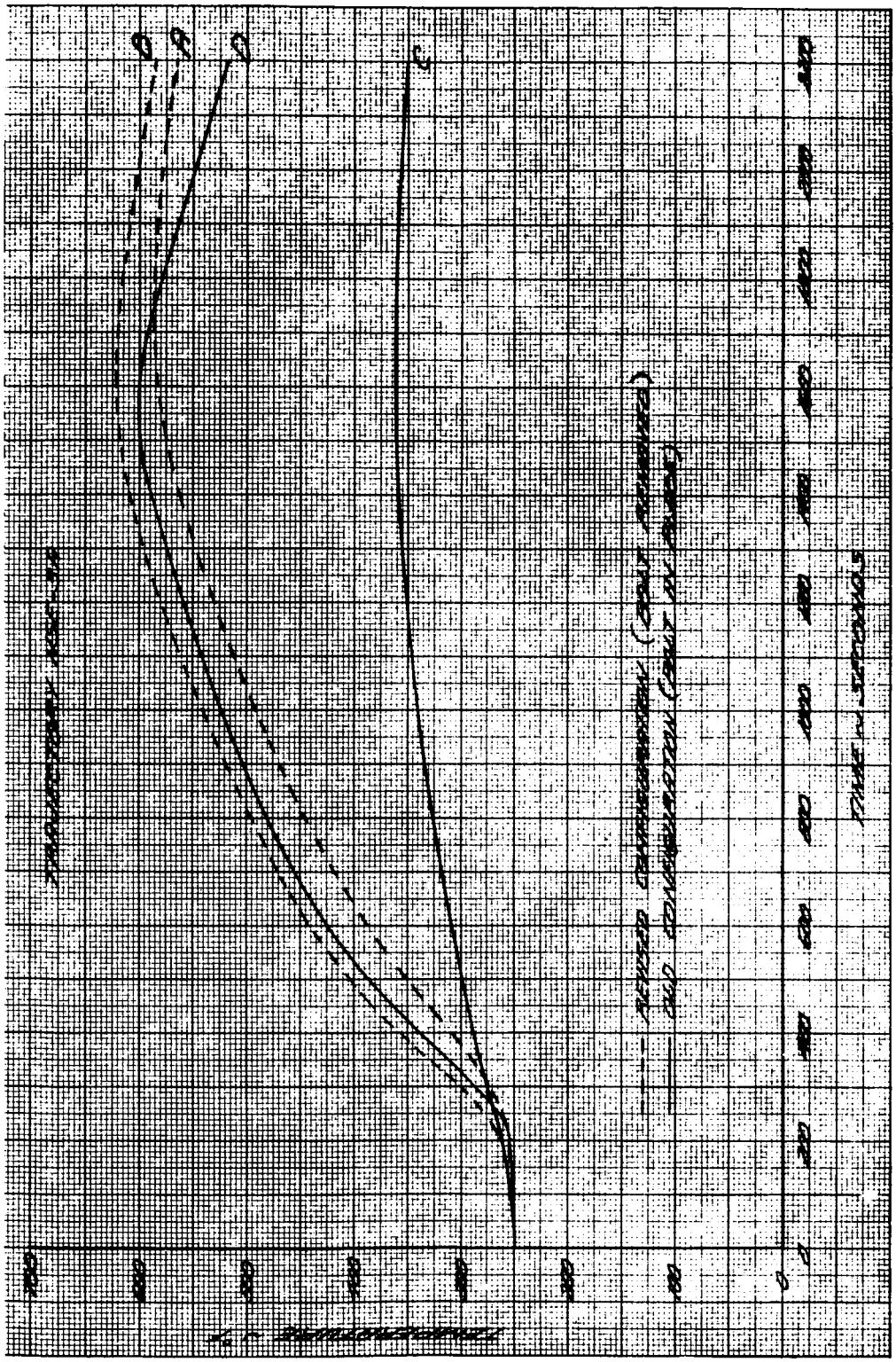

Figure 2 COMPARISON OF TEMPERATURE HISTORIES FOR THE FORWARD PITCH ENGINE ATTACHMENT BOLTS

1.2 Two-Dimensional Areas

1.2.1 Intercompartment Gap at Xc = 112.25 inches

The intercompartment gap at Xc = 112.25 inches has been analyzed two-dimensionally for trajectory HSE-6 and HSE-3A. Since the gap separates the forward compartment from the nose cone, its effect is felt thermally in both areas. In order to simplify the analysis, the gap seal was assumed to be symmetrical with Xc = 112.25 inches, and only the forward half was analyzed. The matrix consisted of those structural members which form part of the nose cone. This is a conservative assumption, as the nose cone structure is reinforced to a lesser degree than that of the forward compartment and thus has a lower heat capacity than the forward compartment "half". The variation of 5026-39/HC-G thermal properties with temperature was accounted for by means of an effective thermal conductivity, which yields correct one-dimensional temperature responses for each trajectory.

The idealized two-dimensional matrix as analyzed is shown in figure 3. The two-dimensional analysis of the gap produced no overheating for trajectory HSE-3A. Examination of the temperature histories shown on figure 4 reveals that the net effect of the gap seal and its associated structural members is to reduce the temperature response in the immediate area.

No temperature response was calculated at the substructure for trajectory HSE-6. This is the result of the extremely short time after the initiation of reentry that the nose cone flies before jettison. This trajectory was run to gather information on temperature gradients in the ablator.

1.2.2 Roll Engines

A two-dimensional thermal analysis of the roll engines NAA/Avco interface area has been completed for trajectory HSE-3A. The location of the analyses was governed by the two-dimensional temperature histories supplied by NAA, Xc = 32.3 inches, λ = 132.7 degrees. From this point the analysis extended at a constant Xc in a windward direction until a point of one-dimensional heat flow was reached.

An effective thermal conductivity was calculated to account for the temperature dependency of the 5026-39/HC-G material.

The application of the NAA temperature histories is accomplished by the use of the revised interface analysis technique which uses NAA two-dimensional temperature histories as a boundary condition at the interface.

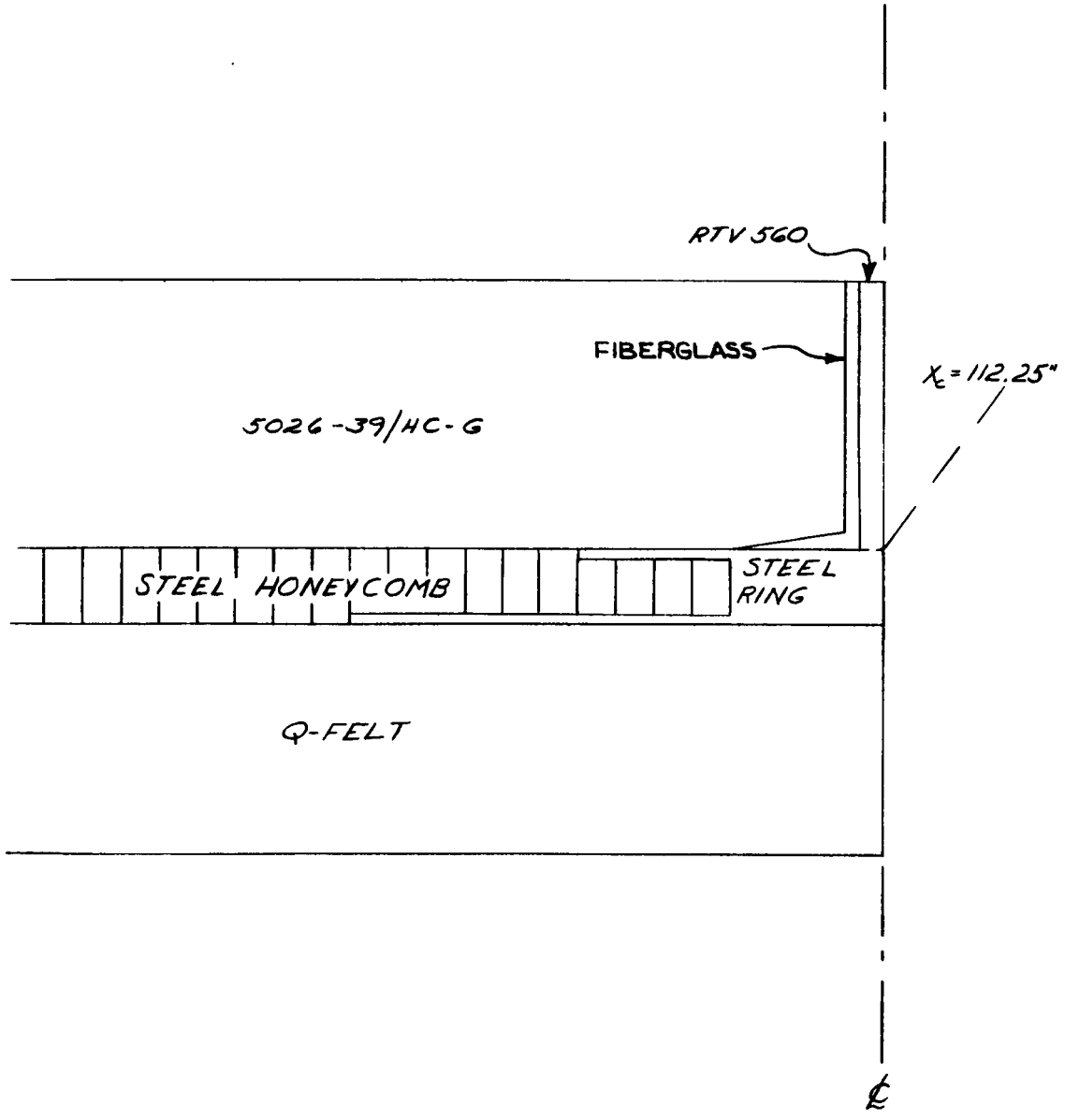

Figure 3 INTERCOMPARTMENT GAP AT X_c = 112.25 TWO-DIMENSIONAL MATRIX

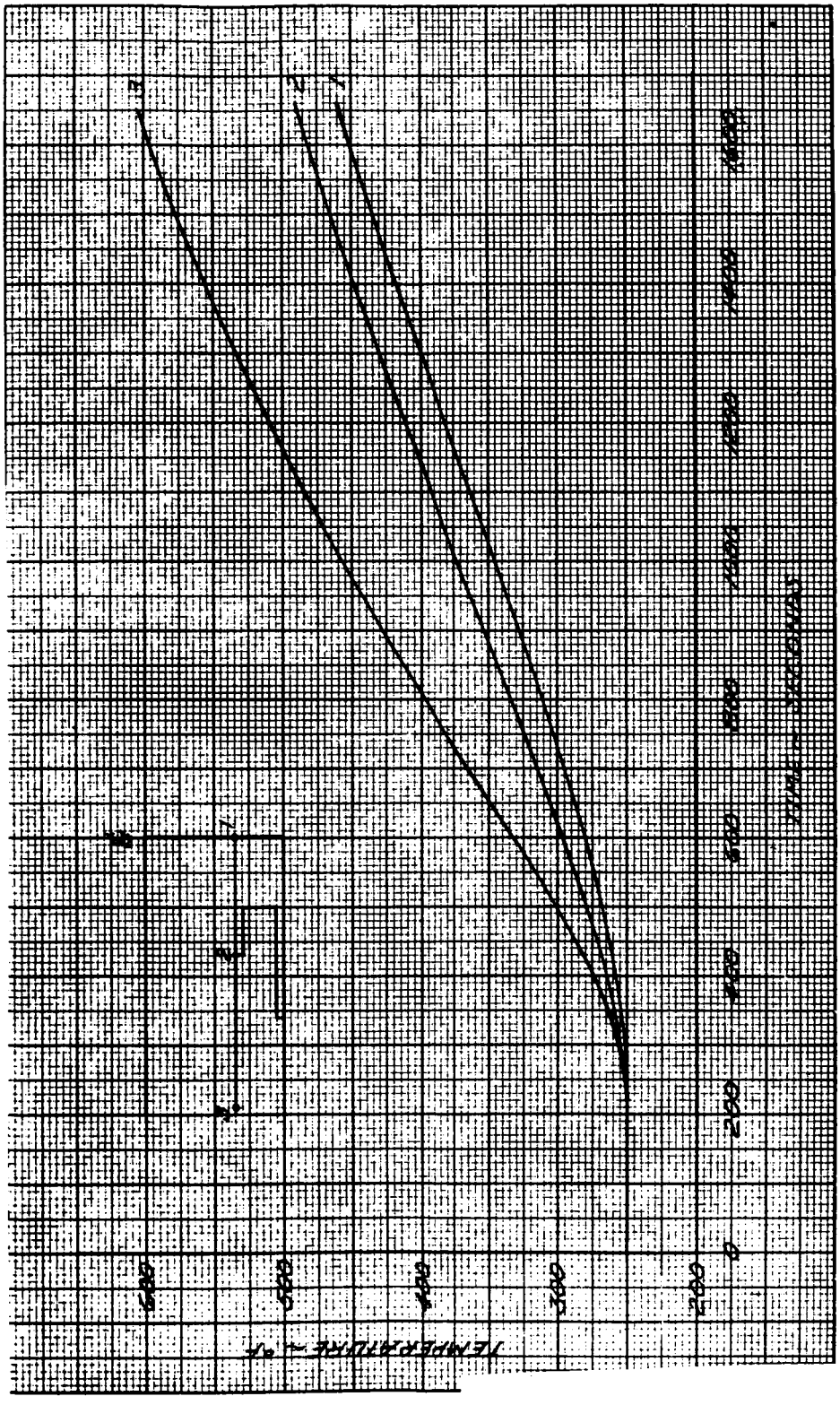

Figure 4 INTERCOMPARTMENT GAP AT X_c = 112.25" 2-D TEMPERATURE HISTORIES TRAJECTORY HSE - 3A

The idealized two-dimensional matrix as analyzed is shown on figure 5. Temperature histories of points in the structure are shown on figure 6. As can be seen, temperatures in the roll engine panel substructure do not exceed 600°F. In fact they are greatly reduced from those temperature levels usually associated with design conditions for trajectory HSE-3A. There are two reasons for this result.

a) The roll engine panel is overdesigned by one-dimensional design methods due to using a design assumption of a nominal substructure and neglecting the true non-nominal honeycomb level structural configuration.

b) The interface temperatures recently provided by NAA do not exceed 600°F, thereby indicating no lateral heat flow from the liner as might be expected.

1.2.3 Leeward Scimitar Antenna

The two-dimensional heat conduction analysis of the leeward scimitar antenna NAA/Avco interface (at Xc = 24 inches, λ = 163° degrees) was completed for the HSE-3A trajectory. Because of the extended length of the antenna in the longitudinal direction, two separate locations (Xc = 24 inches, λ = 163 degrees and Xc = 44 inches, λ = 163 degrees) were considered. A sketch of a typical scimitar antenna interface area is shown in figure 7. Nominal ablator thicknesses reported in the February Progress Report (1964) and appearing also in SEM 196 were used in the analysis.

The two-dimensional temperature responses in depth in the Avco materials were generated by Avco's two-dimensional Program 1459. HSE-3A heating was applied to the surface nodes and the NAA two-dimensional temperature histories (SEM 196) were used for the appropriate nodes along the NAA/Avco interface.

Figure 8 shows the two-dimensional temperature responses at selected depths at the Xc = 24 inches, λ = 163 degrees location.

Figure 9 shows the two-dimensional temperature responses at selected depths at Xc = 44 inches, λ = 163 degrees location. As can be noted the maximum temperature at the bond line does not exceed 490°F.

1.2.4 Aft Compartment Moment Ties

There are 44 aft compartment moment ties located at the toroidal section of the command module. Three-dimensional heat conduction analyses of the substructure, web, and top plate were performed to support the structural analysis. Initial temperatures of -150°F, + 130°F, and + 250°F were considered for trajectories HSE-3A and HSE-6.

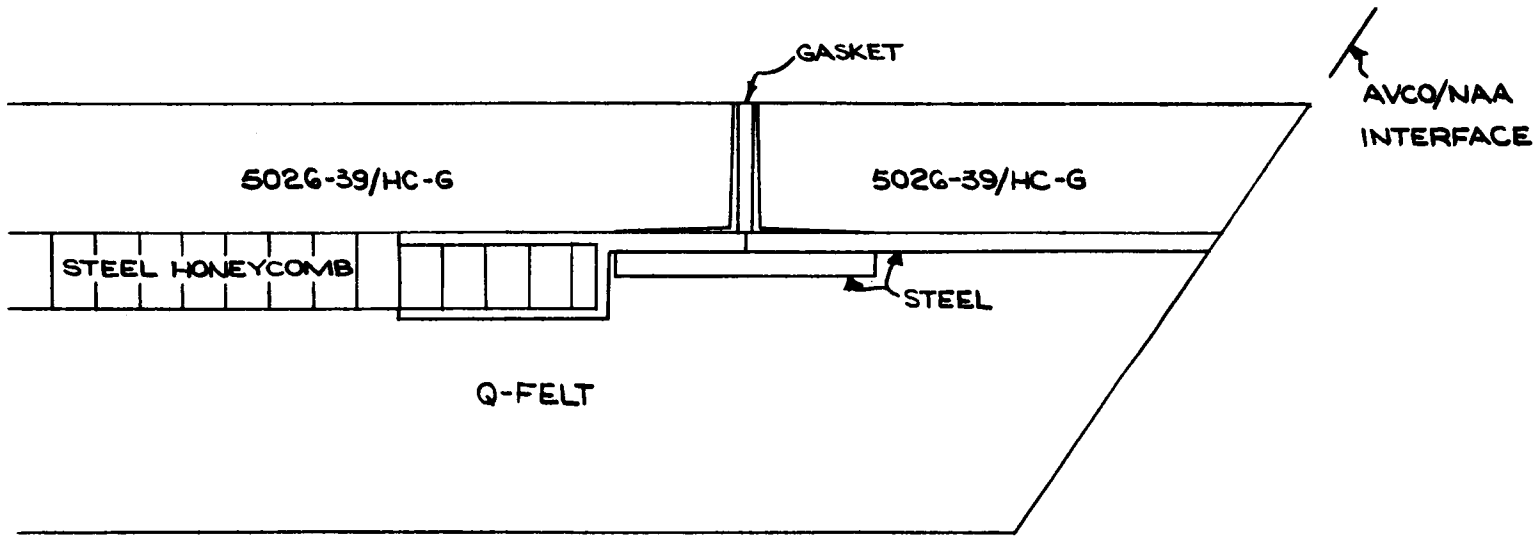

Figure 5 ROLL ENGINE 2-D MATRIX

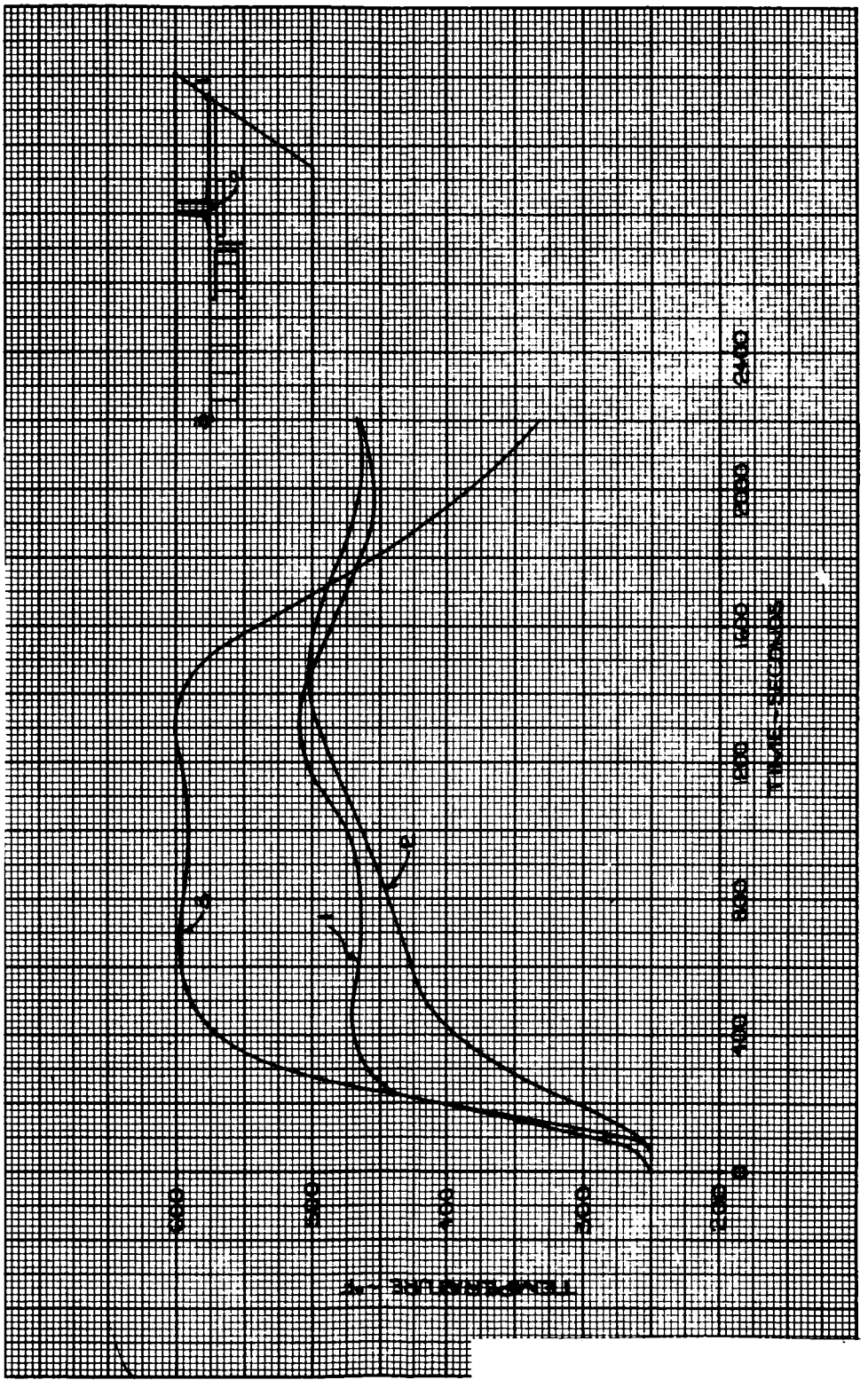

Figure 6 ROLL ENGINE NAA/AVCO INTERFACE 2-D TEMPERATURE HISTORIES

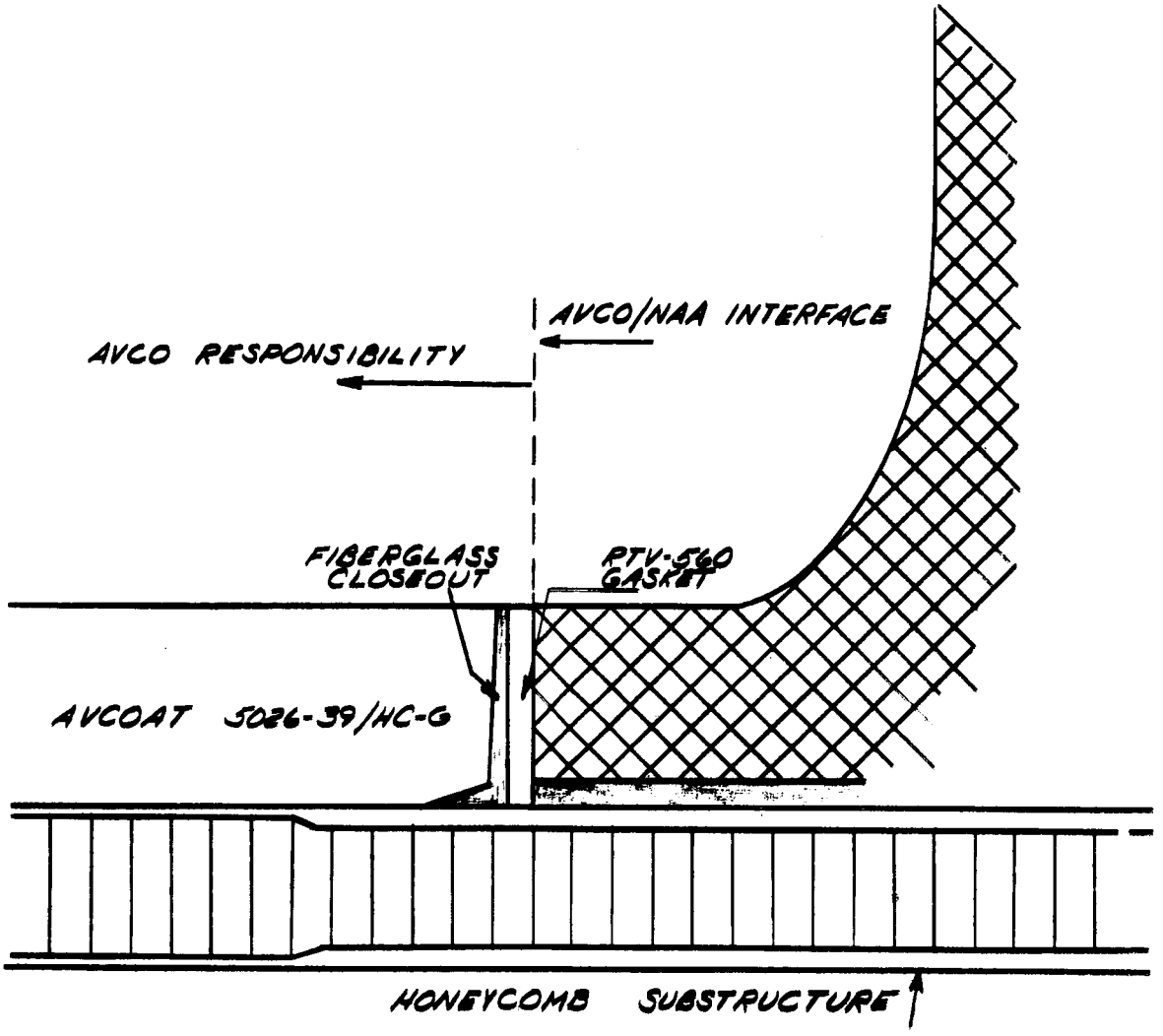

Figure 7 LEEWARD SCIMITAR ANTENNA TWO-DIMENSIONAL MATRIX

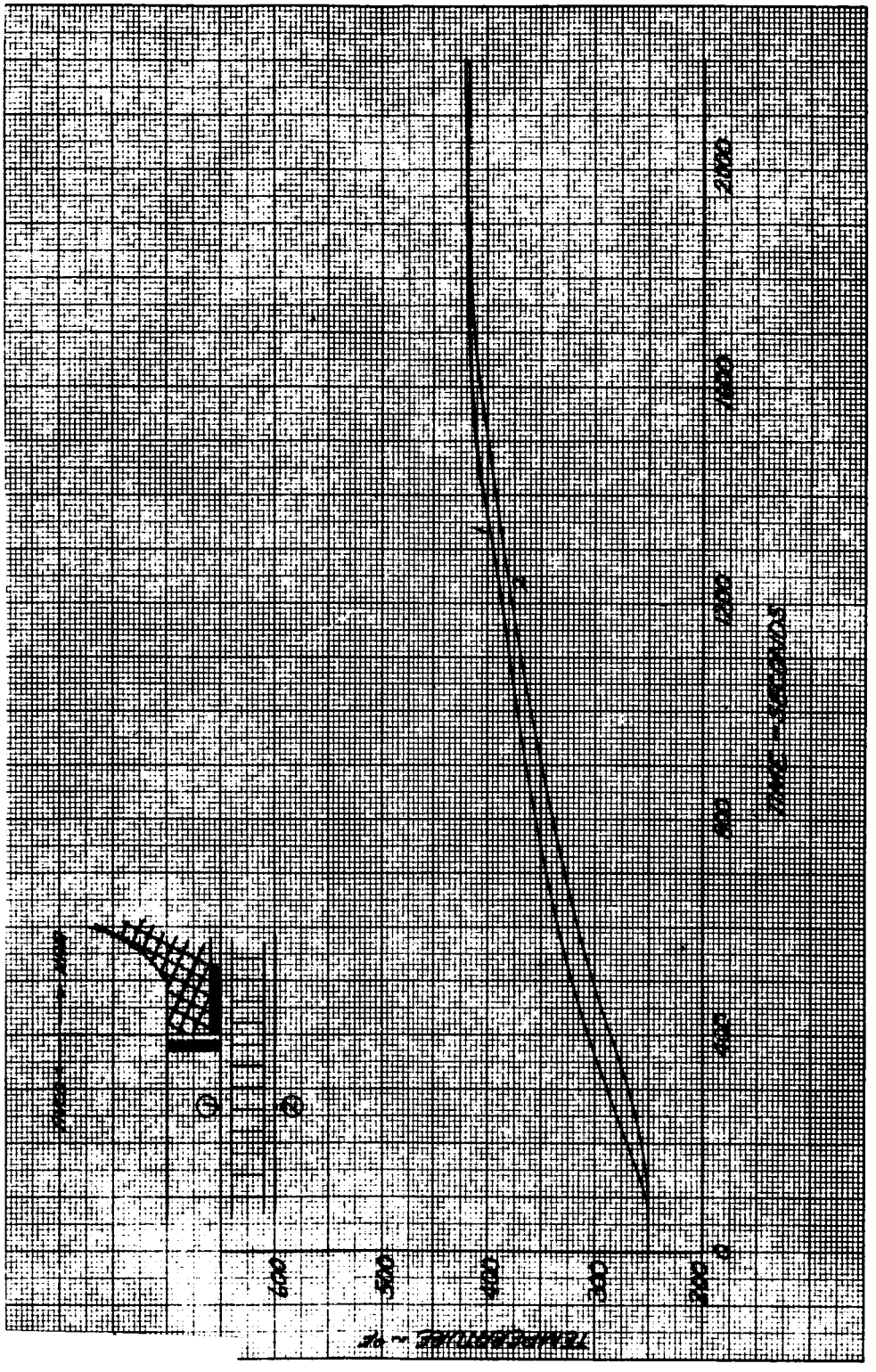

Figure 8 LEEWARD SCIMITAR ANTENNA X_c = 24", = 163-DEGREE TWO-DIMENSIONAL TEMPERATURE RESPONSES

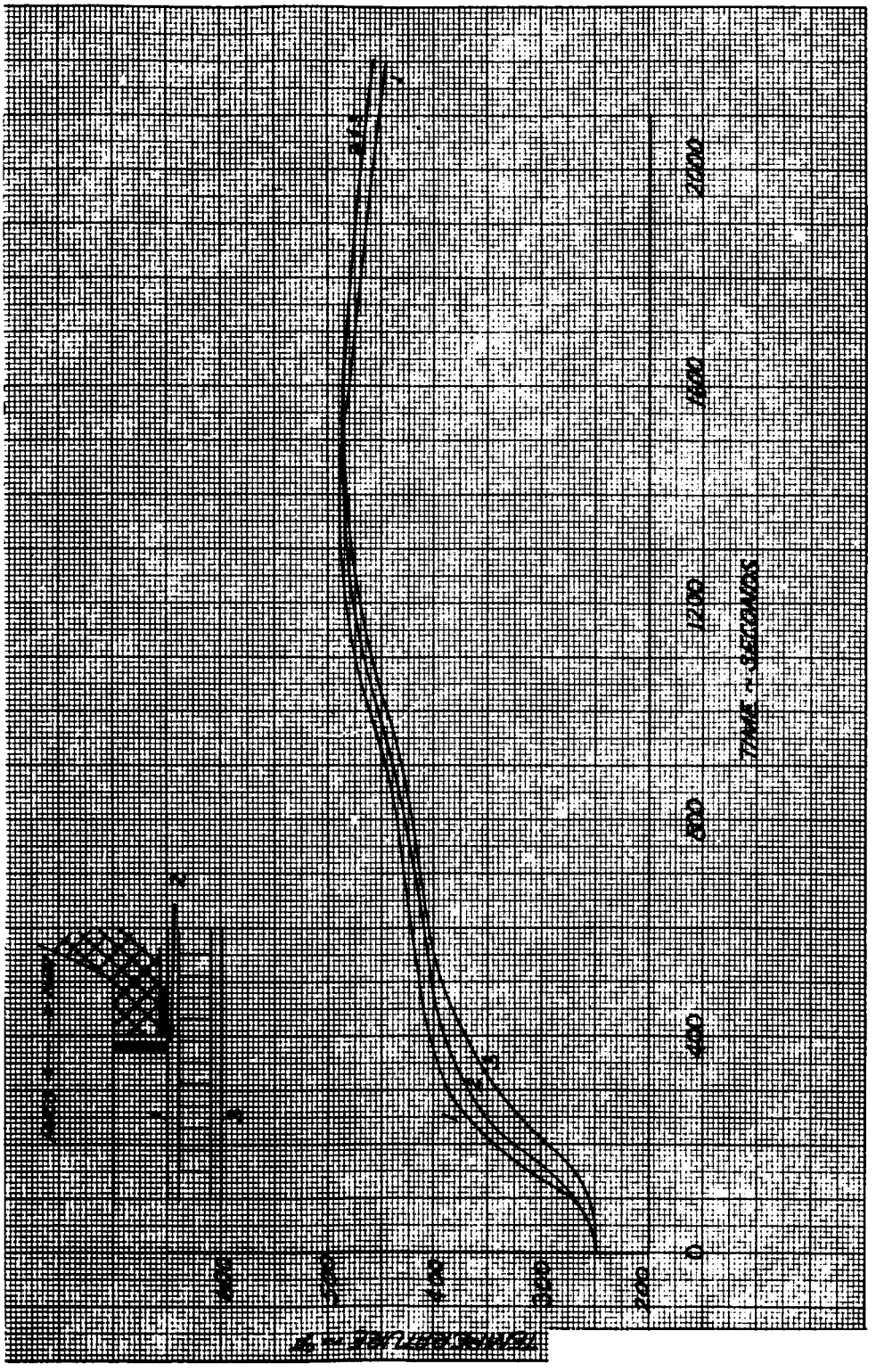

Figure 9 LEEWARD SCIMITAR ANTENNA X_c = 44", = 163-DEGREE TWO-DIMENSIONAL TEMPERATURE RESPONSES

[redacted]

Because of the complex geometry as shown in figure 10, it was necessary to consider an idealized geometry consisting of a rectangular structure section* and trapezoidal web and top plate section. Only the most windward of the 44 equally spaced tension tie was considered in the analysis. Since the space between the tension ties is insulated with Q-Felt, radiation was not considered in the analysis. It was also assumed that for the purpose of this analysis the temperature differences between adjacent ties was small,hence lateral flow of heat could be neglected.

For the tie analyzed, the local total heat input is 107,615 Btu/ft^2 for HSE-6. The standard computational procedures were followed to evaluate the net conducted heat flux to the residual ablator in the vicinity of the windward tension tie. The temperature data shown in figures 11 through 13 show isotherms in the web structure and top plate for HSE-3A for an initial temperature of 250°F.

The maximum temperature obtained in the web was + 475°F at $T_{initial}$ = 250°F. Study of the temperature distribution through the moment tie shows that temperatures closer to the forward end of the tie (Xc = 23.0 - Point A) are lower due to the reduced conduction path to the top plate. Maximum "in depth" gradients range from about 150°F at the aft end of the tie to about 75 degrees at the forward end. Lateral gradients in the substructure are of the order of 110°F and 40°F in the top plate.

Although an analysis of the tension tie was completed for trajectory HSE-6 the results are not presented since virtually no temperature response was noted (hence the gradient was zero). No analyses will be conducted for any other trajectories or any other ties since this case considered herein is felt to be the most severe from a temperature gradient viewpoint.

2.0 Analytical Methods

2.1 Statistical Evaluation of Test Measurement Accuracy

A final report on the study of the enthalpy measurement accuracy in OVERS is being written. The results to date indicate a "three sigma" enthalpy measurement error ranging between 10 and 20 percent, decreasing as enthalpy increases. Inasmuch as these results are extremes, it is felt that the measurement accuracy is reasonable. However, the results will be used as a guide in considering data and in improving the enthalpy measurement in OVERS.

*The local corrugated substructure was treated as a rectangular section.

[redacted]

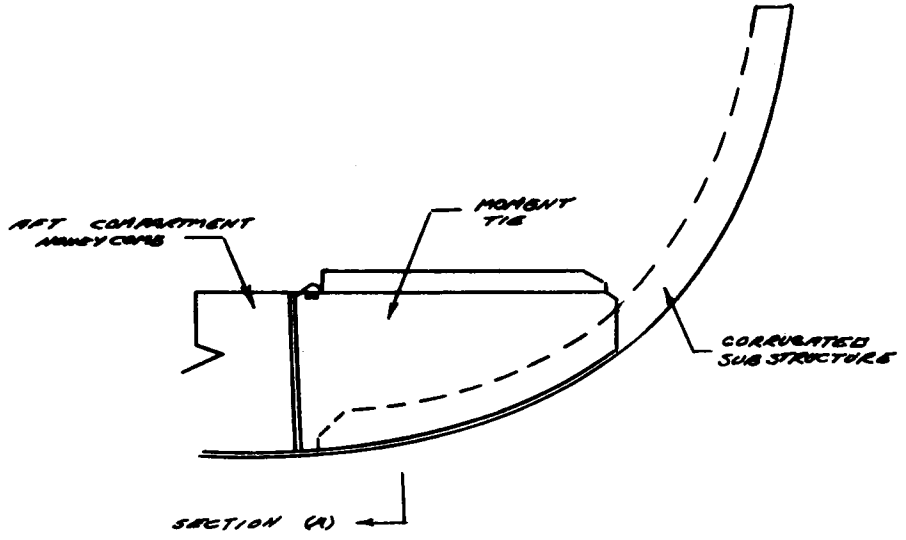

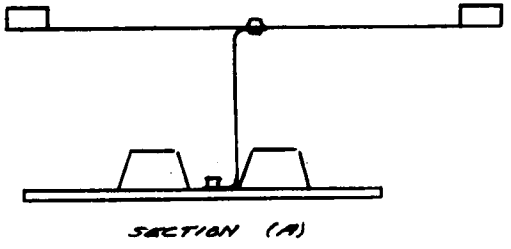

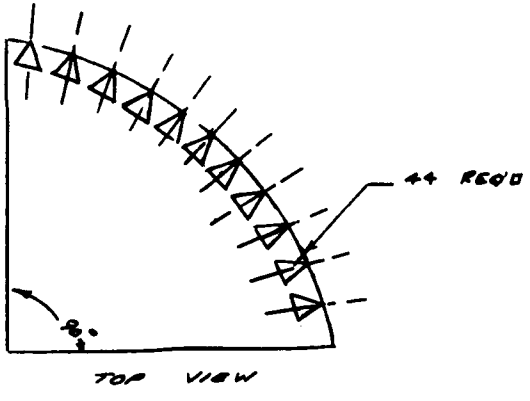

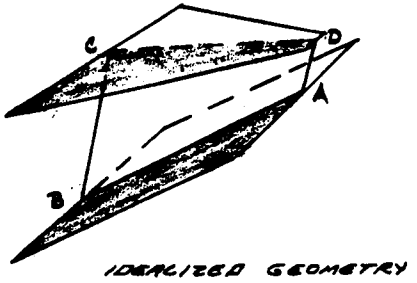

Figure 10 MOMENT TIE GEOMETRY

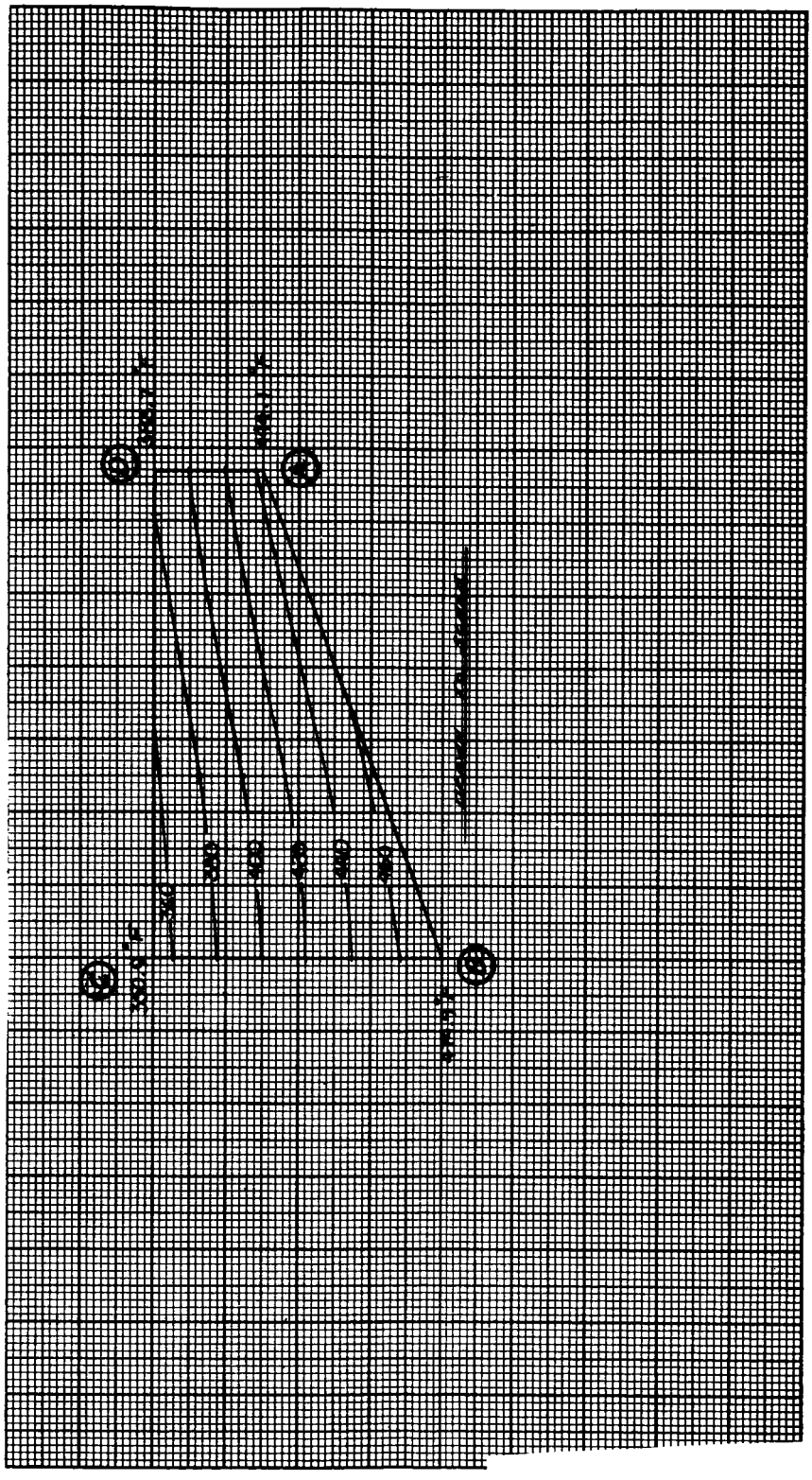

Figure 11 MAXIMUM TEMPERATURE ISOTHERMS--WEB SECTION, AFT COMPARTMENT MOMENT TIE INITIAL TEMP. = +250°F TRAJECTORY HSE-3A

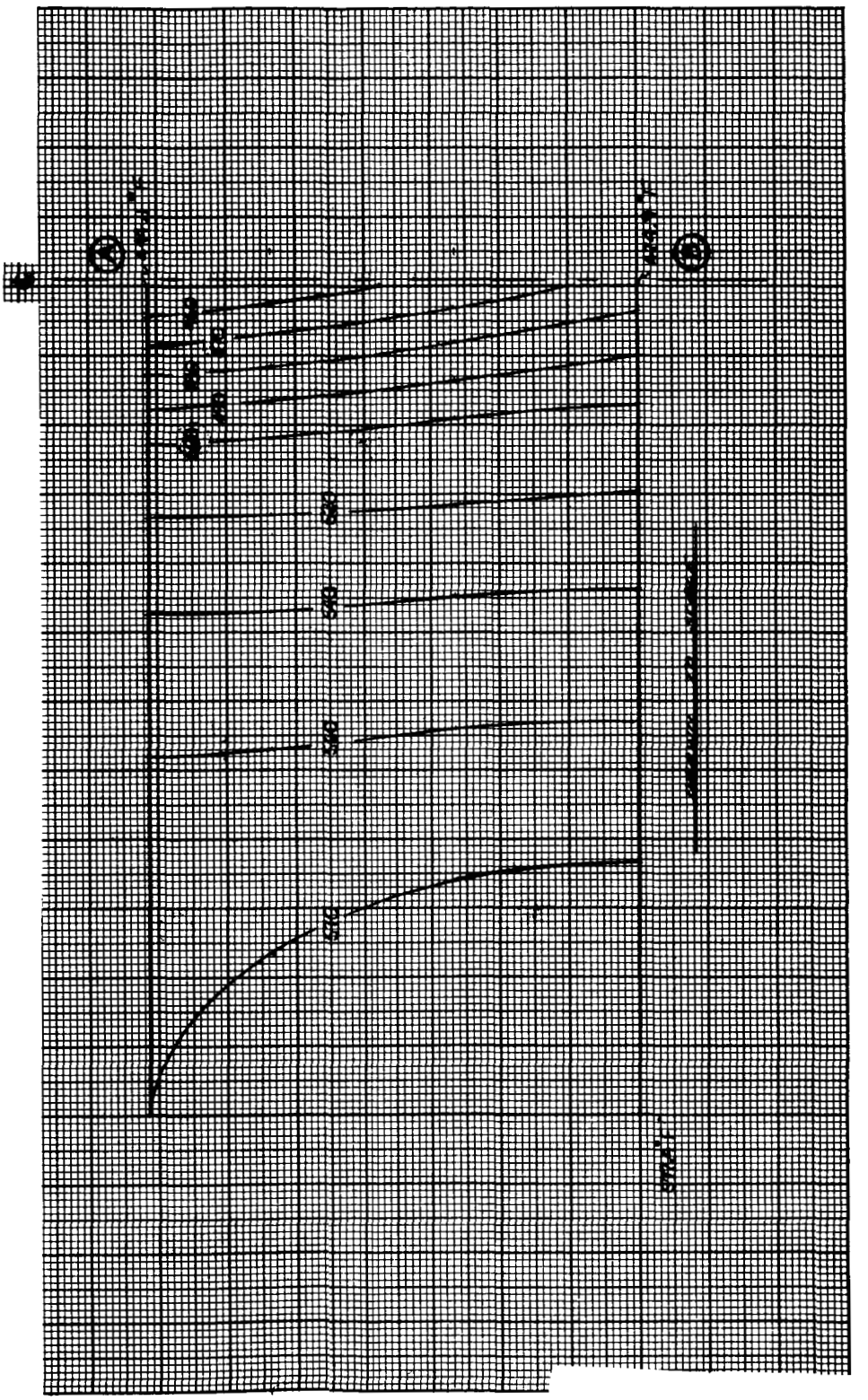

Figure 12 MAXIMUM TEMPERATURE ISOTHERMS--SUBSTRUCTURE SECTION, AFT COMPARTMENT MOMENT TIE--INITIAL TEMP. = +250°F TRAJECTORY HSE-3A

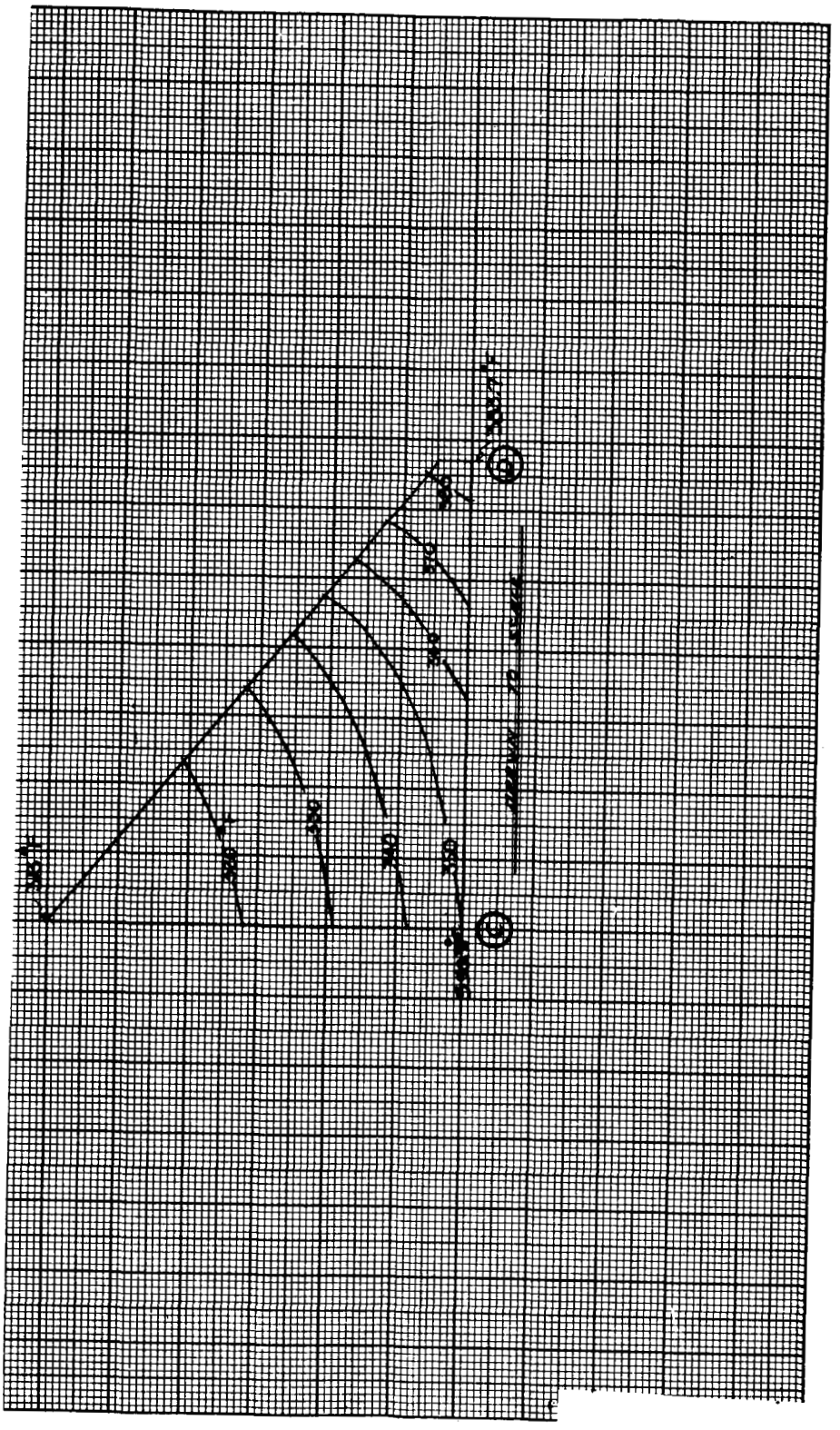

Figure 13 MAXIMUM TEMPERATURE ISOTHERMS--TOP PLATE SECTION,
AFT COMPARTMENT MOMENT TIE, INITIAL TEMP. = +250°F
TRAJECTORY HSE-3A

2.2 Solar Furnace Data Analysis

In the past month, 48 samples of 5026-39/HC-G were tested in the Solar Furnace. These samples were tested at a pressure of one atmosphere and at heat flux levels of 200, 500, 575, 800, and 1100 Btu/ft^2 sec. The data obtained from these tests included length loss, surface temperature of the sample, and reradiated heat flux from the sample surface. Length loss data are presented in figures 14 through 18 for the five heat flux levels. The slope of the linear portion of the plot of length loss versus time (obtained by least squares fit) is used as the ablation rate. As length loss increases, the sample surface moves outside the focal "zone" of the apparatus thus reducing significantly the incident flux and the slopes of the length loss curves. This region of the data was not included in the current analysis. Figure 19 presents ablation rate($\dot{S}$) versus incident radiant heat flux. The inversion of the data between the 500 and 575 Btu/ft^2 sec heat flux levels should be noted. It is suspected that this inversion is the result of experimental error in heat flux.

The sample surface temperature versus incident heat flux is presented in figure 20, and in figure 21 the surface temperature is plotted versus ablation rate ($\dot{S}$). The reradiated heat flux from the sample surface versus incident heat flux is presented in figure 22.

Cold wall thermochemical heat of ablation has been calculated as defined below:

$$\dot{q}^*_{cw} = \frac{\alpha \dot{q}_i}{\rho \dot{S}}$$

$\dot{q}^*_{cw}$ = cold wall thermochemical heat of ablation Btu/lb

$\dot{q}_i$ = incident radiant heat flux Btu/ft^2 sec

α = absorbtivity of sample surface

ρ = sample density lb/ft^3

$\dot{S}$ = surface ablation rate ft/sec

A surface absorptivity of 1.0 was used in order to produce conservative results. The resultant heat of ablation is plotted versus incident flux in figure 23. It is seen that the current data indicate that the design approach for radiative heating is conservative.

These solar furnace tests were conducted under heat flux and pressure conditions of the same magnitude as found in Model 500 Arc tests. Work is underway to compare the results from these two heating environments.

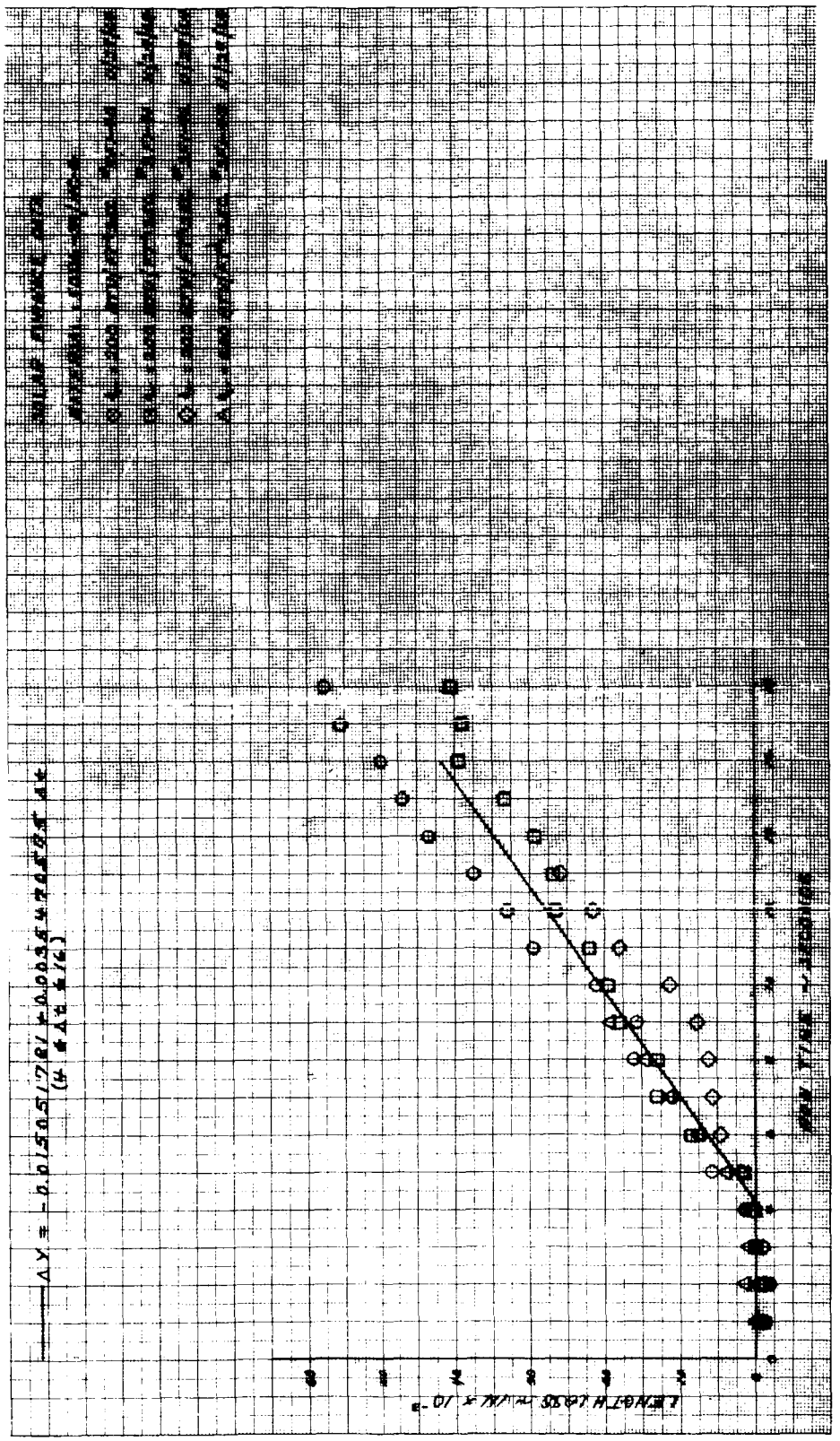

Figure 14 LENGTH LOSS VERSUS RUN TIME

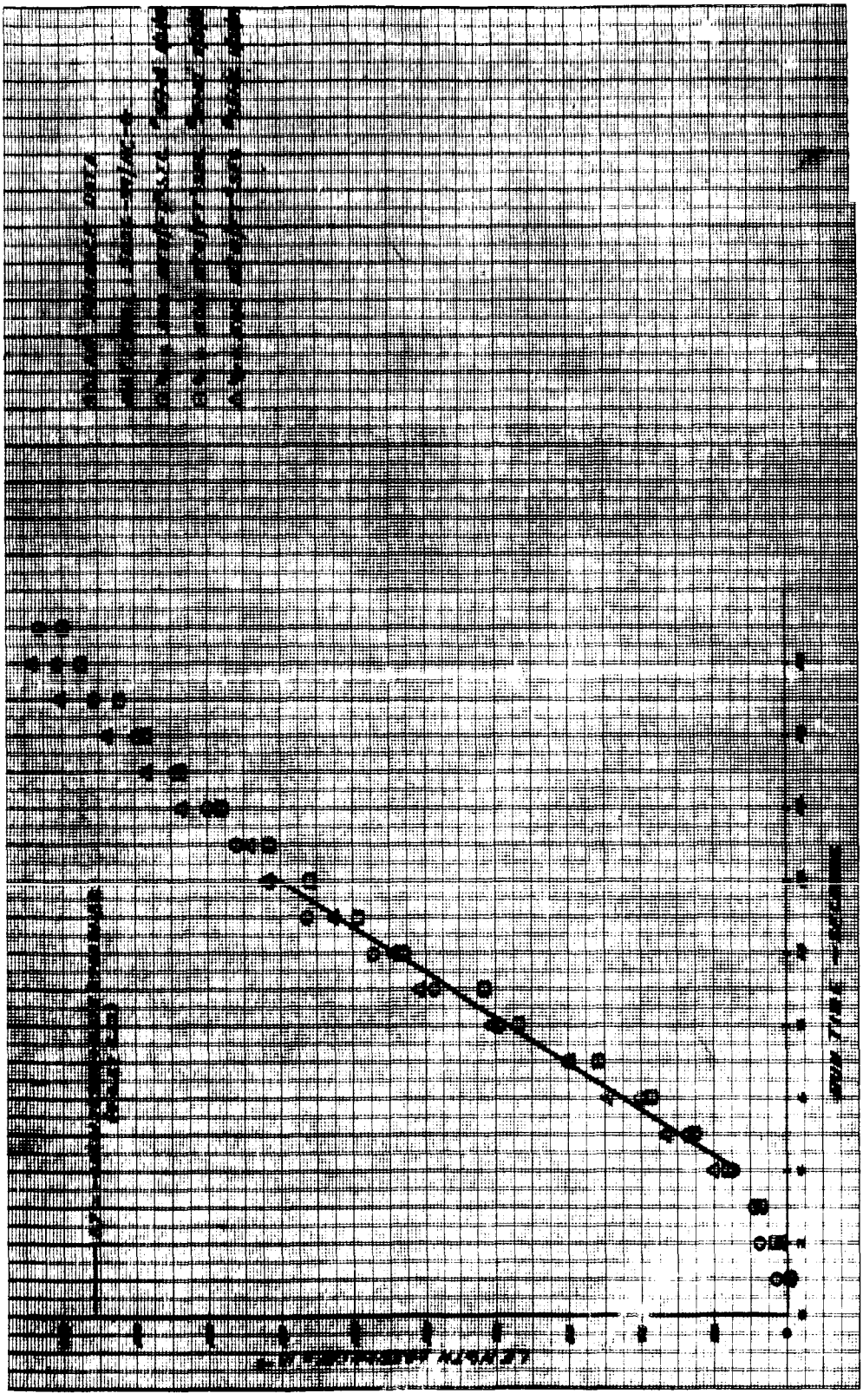

Figure 15 LENGTH LOSS VERSUS RUN TIME

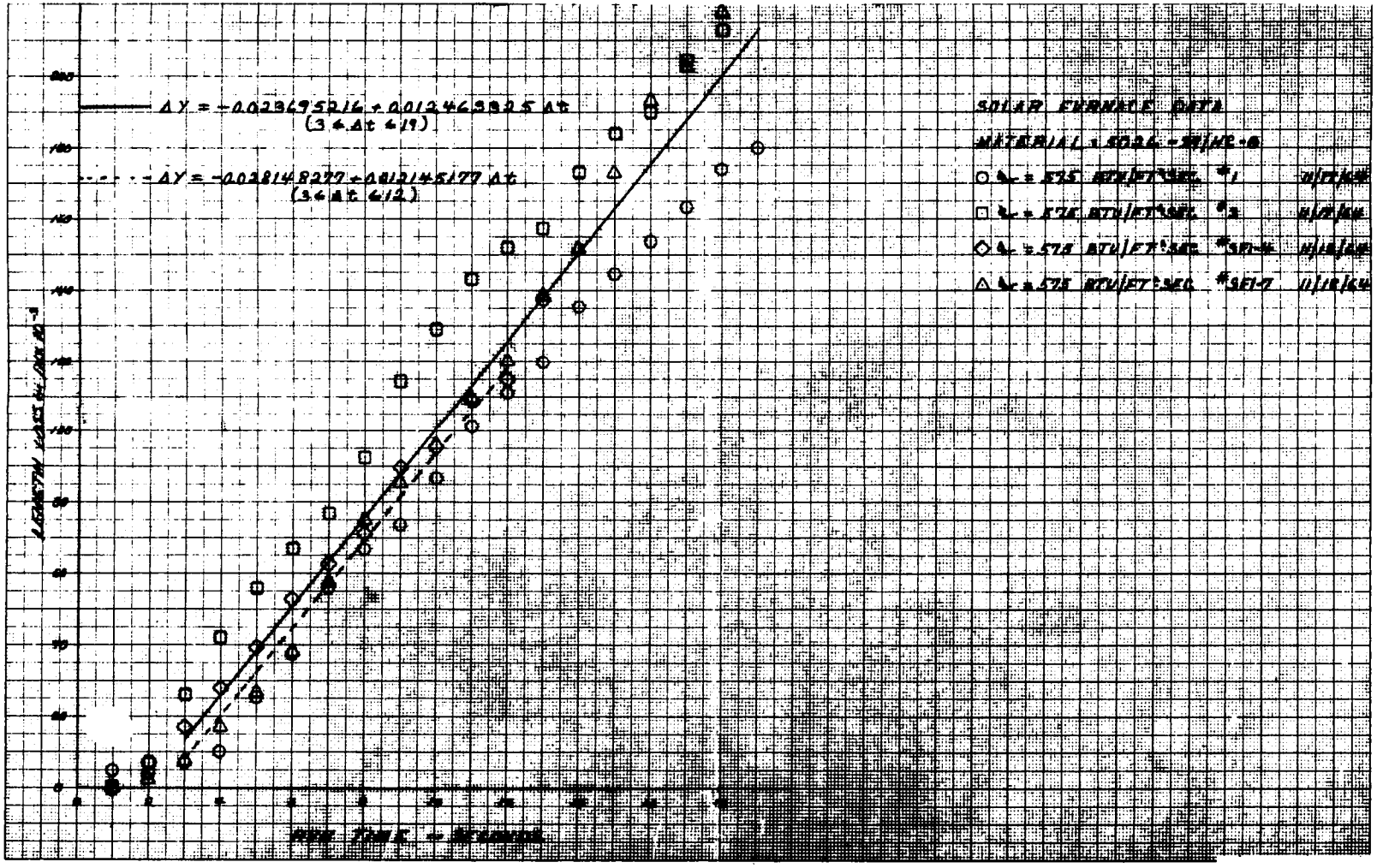

Figure 16 LENGTH LOSS VERSUS RUN TIME

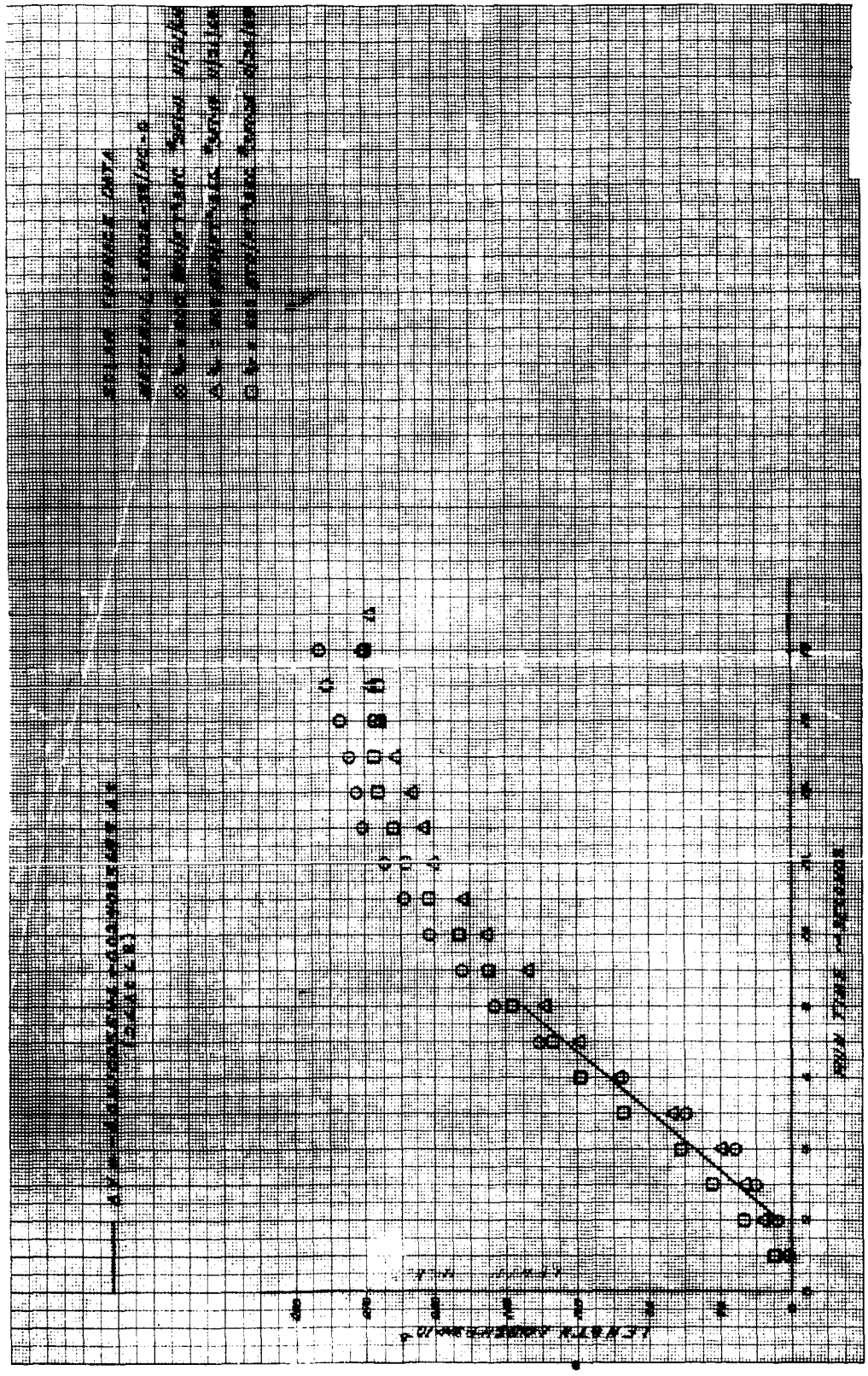

Figure 17 LENGTH LOSS VERSUS RUN TIME

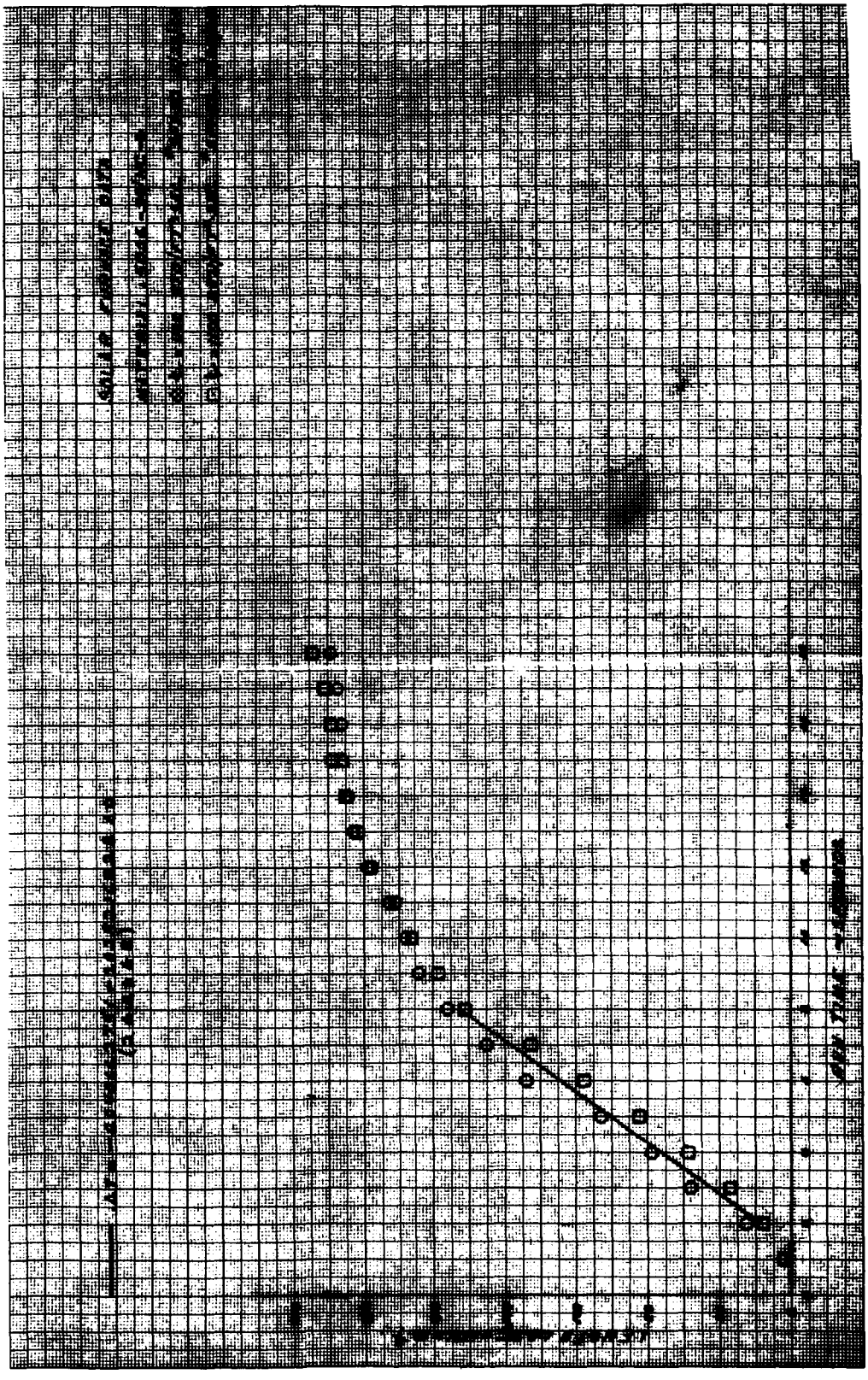

Figure 18 LENGTH LOSS VERSUS RUN TIME

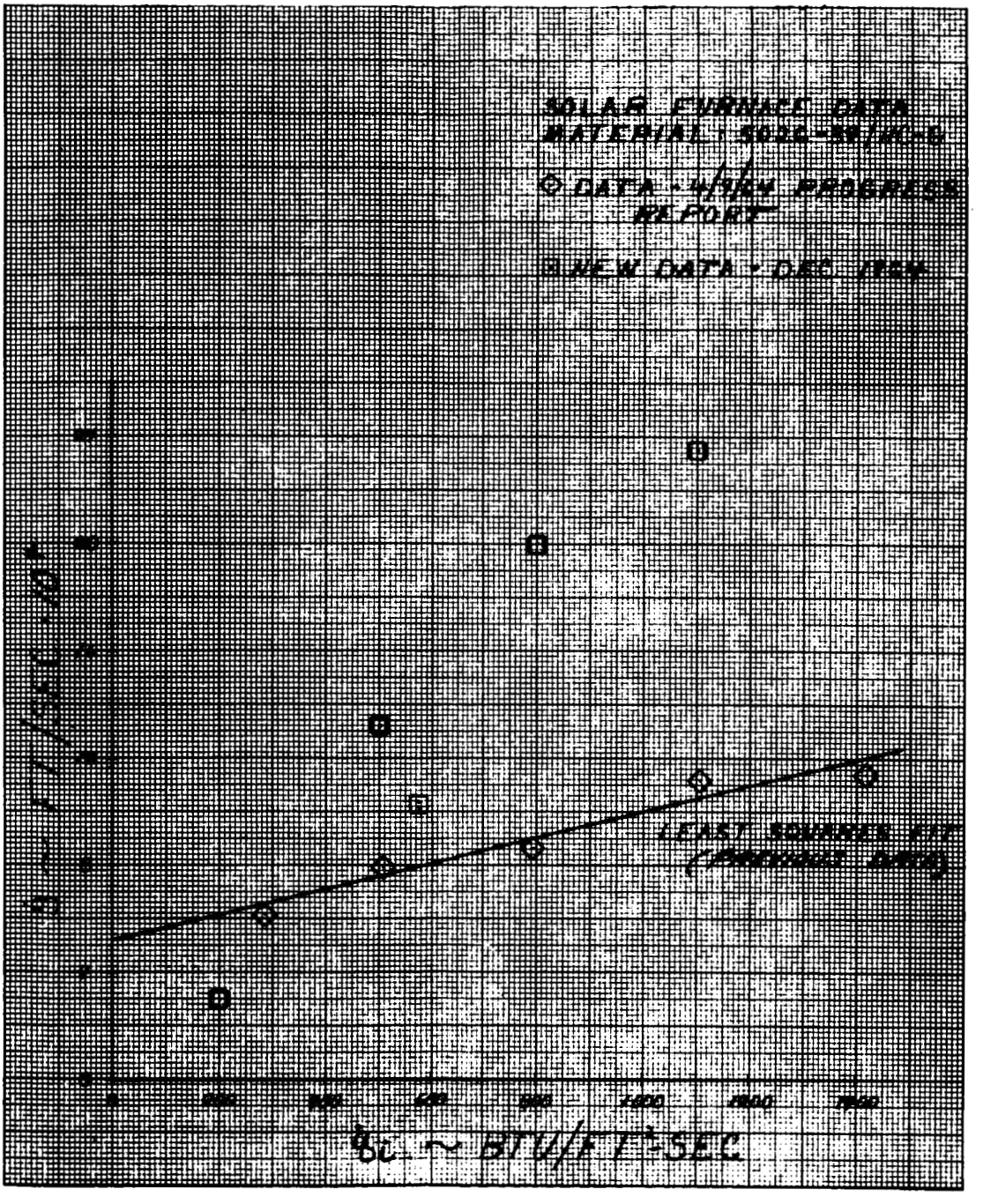

Figure 19 SURFACE RECESSION RATE VERSUS INCIDENT RADIANT HEAT FLUX

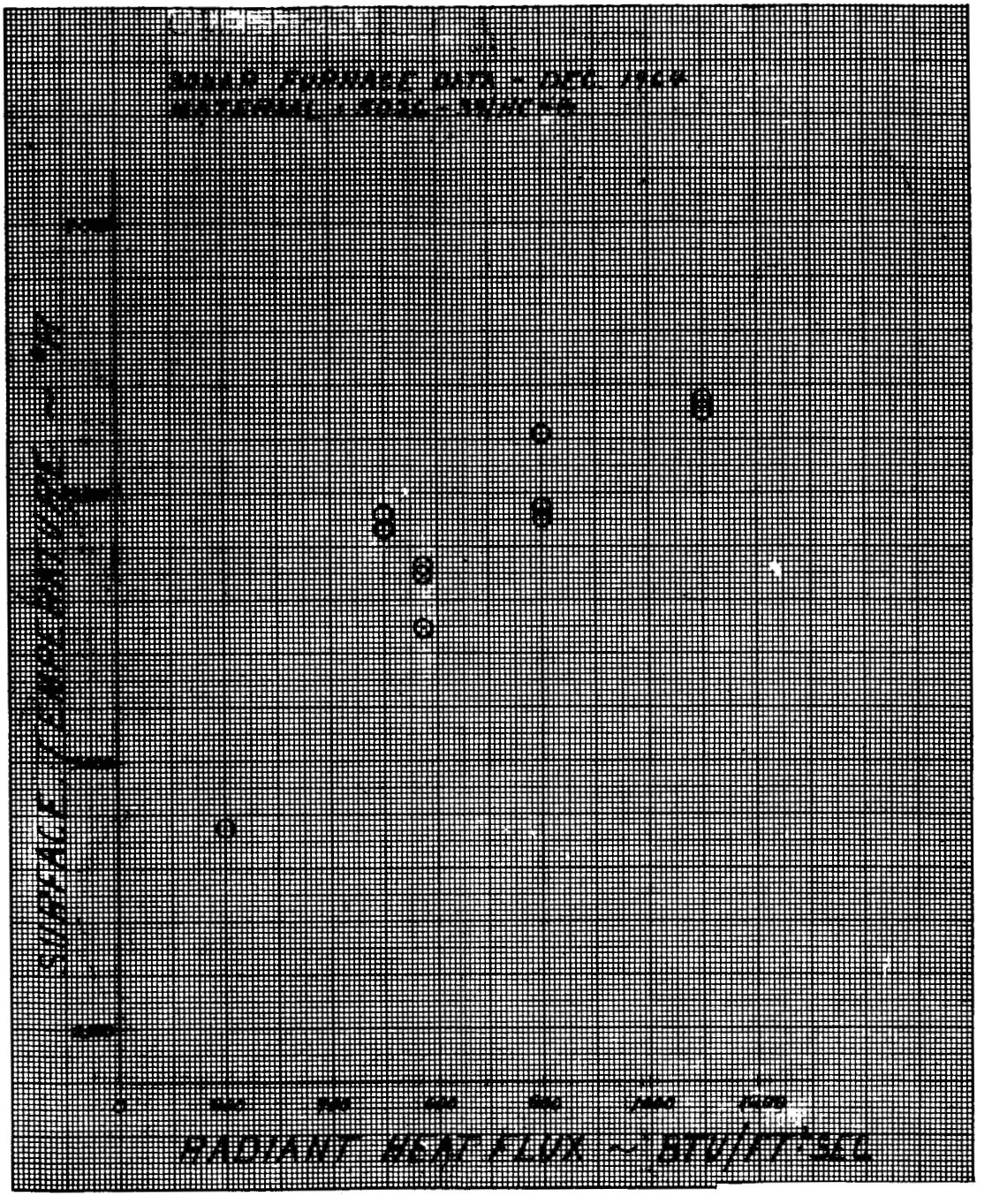

Figure 20 SURFACE TEMPERATURE VERSUS INCIDENT RADIANT HEAT FLUX

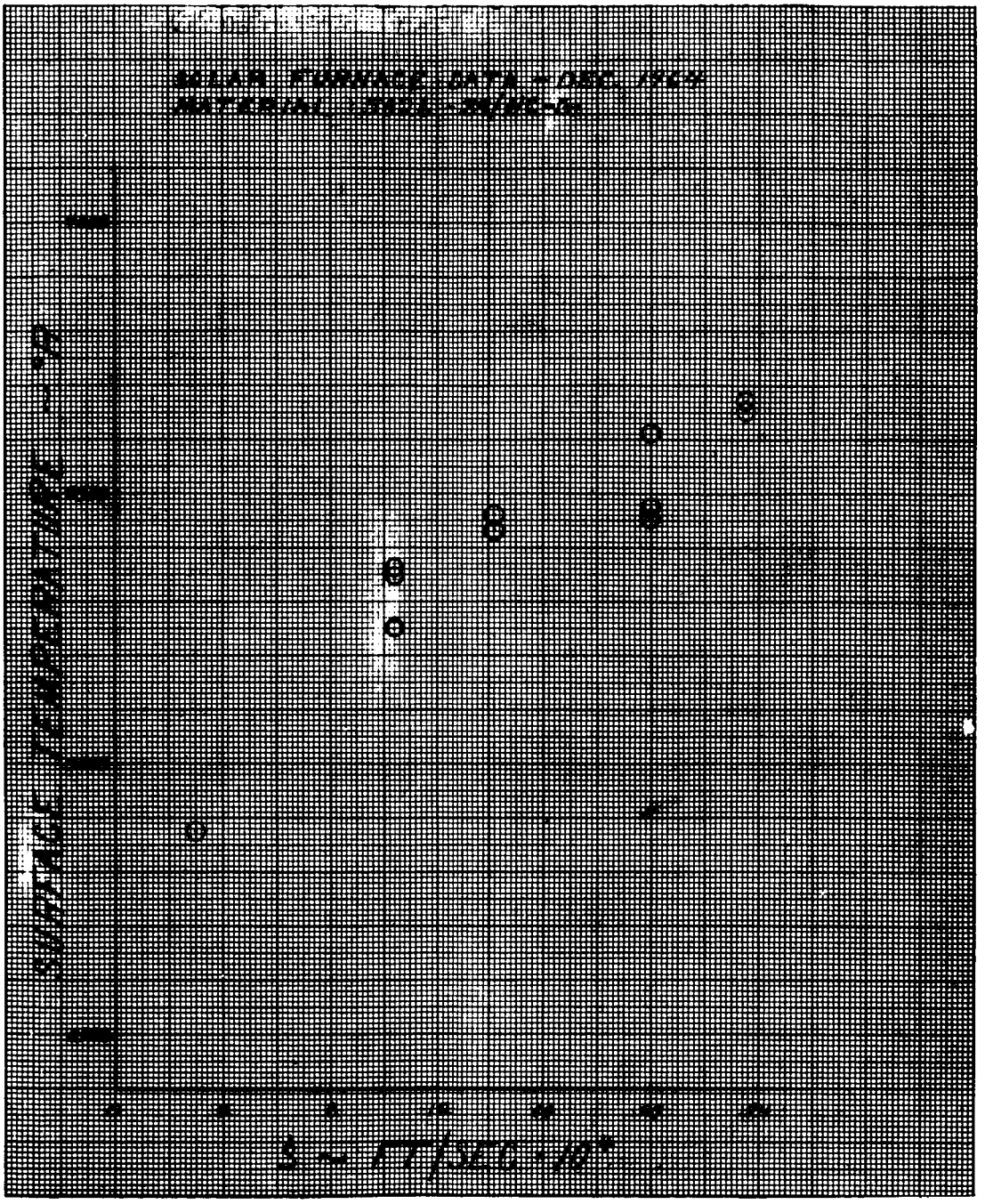

Figure 21 SURFACE TEMPERATURE VERSUS SURFACE RECESSION RATE

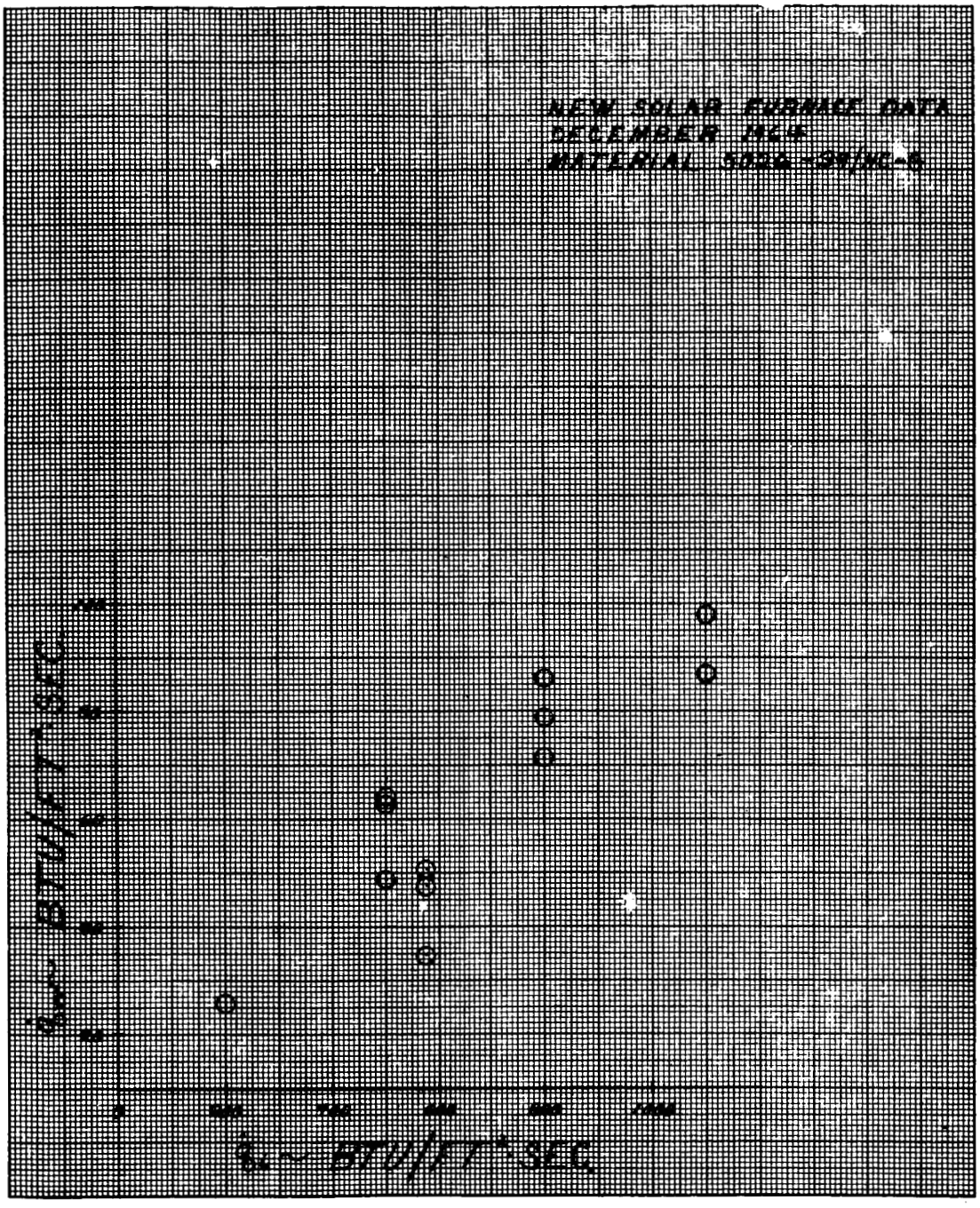

Figure 22 RE-RADIATED HEAT FLUX VERSUS INCIDENT RADIANT HEAT FLUX

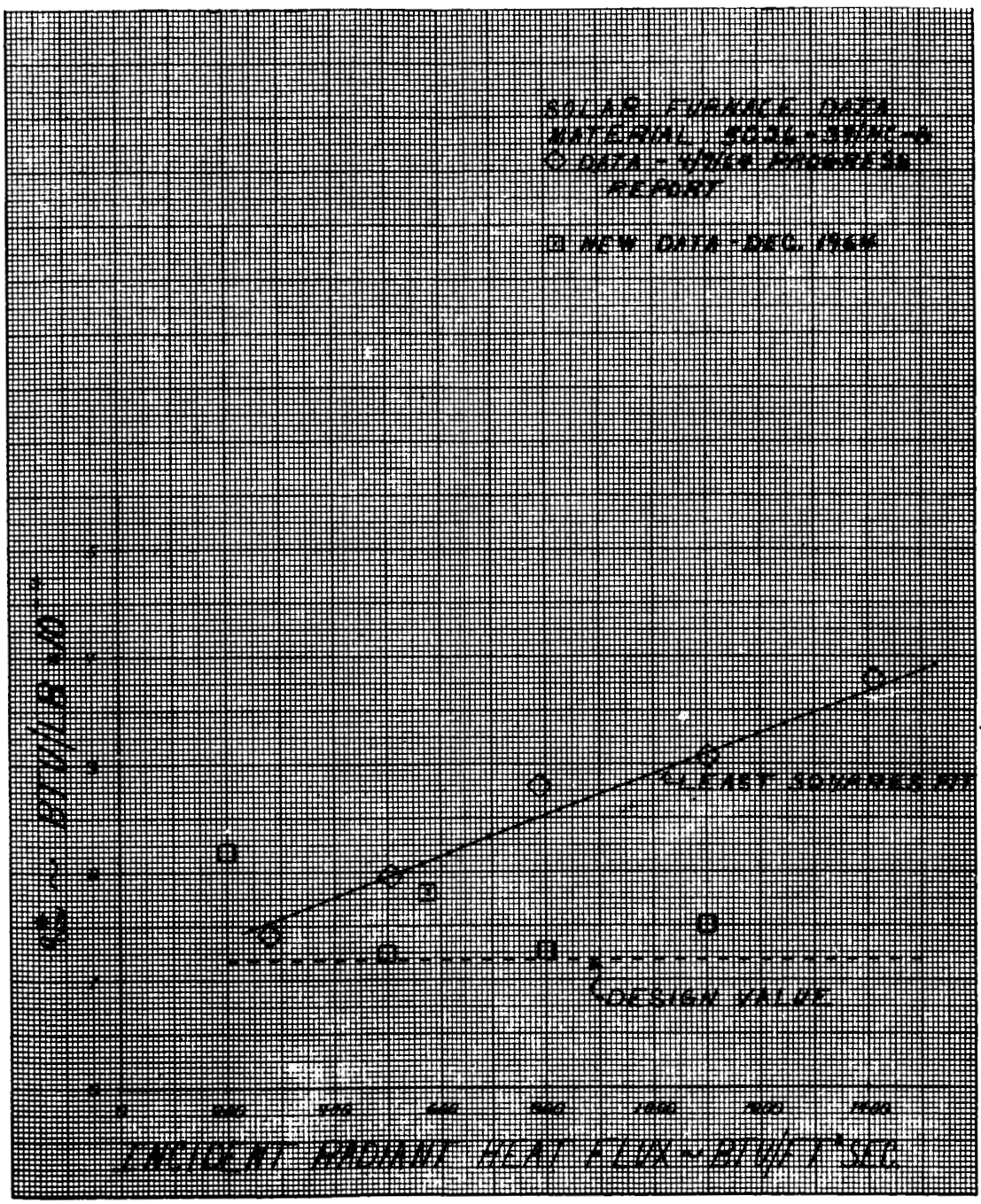

Figure 23 COLD WALL HEAT OF ABLATION VERSUS INCIDENT RADIANT HEAT FLUX

[redacted]

2.3 Surface Recession Studies

Recent data from the OVERS Arc facility were obtained using an optical pyrometer measurement for surface temperature. This measurement is believed to be more accurate than the previously used spectrophotometer measurement. The new data have been compiled on a plot of $\rho_c \frac{\dot{S}}{\sqrt{P}}$ versus surface temperature. Preliminary indications are that it will be possible to distinguish the three combustion regimes for Avcoat 5026-39 HC/G (i.e., the rate, diffusion, and sublimation controlled regimes).

It is planned to predict the surface recession of Avcoat 5026-39 HC/G, assuming combustion as a mechanism. A very flexible set of equations have been programmed at Avco for use with typical heatshield materials.* These equations will be fitted to arc test data and the results will be compared with available chemical analysis for consistency. It is noted that the surface recession-temperature-pressure correlation currently used in program 1600 appears to describe the current data as well as previous data.

3.0 Test Planning and Analysis

3.1 Test Evaluation of Special Design Areas

Test evaluations to support the thermal design of the intercompartment gaps, fixed window areas, air vent and air vent clamp interface areas, and the steam vent interface area were completed. The following summarizes the results of these evaluations.

3.1.1 Intercompartment Gaps

Tests Completed

1) The thermal conductivity of RTV-560 has been measured over the temperature range -100 to +400°F.

2) The laminar thermochemical heat of ablation of RTV-560 has been measured at gas enthalpy levels to 8,000 B/lb and cold wall heat fluxes ranging from 800 to 1400 B/ft^2-sec.

3) The total emittance of RTV-560 has been measured at surface temperatures of approximately 4200°R.

4) The thermal performance of RTV-560 gaskets of varying widths have been determined from radiant lamp tests.

*Brown, J.D., Program 1600-Ablation of Graphite 64-JDB-226.

[redacted]

[redacted]

5) Differential ablation tests of the RTV-560-gasket main-ablator interface have been conducted in the OVERS and Ten Megawatt arcs.

6) The effect of turbulent shear on the ablation performance of RTV-560 has been determined from pipe tests.

7) The effect of exposed steps have been determined from turbulent pipe tests.

8) The radiant heat of ablation of RTV-560 has been measured in the Solar Furnace at heat fluxes between 500 and 1400 Btu/ft^2-sec.

Tests Planned

1) Design verification tests of the ICG seals at Xc = 23.2 inches and Xc = 81.13 inches are planned in the OVERS arc. These tests will be conducted under both HSE-1 and -3A trajectory simulation.

2) OVERS arc tests are planned to determine the allowable unfilled gap width at conditions representative of HSE-3A reentry.

3) OVERS arc tests are planned to determine the effect of exposed RTV-560 steps at conditions representative of HSE-3A reentry.

4) The specific heat of RTV-560 will be measured from -250 to +470°F.

5) Additional laminar thermochemical heat of ablation tests are planned in the OVERS facility to extend the enthalpy range of these measurements.

6) Testing is planned to determine the effect of gap configuration at reentry.

7) A study is planned to determine what effect the expansion of RTV-560 during OVERS arc tests has on local heating.

3.1.2 Fixed Window Areas

Tests Completed

1) Extensive thermophysical, optical, and ablation properties data are available for all materials used in the fixed window areas.

[redacted]

[redacted]

Tests Planned

1) Two full-scale mock-ups of a portion of the side window (also representative of the crew hatch window) will be tested in the radiant lamp facility. These specimens will be instrumented at locations corresponding to those selected for thermal analyses.

2) Two bent panels will be tested in the radiant lamp facility to support the design of the rendezvous window. The first panel will contain calorimeters to measure the heat flux distribution across the panel. The second panel, a full-scale mock-up of the aft edge of the rendezvous window, will be instrumented at locations corresponding to those selected for thermal analyses.

3.1.3 Air Vent Interface Areas

Tests Completed

1) Extensive thermophysical, optical, and ablation properties data are available for all Avco materials used at these interfaces.

Tests Planned

1) Five OVERS two-dimensional tests are planned. The purpose of these tests is to determine the possible effects of flow perturbations caused by a hole in the ablator.

3.1.4 Steam Vent Interface Area

Tests Completed

1) Extensive thermophysical, optical, and ablation properties data are available for all Avco materials used at this interface.

Tests Planned

1) One OVERS two-dimensional strip test is planned for design verification at the steam vent interface. These data will be used in conjunction with data obtained from tests of the air vent interface.

3.2 Additional Test Evaluations

Test evaluations of the following areas are in preparation:

a. Abort tower wells and attach rods

b. Bolt Plugs

[redacted]

c. Close-out members and joints

d. Scimitar antenna interface areas

B. STRUCTURES

Work is in progress on completion of the final stress report for the first four airframes, and the status of the various analyses is given below.

1.0 Volume II Design Information

Work has started on preparation of paragraph 7.0: "Appendix, Ablator Failure Criteria." This section will contain the detailed strain gage correlation and analysis of the failure-criteria-beam test program performed to establish the ablator allowable strain levels.

2.0 Volume III Restrained Curvature Analyses

Section 3.3 "Comparison of Predicted Strains and Test Data" was completed and transmitted to NAA.

Section 5.3 "Reentry Stresses and Strains, Maximum Conditions" was completed and is awaiting reproduction for transmittal to NAA.

3.0 Volume IV Structural Analysis of Forward Compartment Heat Shield

3.1 Paragraph 2.0, Rotationally Symmetric Shell Analyses

Paragraph 2.1, Dexcription of Method of Analysis and Computer Program 1322, was completed and transmitted to NAA/S&ID on 27 November 1964.

Paragraph 2.2, -150°F Soak Condition, was completed and transmitted to NAA/S&ID on 31 December 1964.

Paragraph 2.3, +250°F Soak Condition, has been completed and is presently being reviewed. No interference was found to exist between the forward and crew compartments. The analysis was performed for windward and leeward ablator thicknesses.

Paragraph 2.4, Ascent Loading Conditions, is nearing completion. The condition investigated was C-1 boost max. q for a zero angle of attack, which was the most severe axisymmetric condition, based on SEM 062. The final stresses, strains, and deformations have been determined and the program 1322 results have been plotted. The analysis was performed for leeward ablator thicknesses.

Paragraph 2.5, Abort Loading Conditions, is nearing completion. The most severe axisymmetric condition is max. q non-tumbling abort based on SEM 062. The final stresses, strains and deformations have been determined and the program 1322 results are being plotted. The analysis was performed for leeward ablator thicknesses.

Paragraph 2.6, Reentry, is in progress. The mathematical model has been selected and will consist of 4 regions for both the forward compartment and nose cone. The analysis is being performed for actual windward ablator thicknesses rather than the faired thicknesses.

3.2 Paragraph 3.0, Effects of Cutouts

Paragraph 3.2, Forward Pitch Engine Panel, is continuing for the -150°F soak condition. The model assumes the shell in the vicinity of the cutout to be a flat plate and the continuous closure ring at X_c = 81 is treated as a beam. The model is analyzed using finite difference techniques. The results obtained to date seem to be in error and checking of the basic field equations is in progress.

4.0 Volume V Structural Analysis, Crew Compartment Heat Shield

4.1 Paragraph 2.0, Rotationally Symmetric Shell Analyses

Description of Methods of Analysis, paragraph 2.1, is being reviewed. Work is continuing on all windward meridian analyses of the crew compartment heat shield. Crew-aft compartment interaction loads have been calculated for soak temperature conditions of -150°F and -60°F. The interaction loads together with the thermal environment have been applied on the heat shield using the 1322 program. The program results are being reduced.

Aft crew compartment interaction loads are being calculated for the +250°F soak condition. Deformations and influence coefficients for the aft-crew compartment interaction analysis are being calculated for the conditions of C-1 boost and max. q abort with an angle of attack of zero degrees.

Reentry heating information for the windward meridian during HSE-6 trajectory has been received from the thermodynamics section. Reentry analyses using the 1322 program will start, following an investigation of the heating information.

4.2 Paragraph 4.0, Unsymmetrical Ring Analyses

Paragraph 4.1.1, Method of Analysis and Description of Computer Program 1095X, was completed and transmitted to NAA/S&ID on 3 December 1964.

The unit ring analyses at $X_c = 33.0$ are complete for space flight conditions of -150°F soak, circumferential temperature distribution from +250°F at $\theta_c = 90°$ to -150°F at $\theta_0 = 270°$F, circumferential temperature distribution from -150°F at $\theta_c = 90°$ to +250°F at $q = 270°$F and max. tumbling abort with an angle of attack of 57 degrees. The analyses are being reviewed. The unit ring analysis at $X_c = 68.7$ is complete for the same environments used for the ring analysis at $X_c = 68.7$. The tumbling abort condition with an angle of attack of 57 degrees produces radial deflections on the windward side of the vehicle which exceed those allowed by the stringer slotted holes. A bottoming analysis was done in which the radial deflections of the stringer locations is limited to that allowed by slotted holes.

4.3 Paragraph 5.0, Crew Hatch and Crew Hatch Window

Ablator and steel strains are being calculated at each nodal point on the hatch beam network for the -150°F soak condition. A study was made comparing the strains calculated using an orthotropic plate with those calculated using a beam analogy. Several sections representing the crew hatch were used for the study. The strains calculated using the two methods show very close agreement. Therefore, the beam analogy was selected for the strain calculations since results can be determined quickly and a more comprehensive description of the strains in hatch can be achieved.

The method of analysis and an analytical model have been selected for the crew hatch window-frame interaction analysis. Both the window and frame are being analyzed using finite difference techniques.

A beam network analytical model has been selected for the crew hatch max. q abort condition. Calculations are being made for section properties, flexibilities, and equilibrium equations.

4.4 Paragraph 7.0, Astro Sextant Doors

The analysis to determine the shell-door mismatch at -150°F soak has been started. The door is being analyzed using a beam network analysis similar to the crew hatch analysis. To determine the free thermal deflection, the door is assumed to have a meridional axis of symmetry and an unvarying circumferential ablator thickness. The analysis of the door includes the aluminum backing plate.

5.0 Volume VI, Structural Analyses, Aft Compartment Heat shield

5.1 Paragraph 2.0, Rotationally Symmetric Shell Analyses

Paragraph 2.1, Method of Analysis, is being written.

Paragraph 2. 2, Restraints Due to Bolt Circle, has been completed and is presently being reviewed.

Paragraph 2. 3, 2. 4 and 2. 5 are in progress. Aft compartment heat shield thermostructural analyses have been completed for the space flight environments of -60° F and -150° F using windward meridian ablator thicknesses. Presently, final computer runs are awaited from the Mathematics Department after which analytical results will be plotted. The aft compartment heat shield has been analyzed for a +250° F environment which uses a temperature distribution that is provided in SEM No. AVC 146-case No. 1 - windward meridian. Presently, another +250° F environment is underway which considers a temperature distribution where the aft compartment heat-shield experiences temperatures of +250° F at X_c = 23, +130° F at R_c = 72. 3 and +50° F at R_c = 0. 0 in accordance with NAA internal letter 696-231-64-167, Enclosure (1), 11 May 1964.

6. 0 Unsymmetrical Shell Analysis

As noted last month, a revised test case model, using only a cone with various temperature distributions, has been employed to check out program 1450. Excellent agreement has been obtained between program 1322, which analyzes an axisymmetric temperature input, and program 1450B which analyzes the analogous body forces. Program 1450A, which is set up to handle asymmetric temperature inputs, is still giving unsatisfactory results. However, Avco is not planning to use 1450A to analyze the heat shield because it is limited to a small shell, but the intent was to use it to cross-check 1450B under asymmetric loadings.

The difficulties encountered with the original cone-sphere test-case model are now believed to lie with the junction conditions between regions. This applies to the discrepancies between 1322 and 1450B. In general, the thermal loads (N_T and M_T) are discontinuous at the junctions. In the cone model described above, M_T and N_T are continuous. In program 1322, the thermal load is treated as a thermal load and the machine solution discriminates between the internal mechanical and thermal loads. At a junction, continuity is enforced between the internal mechanical loads of adjacent regions, i. e., meridional moment, meridional membrane force, transverse shear are continuous. With 1450B, the loading is the analogous body forces and the internal moment, computed by 1450B, is the sum of M and M_T and similar sums for other internal forces) and thus, at junctions, the program enforces compatibility between this sum on either side of the junction. This is valid only when M_T and other thermal loads are also continuous.

The obvious resolution of the problem is to input suitable analogous load increments at the junctions, but program 1450B has no provision for such an input. It is anticipated that 1450B will be modified to accommodate external junction loads. In the meantime, noting that the heat shield is not very discontinuous, a continuous model of the crew compartment is being established to overcome these junction problems. In support of the unsymmetrical shell analysis, program 1413A has been modified to compute Fourier coefficients of the thermal loads using a least square technique. Program 1856 has been written to derive geometry input compatible with 1450B, from the AE and EI parameters of the continuous crew compartment model.

7.0 Modification of Rigid Bond Analysis Digital Program

Program 1606 has been modified to allow bending of the substructure. An applied moment or an enforced rotation can be applied to the free edge of the substructure. The modified program is 1606A and has been checked out and placed in production.

C. DESIGN

1.0 General-Considerable Design effort was expended in the area of bolt plugs and sleeves to compensate for the out of tolerance condition on many of the NAA maintenance door bolt locations. Because of the wide range of edge distances present on vehicles 006 and 009, it was necessary to create a bolt plug sleeve and installation drawing (401080) which defines which type of sleeve/plug combination as a function of edge distance is required. Four combinations will be used. The dimensions involved led to the requirement of utilizing a less viscous bonding material and work and tests are presently under way in support of this development.

LA-6828, Access Plug, Pitch Engine, Fwd Compartment, was completed and shows the design for providing accessibility to the six protruding nuts in the forward pitch engine panel area. The manufacturing drawings defining the details of this design for vehicles 006 and 009 were completed. NAA will be responsible for bonding in the molded ablator plug and for installing the molded ablator locking Dutchman plugs as well as sealing this installation. Additional work related to vehicle 009 involved: (1) Incorporation of the tension tie blocks which had previously been deleted; (2) Creating rework sketches defining the hole enlargement for the loose panel fasteners on vehicles 006 and 009 and the relocation of the two (2) end holes to a 0.75 edge distance on

vehicle 009; (3) Redefining the loose panel dimensions for vehicle 009 to compensate for the oversize Forward Pitch Panel; and (4) Evaluating the effect of the vehicle 009 Aft Compartment rework at NAA on the Avco Ablator Design.

Drawings of the new series (402xxx) incorporating the gap splice for the Crew and Aft Compartments were released thereby completing the Design definition of the gap splice for all compartments. Under the direction of Quality Assurance, drawings defining the X-ray results in the Crew Compartment were generated.

The lastest NAA ICD's were reviewed and marked up to reflect Avco's Design requirements. Work continues in the area of manufacturing drawings for vehicle 008 with a large portion of these drawings to be released shortly.

Redesign of the shear pad, either in configuration or material is under discussion. Our possibility is the use of a spirally wound laminated billet which would require a design change.

2.0 NAA EO M28992 requires the installation of nutplates at the loose panel fastener locations and references Avco TWX 5 (10-22-64) as the reason for implementing the change. TWX 5 did not make this request and installation of the nutplates would create manufacturing problems for Avco. Therefore these nut plates should not be installed until after the ablator, however Avco desires to receive the substructure with the full sized holes.

3.0 Weight - The current weight status for vehicles 006 and 009 is the same as in the December report with an ablator weight of 1441.4 pounds for vehicle 006 and 1458.1 pounds for vehicle 009. These weights reflect all heating information through Revision "P" and include perturbations for the shear pads, scimitar antennas, abort tower wells, fixed windows and tension tie blocks.

A graphical comparison was made of the contours produced by the 401098, Revision "F", computer printout and the computer oriented machine tool grinding program. Forty-eight full size layouts of the Crew Compartment were made at selected meridians to establish a similarity of contours.

4.0 Specifications - The Specifications and Standards effort for this reporting period consists of a total of 17 specification change notices being released or awaiting sign-off. Four specification revisions were approved and released and two specifications are being reviewed for revision or awaiting approval of revisions.

A new specification was generated defining the bonding of bolt plug sleeves in support of the bolt edge distance fix for dimensions less than 0.370 inch.

Listed in the table below are the substructure weights for vehicle 006 and 009 as received by Avco. All weights are actual weights and contain the weight of all doors, windows, blocks, and hardwares except as noted. These values were taken for the applicable QATP's.

Compt.	006	009
Fwd Nose Cone	34.3	34.5
Fwd Compt.	147.2	147.6
Crew Compt.	543.2	553.3*
Aft Compt.	484.1	493.6
	1208.8	1229.0

*The weight of the 009 Crew Compartment does not include the weight of the attaching hardware for the doors.

Vehicle 006

APOLLO ABLATOR WEIGHT

ITEM		WEIGHT
FORWARD NOSE CONE	48.5	
5026-39/HC-G (Fwd Nose Cone)		45.1
Closeout - Fiberglass Station Xc 112.25		0.5
Gasket - RTV 560 Station Xc 112.25		0.4
Adhesive - HT 424		1.8
Surface Sealer (Barrier Coat BR-C-8)		0.7

VEHICLE 006

APOLLO WEIGHT SUMMARY
MONTHLY PROGRESS REPORT

January, 1965

	Weight - Pounds							CG (of total) inches			MI (of total) Slug Ft^2		
Compartment	Ablator	Adhesive	Sealer	Fiberglass	Gasket	S&C Pads	Total	Xc	Yc	Zc	Ixx	Iyy	Izz
Forward Nose Cone	45.1	1.8	0.7	0.5	0.4	--	48.5	122.2	-0.1	0.3	1.8	1.5	1.3
Forward	114.7	6.2	2.5	2.1	0.9	--	126.4	93.9	-0.1	3.0	25.3	15.8	14.8
Crew	441.9	22.2	9.0	26.2	5.4	--	504.7	46.1	-0.6	14.4	389.6	230.1	220.6
Aft	686.2	20.6	8.2	6.9	10.8	29.1	761.8	8.7	0.1	5.7	513.5	269.7	256.0
Totals	1287.9	50.8	20.4	35.7	17.5	29.1	1441.4	33.1	-0.2	8.3	935.5	830.2	798.5

1. ρ = 31 lb/ft^3
2. Perturbations include shear pads, tower wells, scimitar antennas, fixed window fairings and tension tie blocks
3. 3 percent estimate for moisture absorption.

Vehicle 006

APOLLO ABLATOR WEIGHT

ITEM	WEIGHT
FORWARD COMPARTMENT	126.4
5026-39/HC-G	114.7
Fwd Compartment	102.5
Tower Wells	9.6
Leeward (2)	4.2
Windward (2)	5.4
Fwd. Comp. Door	1.6
Pitch Eng. Panel	1.0
Closeout - Fiberglass	2.1
Station 112.25	0.5
Station 81.13	1.0
Fwd. Comp. Door	0.2
Pitch Eng. Panel	0.1
Fwd. Compartment	0.3
Adhesive HT 424	6.2
Surface Sealer (Barrier Coat BR-C-8)	2.5
Gasket - RTV 560 (Station 81.13)	0.9

Vehicle 006

APOLLO ABLATOR WEIGHT

ITEM		WEIGHT
CREW COMPARTMENT	504.7	
5026-39/HC-G	441.9	
Crew Compt.		332.3
Crew Hatch		19.0
Crew Hatch Wind.		1.7
Side Window (2)		9.4
Rendezvous Window (2)		22.3
Sex. Teles. Door		9.3
Maintenance Doors		36.3
Type A 0°		4.5
Type A 180°		4.5
Type A 239°		2.6
Type A 301°		2.6
Type B 207° 30'		2.8
Type B 332° 30'		2.8
Type C 270°		2.8
Type E 45°		6.7
Type E 135°		6.7
A. C. Motors		11.6
Pitch		2.2

[redacted]

Yaw (2)		4.8
Roll (2)		4.6
Closeout Members & Bolt Plug Sleeves (F'Glass)	26.2	

Vehicle 006

APOLLO ABLATOR WEIGHT

ITEM	WEIGHT	
Crew Compartment	9.2	
Crew Hatch	1.1	
Crew Hatch Wind.	0.3	
Side Window (2)	1.7	
Rendezvous Window (2)	2.5	
Sex. Teles, Door	0.6	
Maintenance Doors (Fiberglass)	5.8	
Type A 0°		0.7
Type A 180°		0.7
Type A 239°		0.5
Type A 301°		0.5
Type B 207° 30'		0.5
Type B 332° 30'		0.5
Type C 270°		0.5
Type E 45°		1.0
Type E 135°		1.0

[redacted]

[redacted]

A. C. Motors	4.7	
Pitch		0.8
Yaw (2)		1.8
Roll (2)		1.5
Scimitar Antennas (2)		0.6
Umbilical	0.3	
Gaskets - RTV 560	5.4	

Vehicle 006

APOLLO ABLATOR WEIGHT

ITEM	WEIGHT	
Crew Compartment	3.5	
Crew Hatch	0.4	
A. C. Motors	1.4	
Pitch		0.3
Yaw (2)		0.7
Roll (2)		0.4
Maintenance Doors (Gaskets)	0.1	
Type A 239°		0.03
Type A 301°		0.03
Type C 270°		0.06
Sex. & Teles. Door	0.05	
Side Window (2)	0.02	

[redacted]

[redacted]

Vehicle 006

APOLLO ABLATOR WEIGHT

ITEM	WEIGHT	
AFT COMPARTMENT	761.8	
Adhesive - HT 424	22.2	
Surface Sealer (Barrier Coat BR-C-8)	9.0	
5026-39/HC (Aft Compartment)		686.2
Shear Pad (3)		20.5
Compression Pad (3)		8.6
Closeout - Fiberglass		6.9
Shear Pad (3)		0.5
Compression (3)		0.4
C-Band (3)		1.0
Station 23.2		3.3
Bolt Plugs		1.7
Gasket - RTV 560		10.8
Station 23.2		9.6
Compression Pad (3)		0.3
C-Band		0.9
Adhesive - HT 424		20.6
Surface Sealer (Barrier Coat BR-C-8)		8.2

[redacted]

VEHICLE 009

APOLLO WEIGHT SUMMARY
MONTHLY PROGRESS REPORT

January, 1965

	Weight - Pounds							CG (of total) inches			MI (of total) Slug Ft^2		
Compartment	Ablator	Adhesive	Sealer	Fiberglass	Gasket	S&C Pads	Total	Xc	Yc	Zc	Ixx	Iyy	Izz
Forward Nose Cone	46.4	1.8	0.7	0.8	0.6	--	50.3	122.5	-0.1	0.5	2.0	1.5	1.3
Forward	117.3	6.2	2.5	2.3	1.0	--	129.5	94.9	-0.2	4.4	26.8	16.2	15.2
Crew	449.5	22.2	9.0	26.2	5.6	--	512.5	47.6	-0.6	14.3	395.6	232.1	223.9
Aft	690.0	20.6	8.2	7.0	11.1	29.1	766.0	8.6	-0.1	6.1	510.1	265.0	256.6
Totals	1303.2	50.8	20.4	36.3	18.3	29.1	1458.1	33.9	-0.3	8.6	937.5	835.4	810.7

1. ρ = 31 lb/ft^3

2. Perturbations include shear pads, tower wells, scimitar antennas, fixed window fairings, and tension tie blocks.

3. 3 percent estimate for moisture absorption.

[redacted]

Vehicle 009

APOLLO ABLATOR WEIGHT

ITEM	WEIGHT
FORWARD NOSE CONE	50.3
5026-39/HC-G (Fwd Nose Cone)	46.4
Closeout - Fiberglass Station Xc 112.25	0.8
Gasket - RTV 560 Station Xc 112.25	0.6
Adhesive - HT 424	1.8
Surface Sealer (Barrier Coat BR-C-8)	0.7

Vehicle 009

APOLLO ABLATOR WEIGHT

ITEM	WEIGHT
FORWARD COMPARTMENT	129.3
5026-39/HC-G	117.3
Fwd Compartment	103.8
Tower Wells	10.3
Leeward (2)	4.5
Windward (2)	5.8
Fwd. Comp. Door	1.9
Pitch Eng. Panel	1.3
Closeout - Fiberglass	2.3

[redacted]

[redacted]

Station 112.25		0.6
Station 81.13		1.1
Fwd. Comp. Door		0.2
Pitch Eng. Panel		0.1
Fwd. Compartment		0.3
Adhesive - HT 424	6.2	
Surface Sealer (Barrier Coat BR-C-8)	2.5	
Gasket - RTV 560 (Station 81.13)	1.0	

Vehicle 009

APOLLO ABLATOR WEIGHT

ITEM		WEIGHT
CREW COMPARTMENT	512.5	
5026-39/HC-G	449.5	
Crew Compt.		336.7
Crew Hatch		19.3
Crew Hatch Wind.		1.8
Side Window (2)		9.6
Rendezvous Window (2)		22.7
Sex., Teles. Door		9.4
Maintenance Doors		37.2

[redacted]

[redacted]

Type A 0°		4.7
Type A 180°		4.7
Type A 239°		2.6
Type A 301°		2.6
Type B 207° 30'		2.9
Type B 332° 30'		2.9
Type C 270°		3.2
Type E 45°		7.2
Type E 135°		7.0
A. C. Motors	12.2	
Pitch		2.4
Yaw (2)		5.0
Roll (2)		4.8
Closeout Members & Bolt Plug Sleeves (F' Glass)	26.2	

Vehicle 009

APOLLO ABLATOR WEIGHT

ITEM	WEIGHT
Crew Compartment	9.2
Crew Hatch	1.1
Crew Hatch Wind.	0.3
Side Window (2)	1.7
Rendezvous Window (2)	2.5

[redacted]

[redacted]

Sex., Teles. Door	0.6	
Maintenance Doors (Fiberglass)	5.8	
Type A 0°		0.7
Type A 180°		0.7
Type A 239°		0.5
Type A 301°		0.5
Type B 207° 30'		0.5
Type B 332° 30'		0.5
Type C 270°		0.5
Type E 45°		1.0
Type E 135°		1.0
A. C. Motors	4.7	
Pitch		0.8
Yaw (2)		1.8
Roll (2)		1 5
Scimitar Antennas (2)		0.6
Umbilical	0.3	
Gaskets - RTV 560	5.6	

[redacted]

[redacted]

Vehicle 009

APOLLO ABLATOR WEIGHT

ITEM	WEIGHT	
Crew Compartment	3.7	
Crew Hatch	0.4	
A. C. Motors	1.4	
Pitch		0.3
Yaw (2)		0.7
Roll (2)		0.4
Maintenance Doors (Gaskets)	0.1	
Type A 239°		0.03
Type A 301°		0.03
Type C 270°		0.06
Sex., & Teles. Door	0.05	
Side Window (2)	0.02	
Adhesive - HT 424	22.2	
Surface Sealer (Barrier Coat BR-C-8)	9.0	

[redacted]

[redacted]

Vehicle 009

APOLLO ABLATOR WEIGHT

ITEM	WEIGHT	
AFT COMPARTMENT	766.0	
5026-39/HC (Aft Compartment)	690.0	
Shear Pad)3)	20.5	
Compression Pad (3)	8.6	
Closeout - Fiberglass	7.0	
Shear Pad (3)		0.5
Compression (3)		0.4
C-Band (3)		1.0
Station 23.2		3.4
Bolt Plugs		1.7
Gasket - RTV 560	11.1	
Station 23.2		9.8
Compression Pad (3)		0.4
C-Band		0.9
Adhesive - HT 424	20.6	
Surface Sealer (Barrier Coat BR-C-8)	8.2	

[redacted]

[redacted]

D. GROUND TEST

Tests completed are reported below:

1.0 Structural Tests

1.1 Beam Load Tests

Eighteen specimens were tested this past reporting period. All of these specimens consisted of Avcoat 5026-39/HC-G ablator applied to a 22 x 5 x 1/2-inch S.S. sandwich (0.008-inch face sheets) substructure. A typical beam is shown in figure 24.

Specimens APT 642, 643, 747, 749, 752, 755, 758, 759, 760N, 762, 764, 765 were tested as standard beams to provide basic data. Specimens APT 642 and 643 had previously been tested for deflection under compressive ablator load conditions. Specimen APT 749 contained two 1 inch diameter ablator repair plugs located 1 1/2 inches off each specimen edge at the transverse centerline.

Specimens APT 793, 794 were tested to evaluate adhesive versus the standard reference design HT 424 adhesive used to attach the F/G honeycomb to the S.S. substructure. These specimens were identical in all other respects to a regular reference design beam specimen.

Test results are shown in table I.

2.1 Abort Tie Rod Radiant Mockup Test

Abort Tower tie rod specimens APT 817 ANO APT817-1 consisted of a 4.0 x 0.80 x 1.45 inch thick piece of laminated fiberglass attached to an 8.0 x 5.0 x 0.125 inch thick steel plate with HT-424 adhesive and surrounded by Avcoat 5026-39/HC-G. These specimens were subjected to a simulated reentry heating trajectory HSE-3A per curve No. TT-44 for 1.42 inch thick ablator. Maximum of q_{cw} = 11.1 Btu/ft^2/sec and Q_{cw} = 3653 Btu/ft^2 for this trajectory. Figure 25 shows the test setup arrangement and Figure 26 shows specimen apt 817-1 after the completion of its test.

2.0 Thermal Tests

A total of nineteen specimens have been tested during the reporting period. These tests include the following series:

a. instrumented trajectory simulation: AP1737--seven tests

b. q* correlation: AP1718, material RTV--seven tests

[redacted]

[redacted]

TABLE I

BEAM TEST RESULTS

APT No.	Ablator			Cracking		Failure		Type	Remarks
	Thick (in)	Width (in)	Node Direct	Temp. (°F)	Moment (in lb/in)	Temp. (°F)	Moment (in lb/in)		
758	1.0	5.0	Trans.	-150	515	-150	970	F.S.	
759	1.0	5.0	Trans.	-150	455	-150	920	F.S.	
762	1.0	5.0	Trans.	-150	(1) 450	-150	885	F.S	
				-150	(2) 378				
793	1.8	5.0	Trans.	-150	1275	-150	502	B.D	Aerobond Adhesive
794	1.8	5.0	Trans.	-150	1262	-150	1170	B.D	Aerobond Adhesive
642	1.8	5.0	Trans.	R.T.	853	N.A.	N.A.	N.A.	Retest of beams which were previously tested in compression with no failure.
643	1.8	5.0	Trans.	R.T.	820	N.A.	N.A.	N.A.	
763	0.5	5.0	Trans.	-150	225	-150	779	F.S.	
764	0.5	5.0	Trans.	-150	173	N.A.	N.A.	N.A.	
765	0.5	5.0	Trans.	-150	219	N.A.	N.A.	N.A.	
747	2.5	5.0	Trans.	-150	1365	-150	2093	B.D.	See Note (3).
749	1.8	5.0	Trans.	-150	852	-150	585	B.D.	Crack approximately 1 inch away from plugs.
752	1.5	4-5/8	Trans.	-150	820	-150	1210	F.S.	
755	1.5	4-5/8	Trans.	-150	420	-150	1050	B.D.	
760N	1.0	5.0	Trans.	-150	448	-150	980	F.S.	

(1) Cracked outside test section.

(2) Moment at first crack within test section.

(3) APT 749 contained two (2) thicknesses of HT-424 tape due to ablator being removed and replaced as a result of fabrication faults.

[redacted]

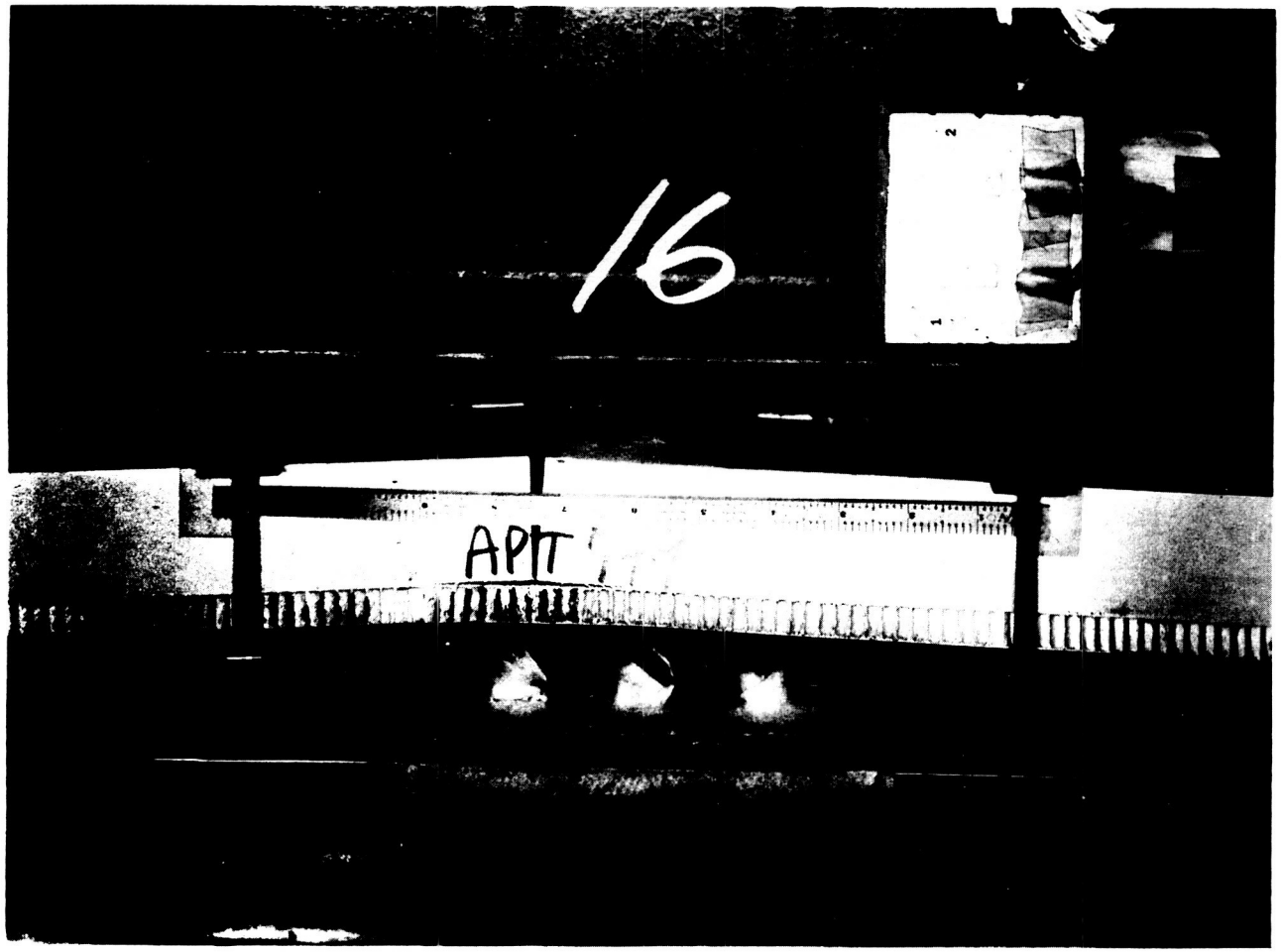

Figure 24 TYPICAL TEST BEAM AT THE COMPLETION OF A LOAD TEST
12742A

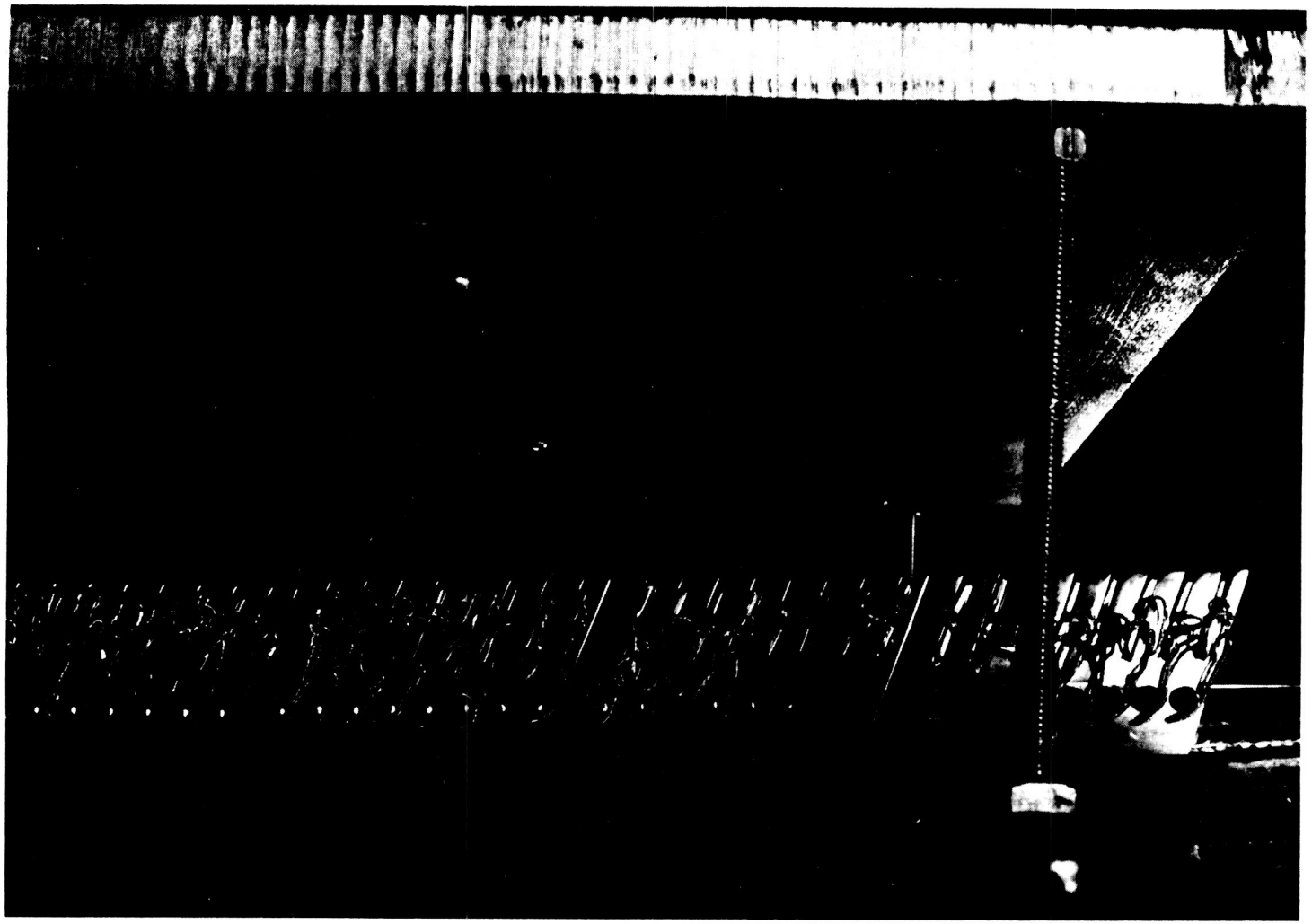

Figure 25 RADIANT HEATED TEST SET-UP FOR SPECIMENS APT 817 AND 817-1 (12741B)

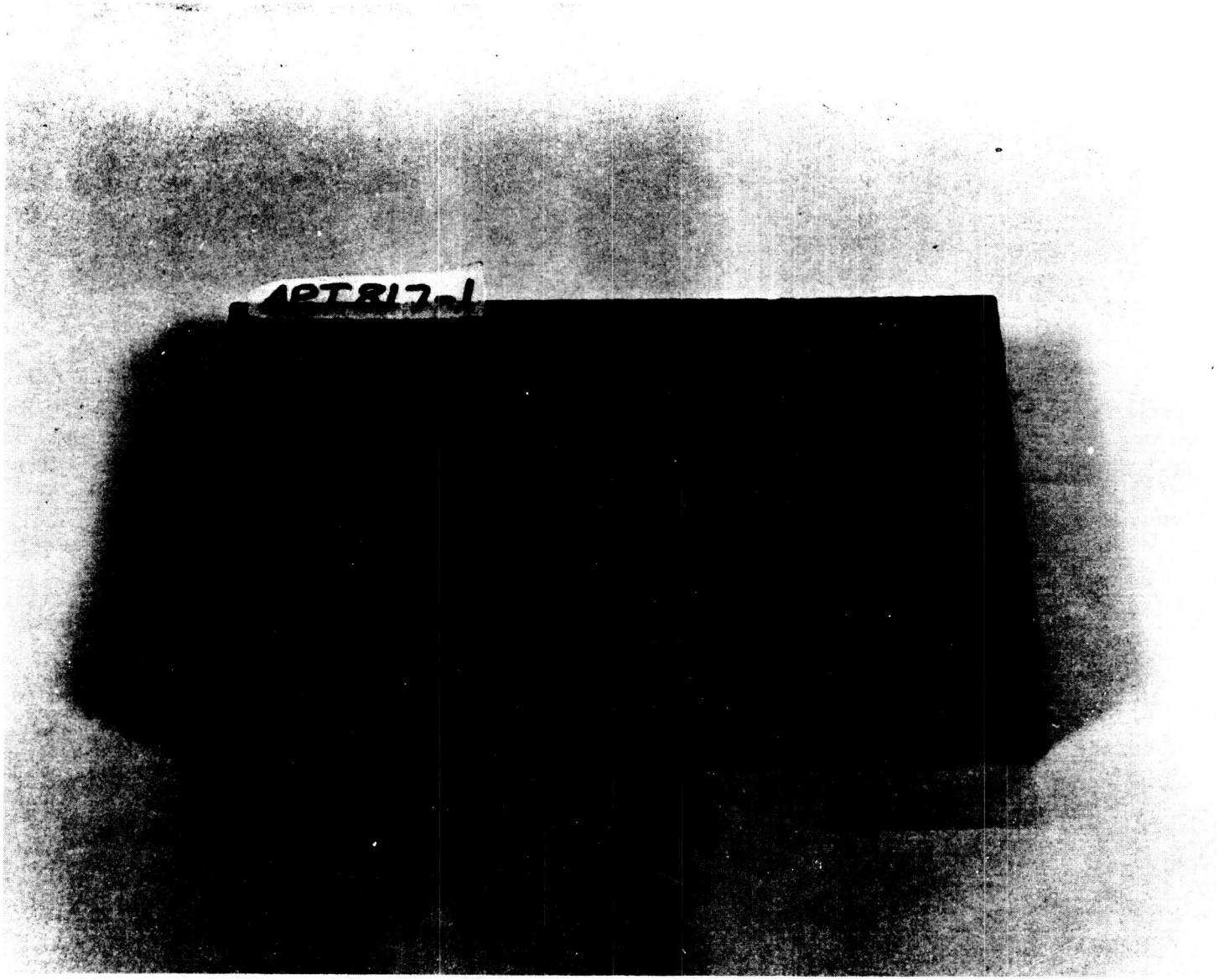

Figure 26 RADIANT HEATED TEST SPECIMEN APT 817-1 AFTER COMPLETION OF TESTING
12790A

c. q^* correlation: AP1816, material 5026-39/HC-G--two tests

d. Westinghouse Micarta, AP1848, material fiberglass-two tests

e. alternate shear-compression pad material AP1852--material RPD Asbestos phenolic--one test

Series AP1718, AP1816 and AP1720 have been completed and the test data reported herein.

The test data for the seven trajectory specimens will be reported in next month's report, when the reduction of the test data will have been completed for the entire series (AP1737). Thermocouple data is also in the process of being reduced.

Table II presents a summary of the ablation data for series AP1816, AP1720, AP1718, AP1826, AP1848, AP1852.

Series AP1718 consist of RTV material wrapped in fiberglass and mounted on a backplate. The following generalities may be made:

a. severe horizontal cracking occurred at the char layer

b. radial and axial expansion of the material made length loss measurements meaningless

c. expansion stresses were severe enough to cause both separation from the backplate and displacement from the fiberglass wrap, e.g., AP1718-6

d. all weight loss must be viewed with caution due to loss of surface char.

Figure 27 presents a typical pre-test specimen and figures 28 and 29 are post test photographs of four of the AP1718 RTV series.

Series AP1720 were specimens of fiberglass. Figure 30 is a typical pre-test specimen and figure 31 is a typical post test photograph. This program was cancelled prior to completion due to unsatisfactory performance of the material. As may be observed in the photograph, there was extreme separation of the laminates that often penetrated through to the back surface. These cracks were observed to occur during testing and to enlarge during cooling. The emissivities of samples -11, -13, and -15 appear low. Specimen -15 delaminated at a section which exposed the thermocouples; as a result the thermal data is very questionable and will be noted when it is reduced.

Series AP1816 was run to determine q^* heat of ablation characteristics for 5026-39/HC-G material. Figure 32 is a typical pre-test specimen and figure 33 is a typical post test photograph. A nominal heat flux of 100 Btu/ft2-sec was

requested over a wide enthalpy range. The maximum heat flux obtainable at low enthalpy condition was 80 Btu/ft^2-sec.

Series AP1848 pictured in figures 34 and 35 were tested to further evaluate the performance fiberglass (Westinghouse Micarta). The vertical cracks extending into the virgin material are portrayed in the cross section photograph (figure 35).

A second series, AP1852, was tested to evaluate an alternate material for the compression shear pad: RM41 RPD Asbestos phenolic with 37 percent resin. Figures 36 and 37 indicated that the vertical cracking has been greatly reduced, that the bond is still intact and that cracking does not extend into the virgin material.

Four specimens of 5026-39HCG (AF1807) have been tested with air as the working gas in the low enthalpy Model 500 Arc. These data are presently being reduced. The final data for the oxidation tests of 5026-39/HCG (AP1750) are presented. These tests were conducted at a low level of heat flux and enthalpy to determine the effects of the different gases on the material performance and to try to further understand the ablation mechanism.

All of the test conditions and results for the oxidation tests carried out with argon, nitrogen, and air as the working gases are presented on table I. These tests were conducted at heat fluxes ($\dot{q}_c$) and gas enthalpies (H) as similar as possible to determine the effects of the different gases on the ablation behavior of the 5026-39/HCG material (AP1750). In all tests with the different gases it was observed that the resin degraded and the silica melted, flowed, and was blown off the sides of the specimen. The specimens tested with argon is shown in figure 38.

The tested surface of all the specimens was examined with a microscope and the following peculiarities were noticed.

1. The surface of the ones tested with nitrogen did not reach as high a temperature as those tested with the other two gases.

2. There were bluish streaks or marks in the char layers and on the surfaces of the specimens tested with argon and nitrogen. The char layers on these specimens were thicker than the ones on the specimens tested in air, but there was no indication of the bluish marks on the specimens tested in air.

Except for these two peculiarities the surface of the specimens tested with the different gases appeared the same.

[redacted]

TABLE II

OVERS ABLATION DATA

Sample No.	Run No.	Density	$\dot{m}_{gas}$ x 10^{-3}	P_{impact}	Btu/lb H x 10^3	Btu/ft^{2}sec $Q_{conv.}$	Time (sec)	L (inches)	W (gms)	Surface Temp. (°K) Corr.	Watts/cm^2	Emissivity
AP1816-13*	586-7	0.491	7.0×10^{-3}	11.2	5.10	80	120	0.15	38.5	1860	49	0.71
-14	586-8	0.491	7.0	11.2	5.1	80	240	0.27	46.1	1860	43	0.63
-15	571-16	0.493	6.2	--	4.8	91	300	0.35	56.7	--	55	--
-10	564-10	0.504	3.6	7.4	7.5	97	120	0.19	34.4	1970	65	0.76
-11	564-6	0.504	3.2	6.8	7.4	97	240	0.34	33.0	1940	54	0.66
-9	564-5	0.506	3.2	--	7.3	94	300	0.41	42.4	1960	64	0.76
-12	562-7	0.506	2.0		10.6	103	120	0.15	20.5	1960	64	0.77
-5	562-6	0.509	2.0		10.6	103	240	0.31	33.1	2010	66	0.71
-7	562-8	0.509	2.0		10.6	105	300	0.38	37.0	1960	63	0.75
-3	563-9	0.510	1.6		13.2	102	120	0.15	22.4	2040	68	0.69
-6	563-7**	0.511	1.6		13.5	100	240	0.36	34.7	1970	71	0.83
-8	563-6	0.512	1.6		13.5	104	300	0.34	41.9	1985	57	0.65
-2	571-20	0.513	1.1		18.0	106	120	0.12	30.0	1900	55	0.74
-4	571-20	0.513	1.1		18.0	106	240	0.24	39.4	1890	55	0.75
-1	571-18	0.514	1.2		18.8	106	300	0.32	41.7	1975	67	0.77
*Average ϵ_{avg} = 0.75 used for correcting surface brightness temperatures.												
**Voltage varied during test; therefore, all ablation and aerodynamic data should be viewed with caution.												
AP1720-4*	565-21	1.846	6.0	10.7	5.4	99	180	N/A	41.2	1850	57	0.85
-9	565-20	1.847	5.7	9.9	5.3	99	300	N/A	61.4	1825	49	0.77
-14	564-14	1.848	4.0	8.5	6.8	93	60	N/A	17.8	1750	40	0.75
-18	564-13	1.848	4.0	8.5	7.2	93	180	N/A	31.6	1785	48	0.83
-16	564-12	1.849	4.0	8.5	7.0	96	300	N/A	49.5	1795	48	0.82
-11	569-25	1.851	1.5	5.6	11.5	100	60	N/A	10.5	1926	48	0.62
-13	569-24	1.851	1.5	4.6	11.8	100	180	N/A	25.3	1870	45	0.64
-15	565-6	1.853	1.2		11.5	61	200	N/A	19.0	1605	21	0.55
*Average ϵ_{avg} = 0.70 used for correcting surface brightness temperature.												
AP1718-5*	556-7	1.428	1.1		18.2	100	180	N/A	--	1960	70	0.83
-11	556-6	1.430	1.1		18.0	100	310	N/A	--	1990	69	0.77
-2	555-10	1.431	1.1		18.2	105	300	N/A	--	1940	61	0.76
-12	573-7	1.432	5.0	8.4	4.8	21	180	N/A	14.7	1455	22	0.87
-1	573-8	1.433	5.0	8.4	5.4	22	300	N/A	--	1565	24	0.72
-14	573-9	1.434	5.0	9.1	5.6	20	420	N/A	36.1	1525	27	0.87
-10	565-9	1.436	2.0	6.6	10.3	100	180	N/A	28.0	1955	57	0.69
-13	565-10	1.436	1.3	5.8	10.3	100	300	N/A	33.7	1920	50	0.65
-9	580-16	1.435	1.5	6.4	10.5	101	420	N/A	--	1850	64	0.96
-3	565-15	1.436	1.1		10.8	61	180	N/A	--	1660	29	0.68
-6	565-17	1.436	1.2	4.5	10.6	61	300	N/A	--	1710	37	0.77
-8	580-18	1.436	1.2	4.1	9.9	60	420	N/A	--	1720	45	0.91
-4	571-12	1.437	0.6	--	10.1	20	167	N/A	11.0	1475	12	0.46
-15	571-12	1.439	0.6	--	10.1	20	300	N/A	13.7	1370	12	0.61
-7	580-20	1.441	0.6		10.5	20	420	N/A	--	1395	17	0.79
*Average ϵ_{avg} = 0.75 used in correcting surface brightness temperatures.												
AP1826-1	558-16		1.1	4.2	10.0	60	200	0.004	34.6	1540	29	0.91
AP1848-1*	579-4		1.3	4.7	10.9	61	200			1435*	--	--
-2	579-5		1.3	6.0	10.4	56	200			1435*	--	--
*Average ϵ = 0.70 used for correcting surface brightness temperatures.												
AP1852-1	583-23		1.1	4.4	10.8	65	200			--	--	--

Figure 27 TYPICAL SPECIMEN, AP 1718, RTV-560
12426B

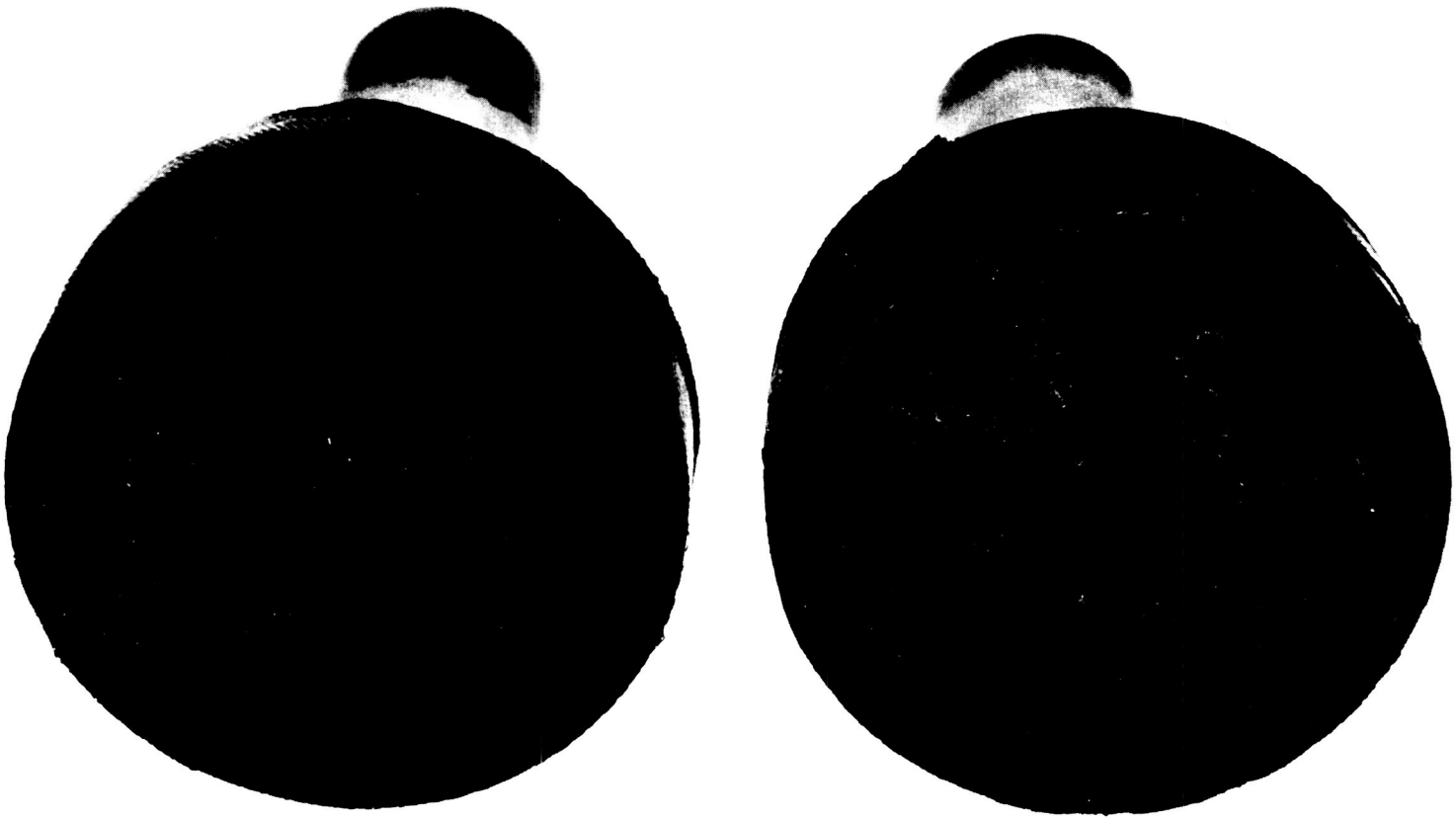

Figure 28 RTV-560 MATERIAL, AP 1718-4 AND 1718-15
12781H

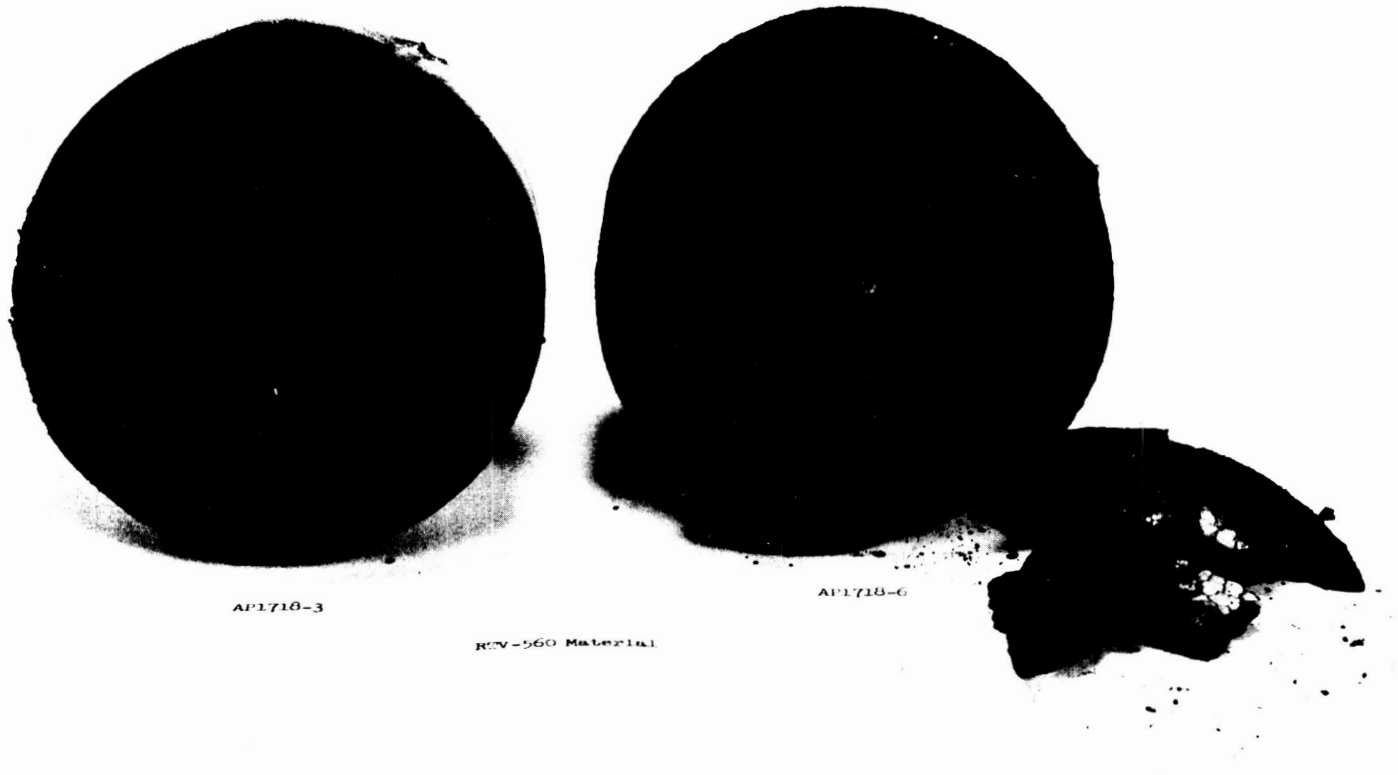

Figure 29 RTV-MATERIAL, AP 1718-3 AND AP 1718-6
12583U

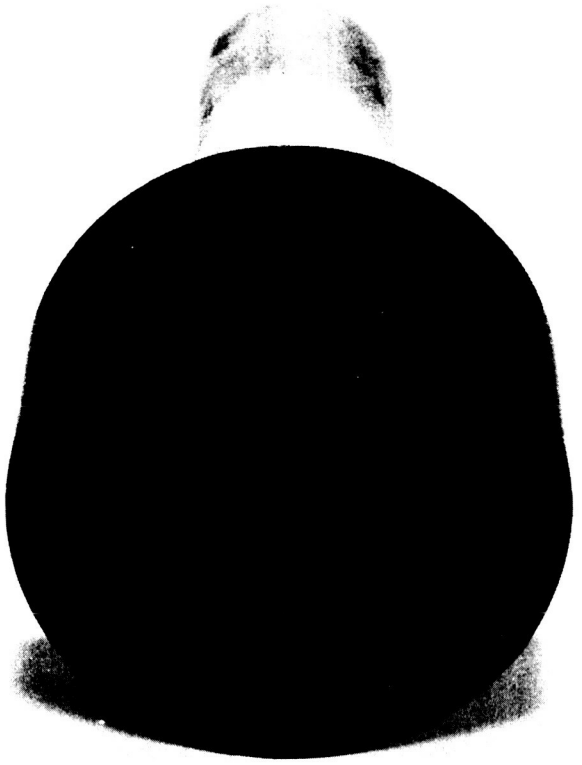

Figure 30 SCP F/G MATERIAL, TYPICAL SPECIMEN AP 1720
12583H

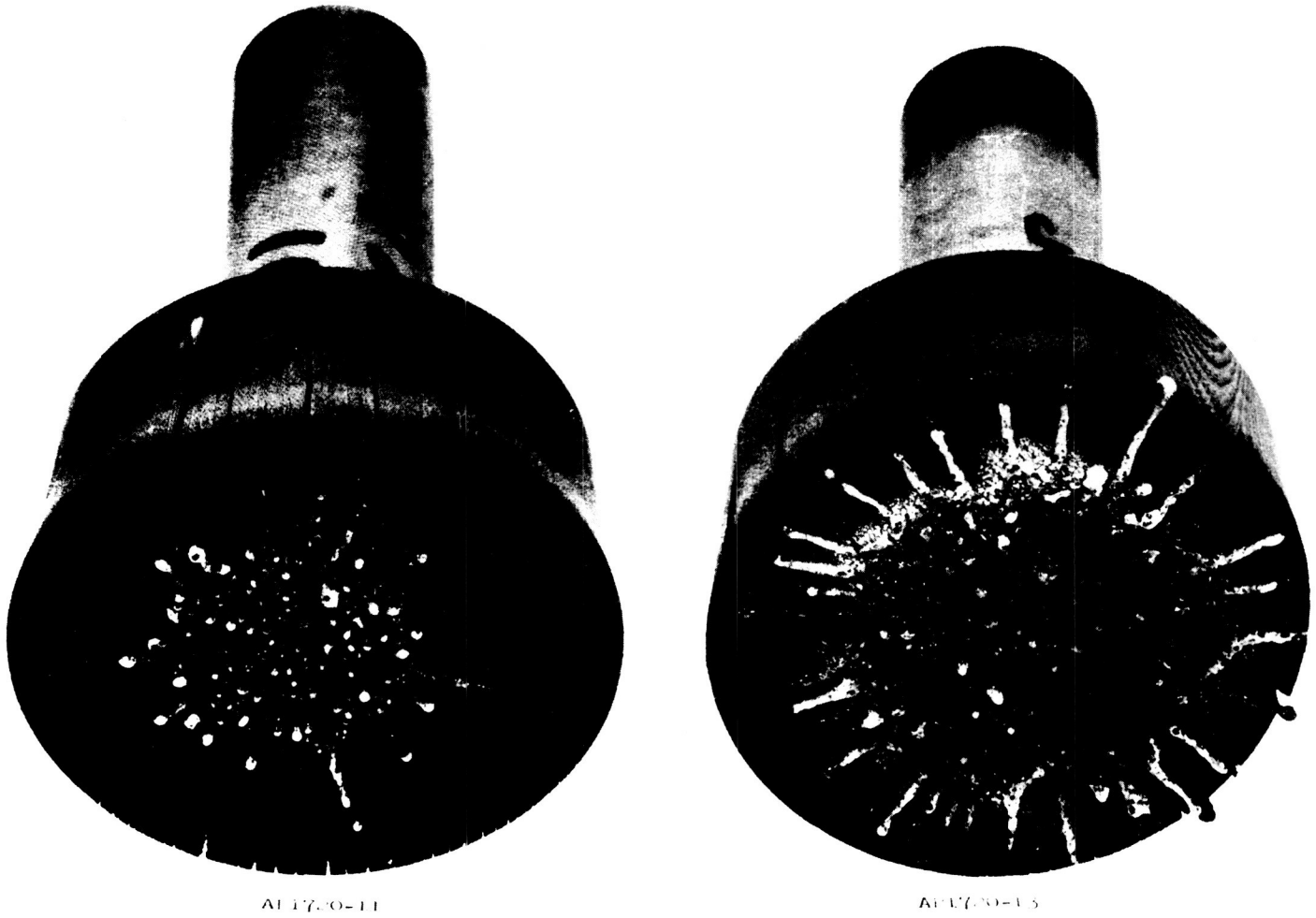

AP 1720-11

AP 1720-13

Figure 31 F/G MATERIAL, AP 1720-11 AND AP 1720-13
12781C

Figure 32 TYPICAL SPECIMEN, AP 1816, 5026-39/HCG
12426J

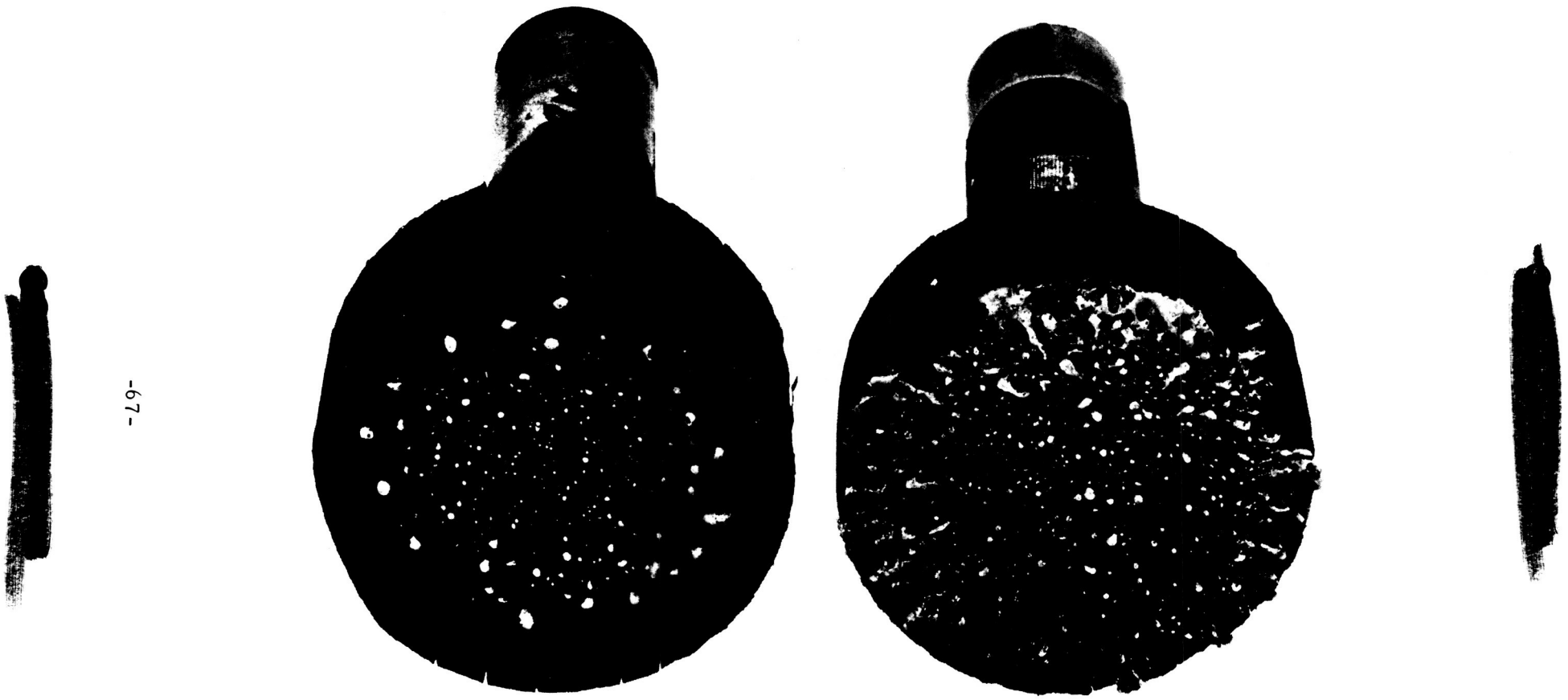

AP1816-4 AP1816-15

Figure 33 5026-39/HC-G MATERIAL, AP 1816-4 AND AP 1816-15
12781D

[redacted]

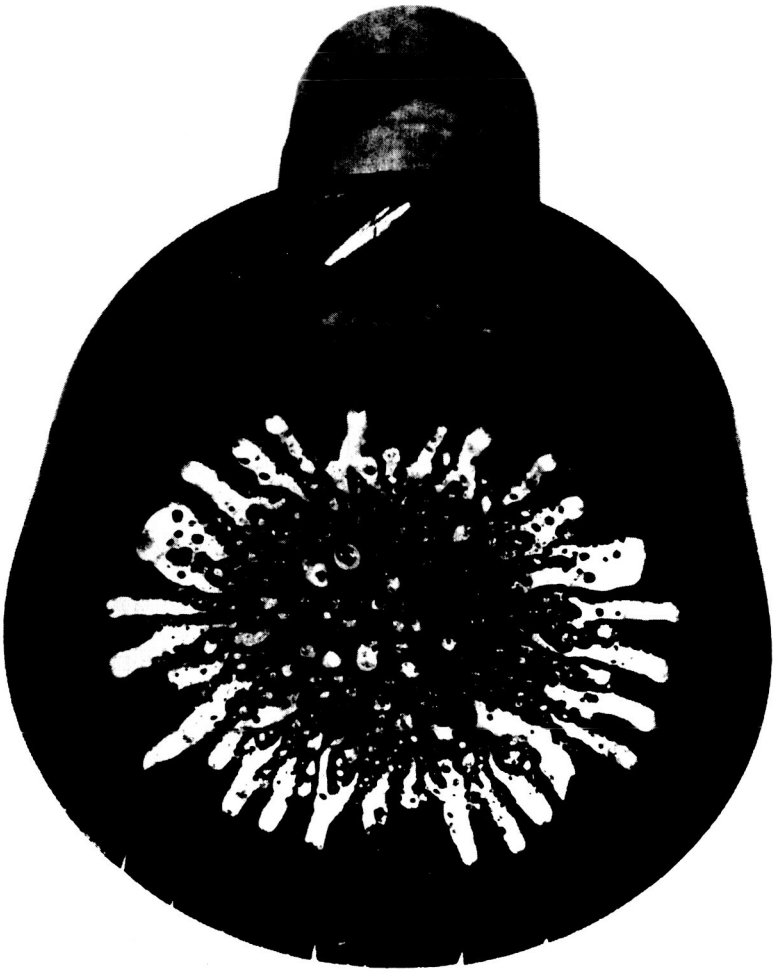

AP1848-1

Figure 34 AP 1814-1, MATERIAL: F/G
12744B

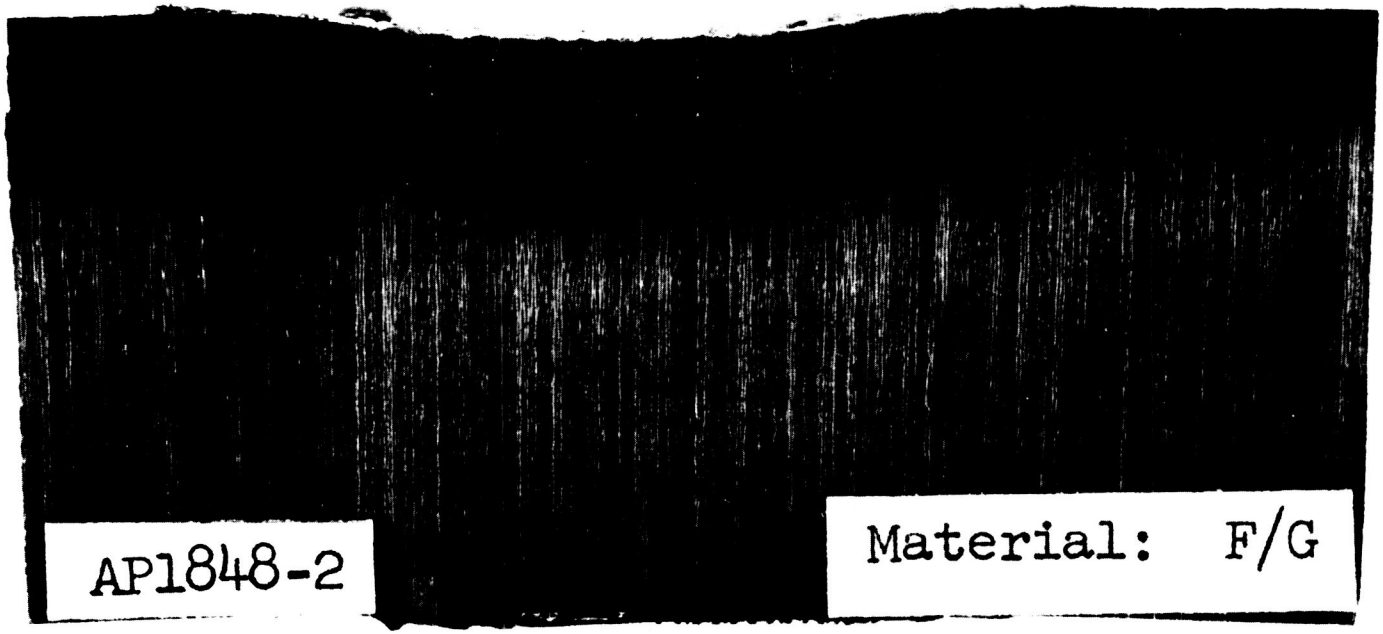

Figure 35 AP 148-2, MATERIAL: F/G
12744C

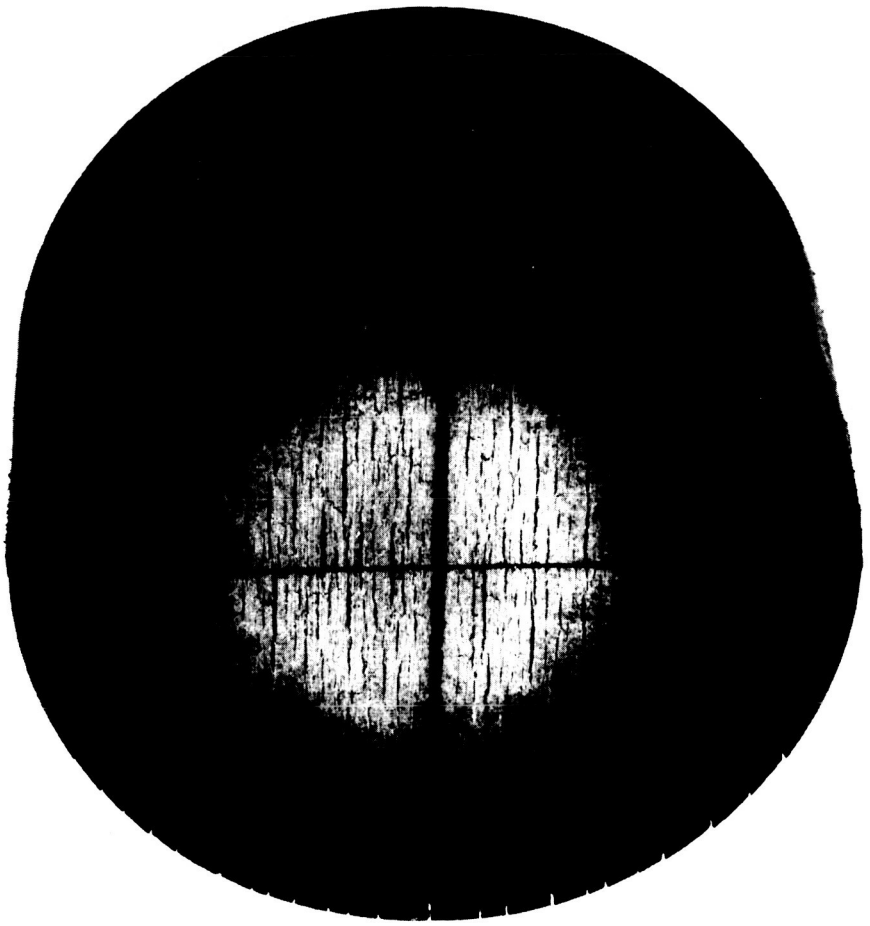

Figure 36 AP 1852-1
12781L

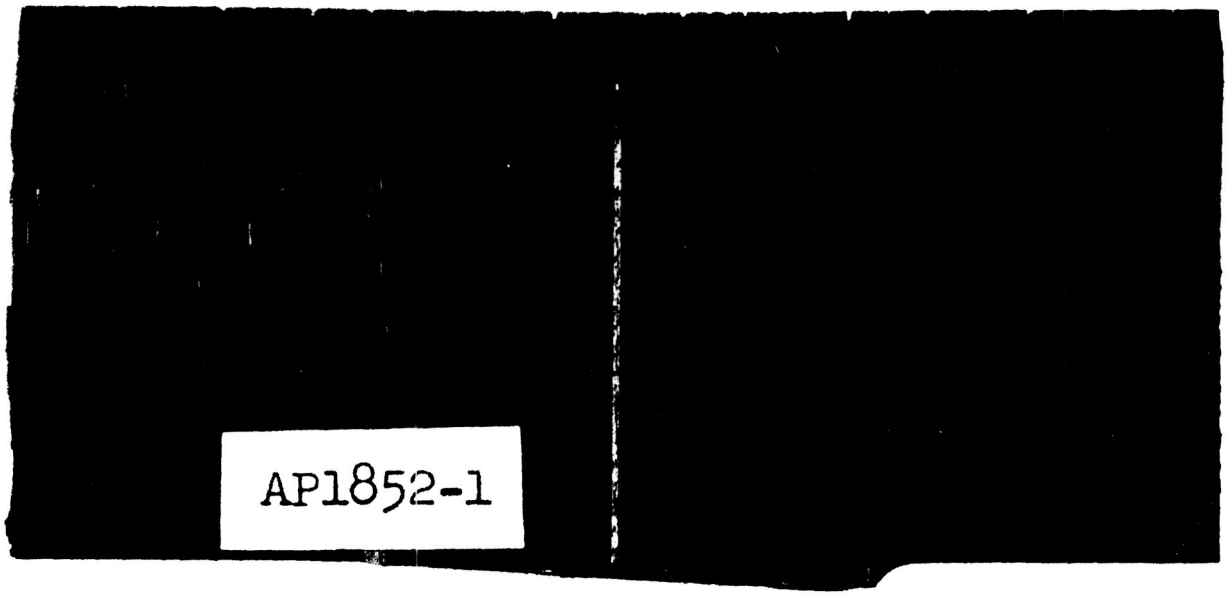

Figure 37 AP 1852-1
12781N

No.	16	5	1	8	18	7	4
$H(Btu/lb)$	702	843	866	887	1008	1082	1317
$q_c(Btu/ft^2 sec)$	182	173	163	127	182	190	195

Figure 38 5026-39HCG SPECIMENS TESTED WITH ARGON
12581A

[redacted]

The char depths (ΔX_c) of the specimens were measured with a measuring microscope. The specimens tested with air had the thinnest char layer, those tested with argon were thicker (2-3 times those tested in air), and the ones tested with nitrogen were about a factor of 10 thicker than those tested in air (see table I). A higher surface temperature (T_T) was exhibited by the argon tested specimens.

At the constant heat flux and enthalpy conditions, the ablative rates (V) of the specimens tested with air were about three times higher than those tested with nitrogen and argon (neglecting the scatter in the data). The oxygen in the air combined with the carbon on the char surface causing a faster recession rate and thinner char layer. These recession rates were measured from silhouette movies taken at one (1) frame per second.

Although the surface eroded at different rates and had varying char thicknesses, the average total emittance (ϵ_T) of the specimens tested with argon and nitrogen were the same (~ 0.7) and higher than the average value for the air tested specimens (~ 0.6). The specimens tested with air generally had radiation values equivalent to the values of those tested with nitrogen and surface temperature values between the ones tested in argon and nitrogen.

The thermochemical (q^*) and cold wall heat of ablation (q_c^*) results are presented in table III. Other data are presented in table III; they are air flow ($\dot{m}$), stagnation pressure (P_s), the length loss of the specimen ($\Delta \ell$), and the time of each run (t).

The 20°C/min test of honeycomb material performed on the differential scan calorimeter has been completed and the data has been reduced. It is presently undergoing analysis. In addition, a 10°C/min run has been performed and a 5°C/min test is in progress.

A test run was made on an Armco Iron Standard material in the high temperature radial conductivity apparatus with excellent correlation being achieved with lower power level measurements. This test reaffirms the previous calibration with greater confidence being given to subsequent measurements.

Three materials were tested for thermal conductivity from - 260°F to 600°F, as part of a study to determine the effect of cell orientation on conductivity. (Heat flow normal to cell axis symmetry).

Forty-eight samples of 5026-39/HC-G were exposed to thermal radiation in the solar furnace. The information obtained from these exposures are shown in figure 39 through 46. The recession rates of individual samples of 5026-39HC-G at five different flux levels are shown in figures 39 through 43 whereas figures 44 through 46 show the effect of incident radiant flux on recession rate, surface temperature and surface reradiation, respectively.

[redacted]

TABLE III

TEST CONDITIONS AND RESULTS OF OXIDATION TESTS OF 5026-39/HCG (AP1750)

Specimen 5026-39/HCG	Gas	H (Btu/lb)	$\dot{q}_c$ (Btu/ft^{2}sec)	$\dot{m}$ (lb/sec)	P_s (Atm)	$\dot{V}$ (in/sec)	q_r (Btu/ft^{2}sec)	T (T_R)	ϵ_T	ΔX_o (in)	q^* (Btu/lb)	q_c^* (Btu/lb)	Δl (in)	t (sec)
16	Argon	702	182	25.2×10^{-3}	1.35	0.0129	74.8	3680	0.80	0.079	--	5330	0.388	30.00
5	Mol. wt. = 40	843	173	17.2	1.20	0.0086	77.5	3930	0.70	0.102	160	8140	0.244	30.10
1	Mol. wt. = 40	866	163	17.2	1.22	0.0115	72.0	3935	0.65	0.099	219	5590	0.331	30.00
8	Mol. wt. = 40	887	127	5.4	1.04	0.0034	52.5	3610	0.65	0.126	1700	12,550	0.114	29.95
18	Mol. wt. = 40	1008	182	17.1	1.24	0.0125	79.9	3980	0.70	0.061	633	5720	0.361	30.00
7	Mol. wt. = 40	1082	190	14.0	1.19	0.0128	80.2	4055	0.65	0.077	845	5770	0.371	30.00
4	Mol. wt. = 40	1317	195	9.1	1.12	0.0089	79.9	3895	0.75	0.092	2040	8240	0.268	30.10
15	Air	951	155	34.4	1.52	0.0373	28.3	3270	0.51	0.036	-167	1593	0.369	10.50
9	Mol. wt. = 28.97	1003	175	36.7	1.64	0.0360	51.1	3540	0.68	0.021	-455	1811	0.331	8.50
3	Mol. wt. = 28.97	1070	168	32.3	1.51	0.0619	53.1	3760	0.56	0.029	-302	1069	0.975	15.90
10	Mol. wt. = 28.97	1147	201	28.6	1.41	0.0334	45.5	3520	0.62	0.026	-116	2257	0.329	10.30
12	Mol. wt. = 28.97	1596	180	19.0	1.18	0.0324	81.9	4150	0.58	0.046	-396	2158	0.388	15.90
2	Nitrogen	849	122	33.5	1.43	0.0013	25.6	2750	0.94	0.219	-1502	35,083	0.018	31.30
17	Mol. wt. = 28.00	1059	183	42.0	1.78	0.0107	32.0	3130	0.70	0.222	320	6416	0.075	16.60
19	Mol. wt. = 28.00	1080	158	31.7	1.43	0.0081	35.8	3170	0.74	0.358	16	7407	0.194	30.00
14	Mol. wt. = 28.00	1125	176	35.0	1.63	0.0183	45.5	3400	0.71	0.344	-259	3847	0.361	30.05
13	Mol. wt. = 28.00	1267	174	29.4	1.46	0.0247	73.0	3980	0.61	0.191	-773	2658	0.471	30.10
11	Mol. wt. = 28.00	1831	190	18.7	1.22	0.0088	113.0	4400	0.63	0.197	-2303	8097	0.225	29.90

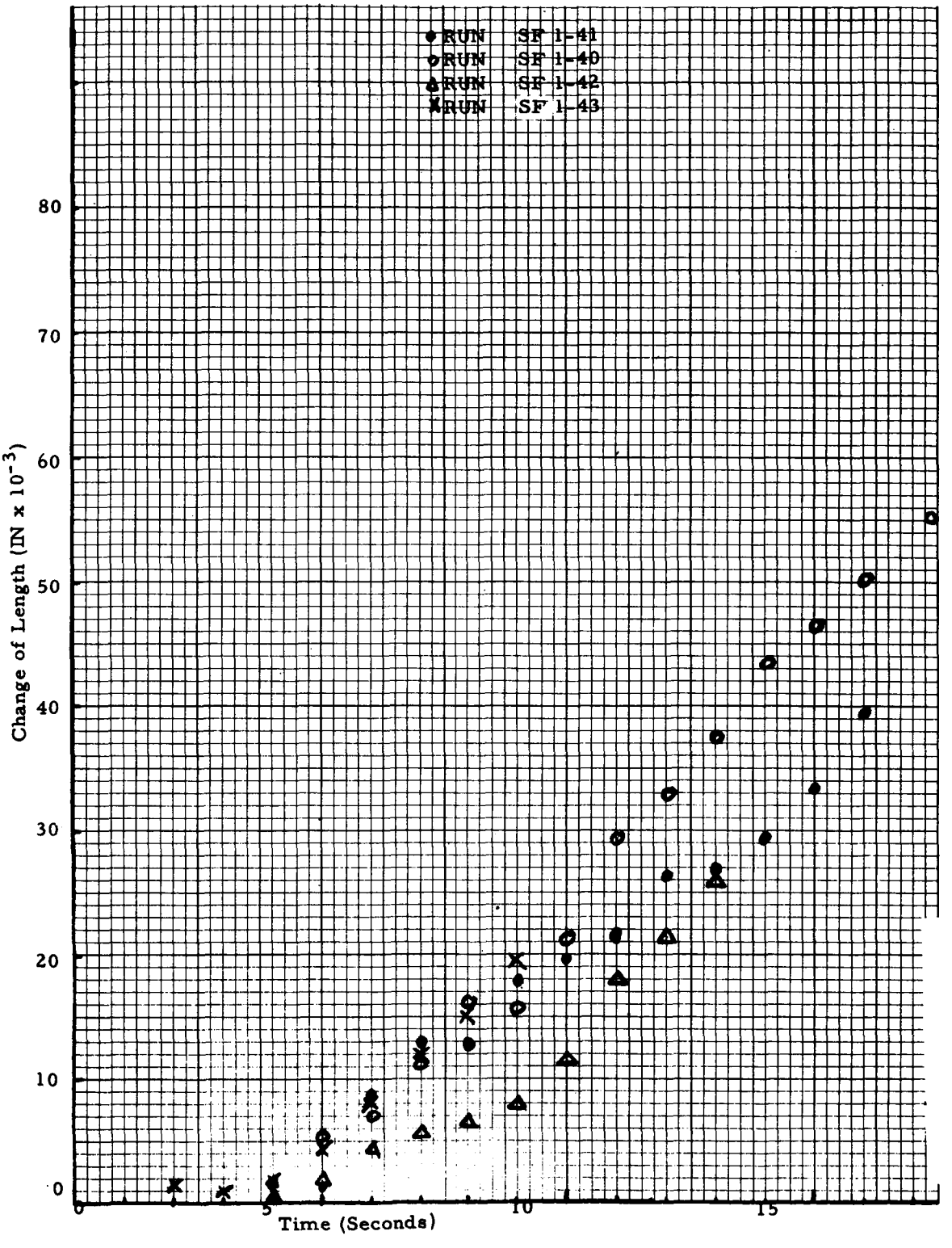

Figure 39 ABLATION OF 5026-39 H/CG UNDER RADIANT FLUX OF 200 BTU/ FT^2 SEC

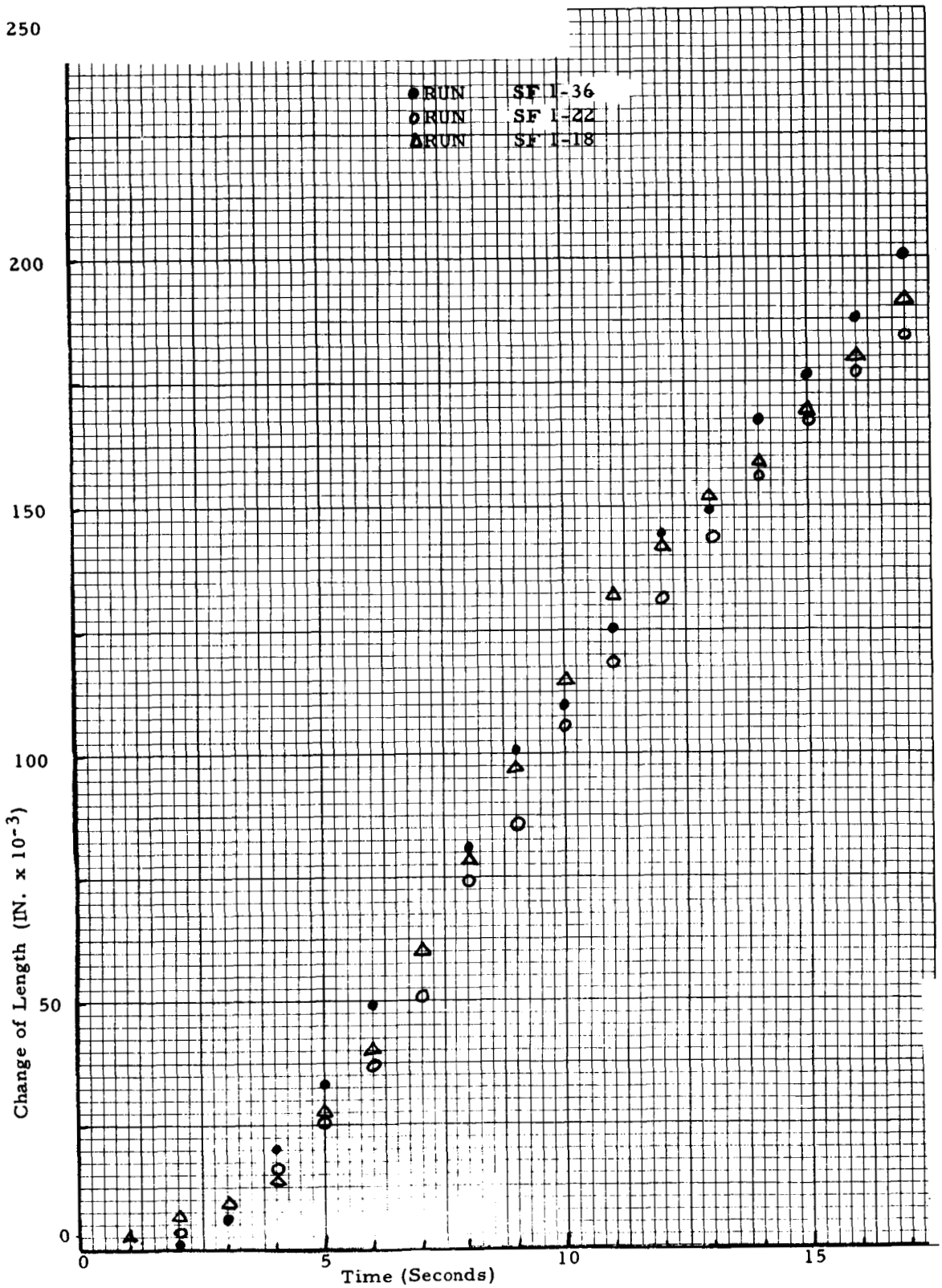

Figure 40 ABLATION OF 5026-39 H/CG UNDER RADIANT FLUX OF 500 BTU/ FT^2 SEC

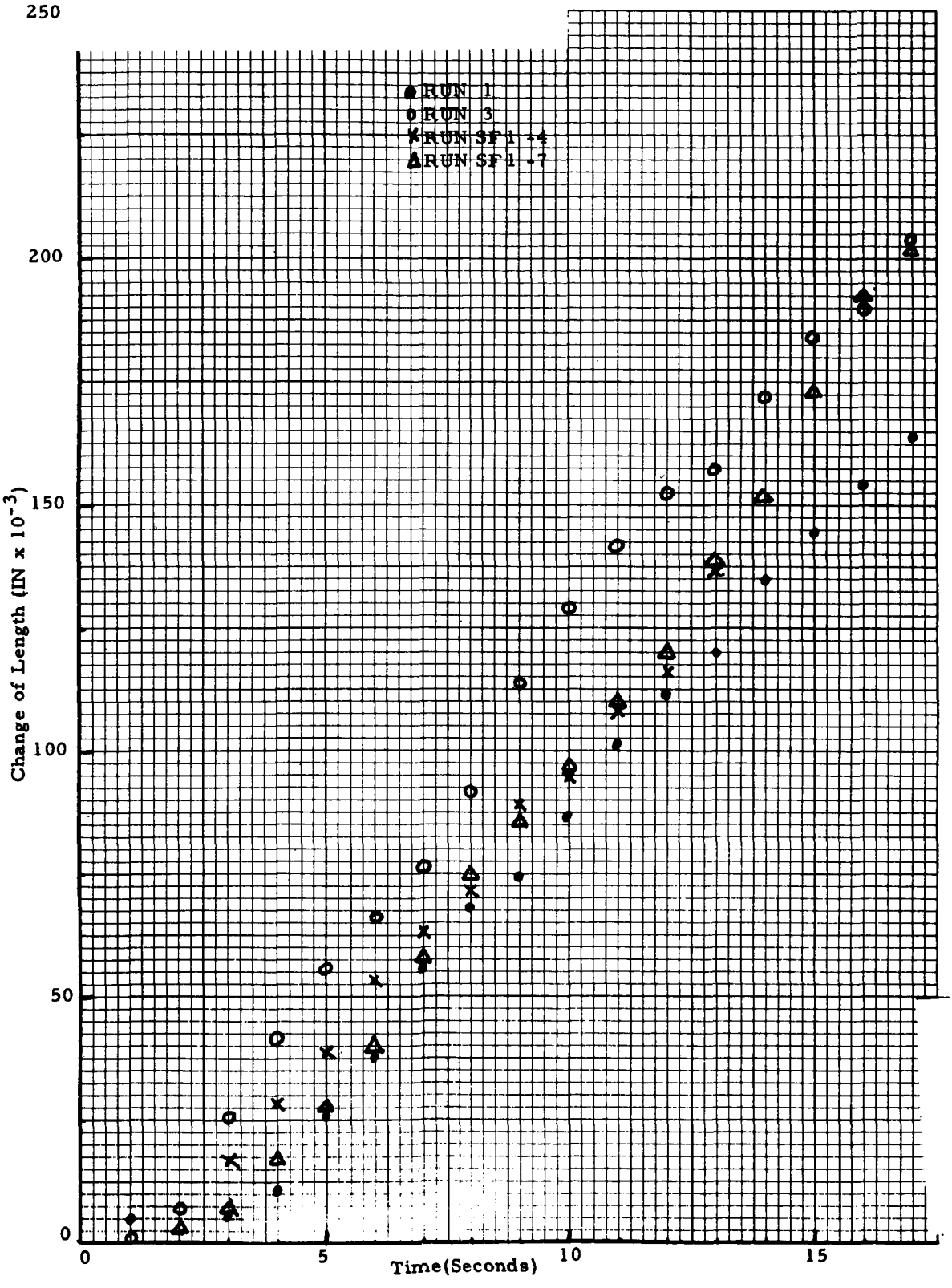

Figure 41 ABLATION OF 5026-39 H/CG UNDER RADIANT FLUX OF 575 BTU/ FT^2 SEC

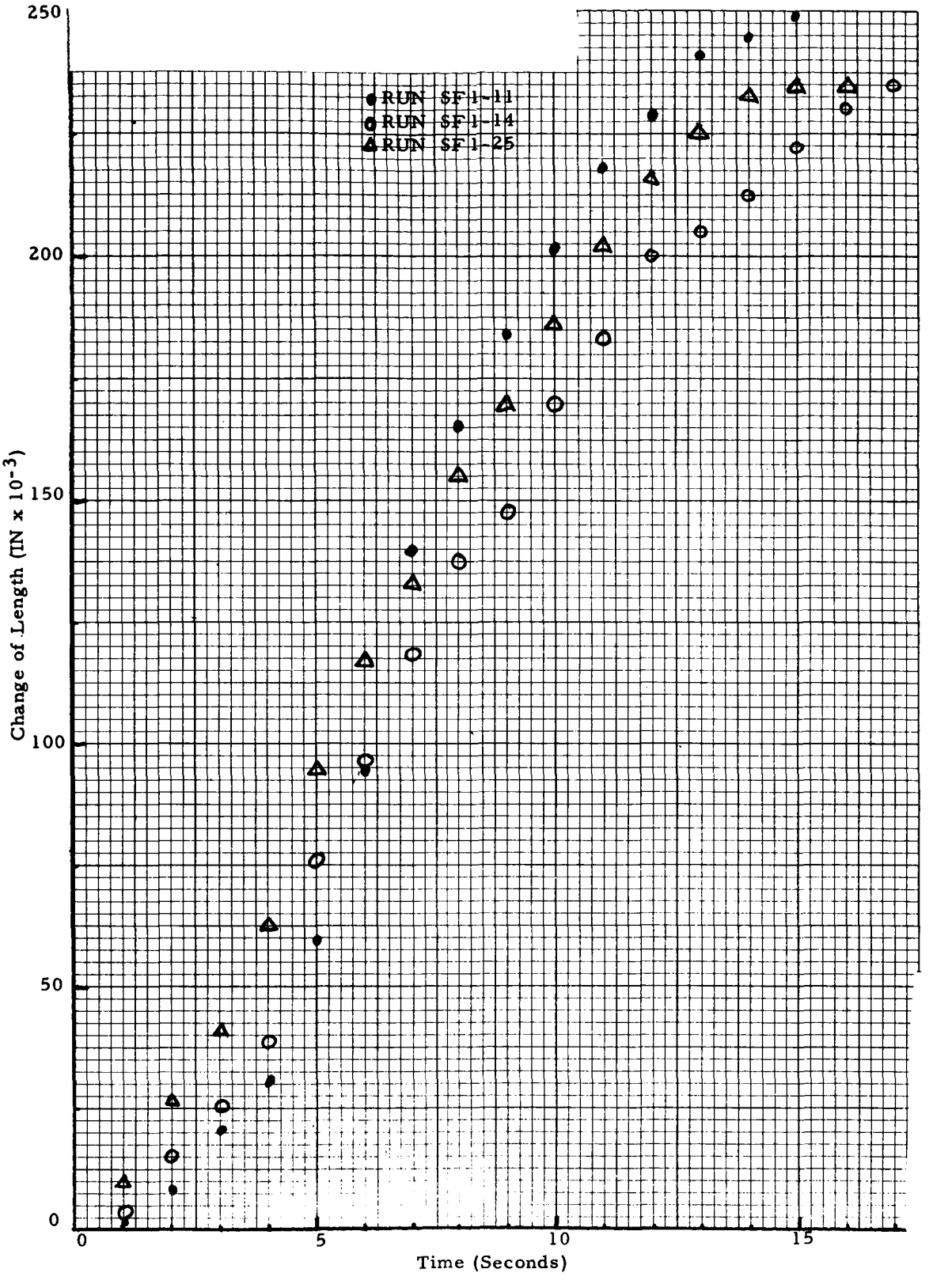

Figure 42 ABLATION OF 5026-39 H/CG UNDER RADIANT FLUX OF 800 BTU/ FT^2 SEC

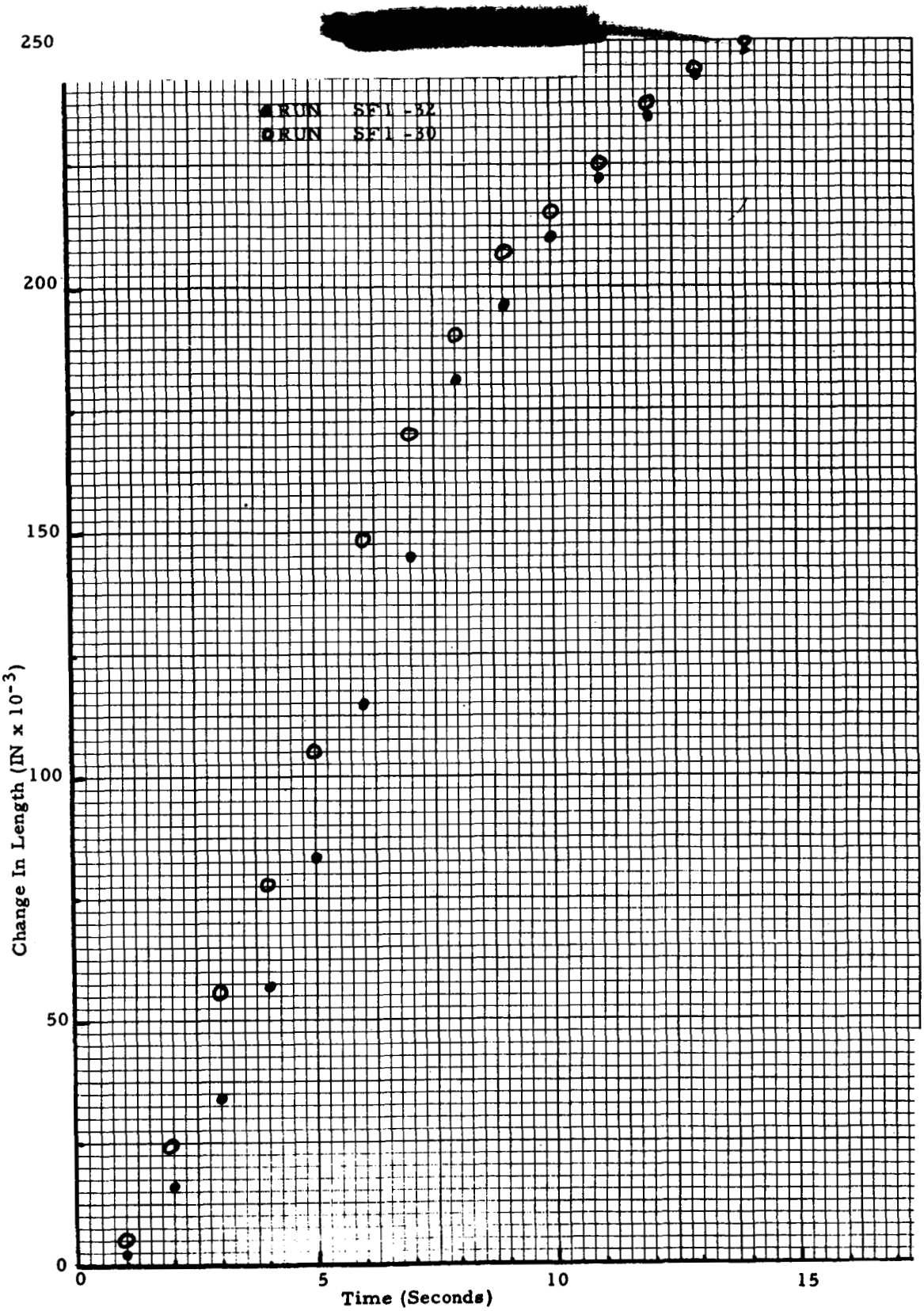

Figure 43 ABLATION OF 5026 [illegible]/CG UNDER RADIANT FLUX OF 1100 BTU/ FT^2 SEC

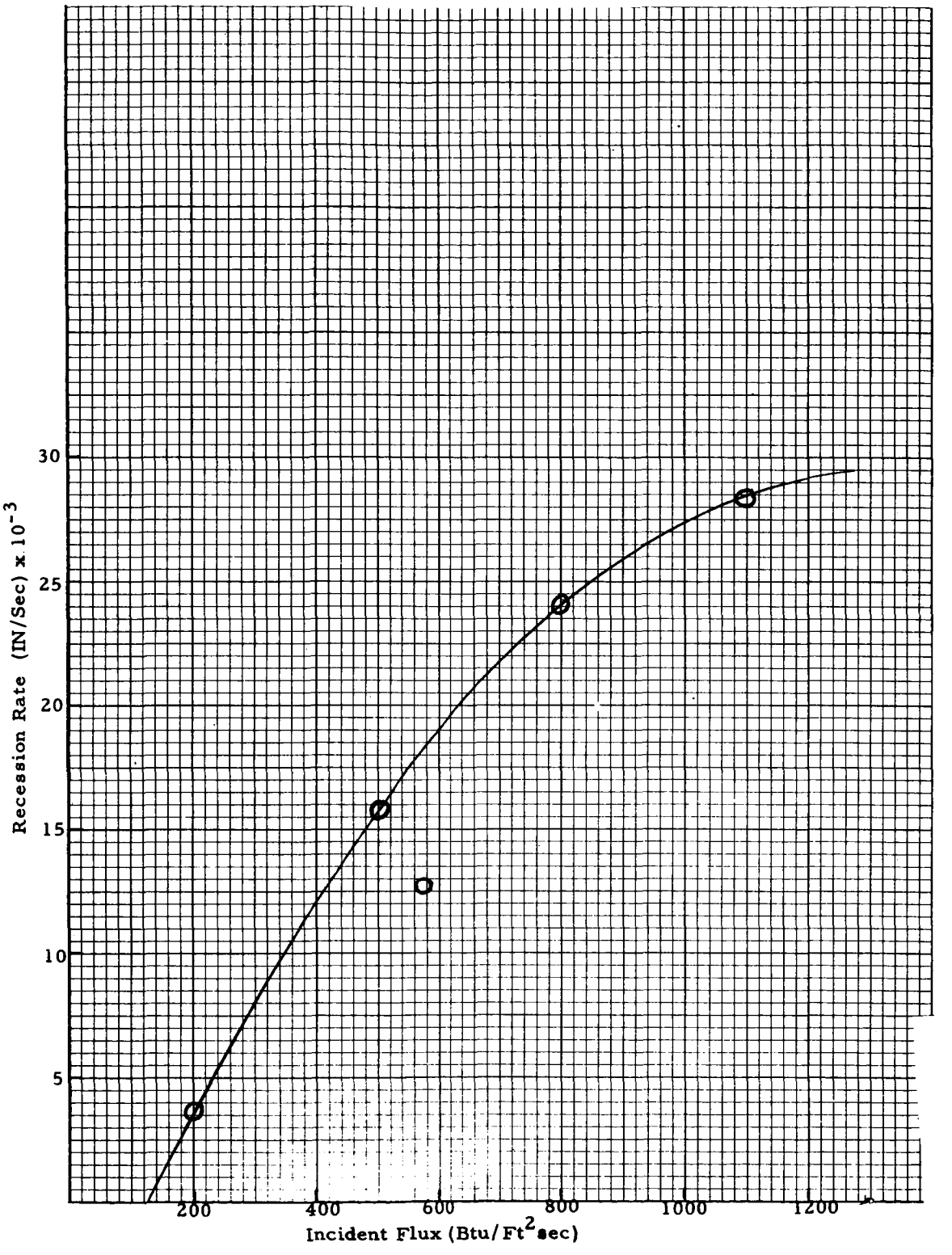

Figure 44 RECESSION RATE AS A FUNCTION OF INCIDENT RADIANT HEAT

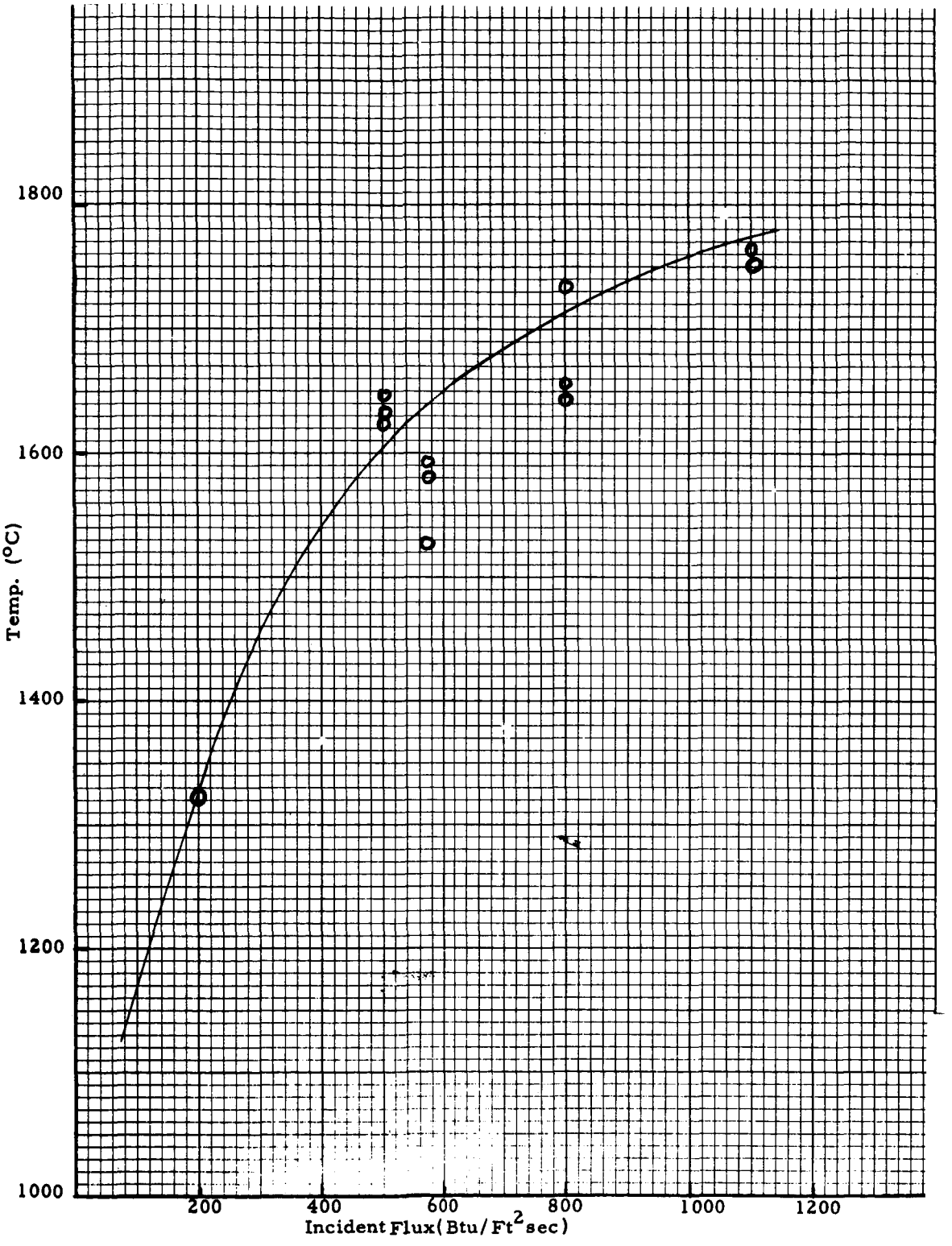

Figure 45 SURFACE TEMPERATURE OF 5026-39 H/CG AS A FUNCTION OF INCIDENT RADIANT HEAT

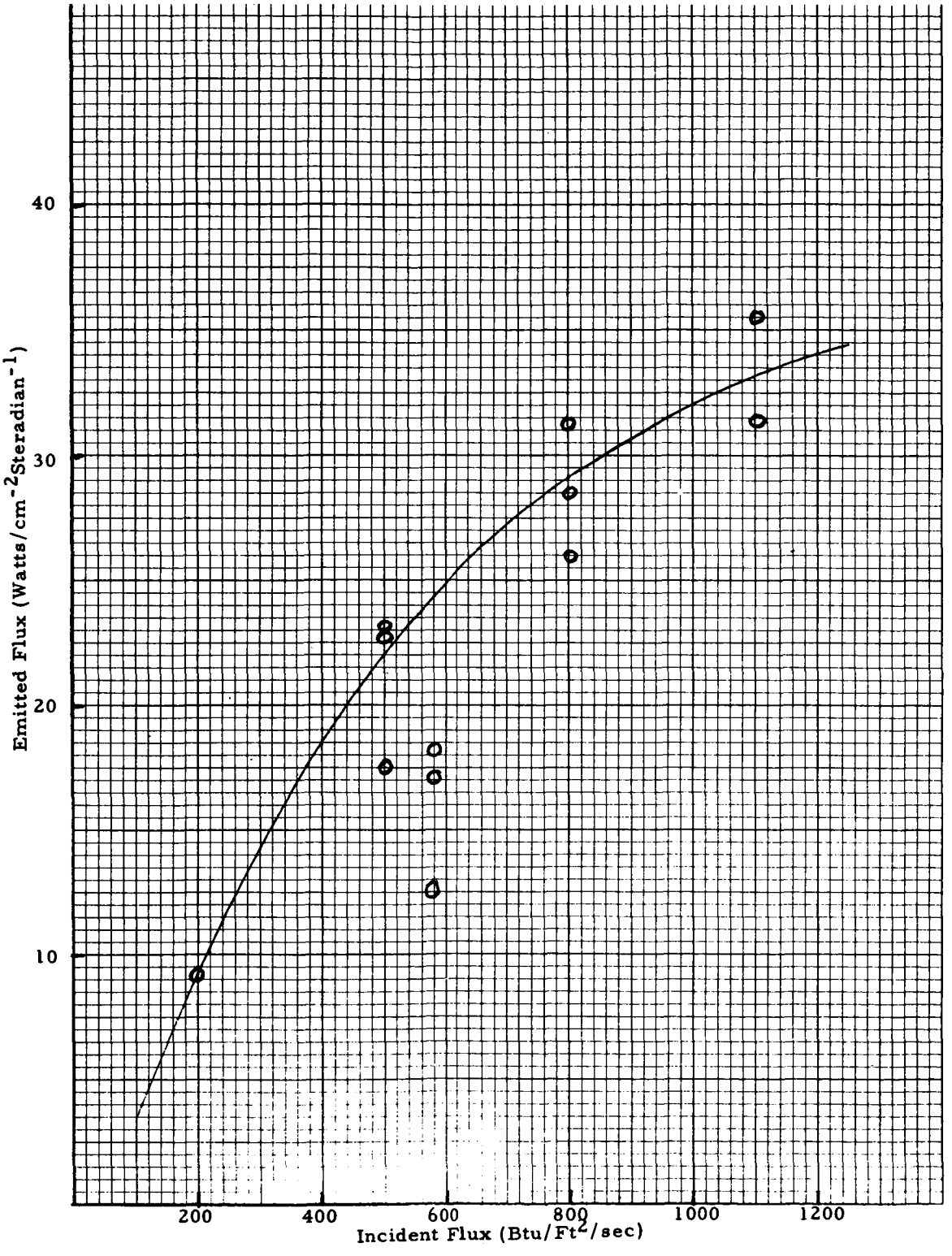

Figure 46 RADIATED FLUX EMITTED BY 5026-39 H/CG AS A FUNCTION OF INCIDENT RADIANT HEAT

Test No.	A. P. No.	Material	Density	K	Temp°F
537	1818-2	5026-39/HC-G (1)	32.73	0.010	-260
				0.063	250
				0.069	600
541	1818-4	5026-39/HC-G (1)	32.4_9	0.01_0	-260
				0.05_9	250
				0.06_4	600
542	1818-3	5026-39/HC-G (1)	32.7_6	0.01_0	-260
				0.06_0	250
				0.06_6	600

Note: Density units are in lbm/ft^3
K units are in Btu/hr-ft-°F

The recession rates of 5026-39/HC-G were determined from motion pictures of the specimen during exposure.

The surface temperature of 5026-39/HC-G was determined from measurements with a radiation pyrometer sensitive to radiation between 0.75 and 0.85 μ. The flux radiated by the ablating surface was measured with a thermistor bolometer sensitive to radiation between 0.2 and 15 μ. In both the surface temperature and emission measurements a rotating sector[2] was used to separate the emitted and reflected radiation. The apparent anomalies, i.e. the inversion of the recession rate, emission and surface temperature between incident flux levels of 500 and 575 Btu/ft^2sec and the excessive reradiation at the higher flux levels require additional study.

Hemispherical emittance measurements were made using the 14 inch, liquid nitrogen cooled sphere, at pressures less than 10^{-4} mm/Hg.

The hemispherical emittance of 5026-39/HC-G, pre-charred at 2000°F, has been measured to be 0.91 at 1425°F.

[2]Laszlo, T.S., R.E. Gannon, and P.J. Sheehan, "Emittance Measurement Above 2000°C" J. Solar Energy, Vol. 8, No. 4, December 1964.

[redacted]

II. MANUFACTURING

Application of the ablative heat shield to AFRM 006 has been largely completed, but in several cases, extensive repairs are still in process. Ablator has been gunned into the honeycomb of the nosecap and forward compartments of AFRM 009, and gunning is about to begin on the crew compartment. The aft compartment of this vehicle was returned to NAA/S&ID for structural modification. Current status of each compartment of each vehicle is as shown below:

Operation	AFRM 006 COMPARTMENT			
	Nosecap	Forward	Crew	Aft
Weight and C.G. Determination	complete	complete	complete	complete
X-Ray	complete	complete	complete	complete
Dimensional Inspection	complete	complete	complete	complete
Edgemember and Honeycomb Prefit	complete	complete	complete	complete
Cleaning and Priming Substructure	complete	complete	complete	complete
Bonding of Edgemembers and Honeycomb	complete	complete	complete	complete
Contour Machining of Honeycomb	complete	complete	complete	complete
Inspection of Honeycomb Bond	complete	complete	complete	complete
Repair of Defective Bond Areas	complete	complete	complete	complete
Gunning of 5026-39 Ablator	complete	complete	complete	complete
Cure and Postcure	complete	complete	complete	complete
Installation of Bolt Plug Housings	-	complete	in process	-
Installation of Gaskets	-	complete	-	-

[redacted]

[redacted]

Operation	AFRM 006 COMPARTMENT (Cont'd)			
	Nosecap	Forward	Crew	Aft
Machining of Compartment	complete	complete	in process	in process
Radiographic Inspection	complete	complete	in process	-
Repair of Defective Areas	complete	complete	-	in process*
Application of Pore Sealer Coat	in process	in process	-	-

* Extensive repairs including replacement of large areas

Operation	AFRM 009 COMPARTMENT			
	Nosecap	Forward	Crew	Aft
Weight and C.G. Determination	complete	complete	complete	complete
X-Ray	complete	complete	complete	complete
Dimensional Inspection	complete	complete	complete	complete
Edgemember & Honeycomb Prefit	complete	complete	complete	-*
Cleaning & Priming Substructure	complete	complete	complete	
Bonding of Edgemembers & Honeycomb	complete	complete	complete	
Contour Machining of Honeycomb	complete	complete	complete	
Inspection of Honeycomb Bond	complete	complete	complete	
Repair of Defective Bond Areas	complete	complete	in process	
Gunning of 5026-39 Ablator	complete	complete	-	
Cure and Postcure	complete	complete	-	

*Work stopped on aft compartment per NAA/S&ID direction. Compartment returned to NAA/S&ID for structural modification.

[redacted]

[redacted]

The nosecap and forward compartments of AFRM 006 have completed all final repairs and are in process of having pore sealer applied prior to application of the final moisture barrier coating. In the process of making these repairs, it was discovered that ablator thickness in a region near the spherical tip of the nosecap was as much as 0.300 inch below the design value. Investigation showed that the machining of the ablator was at fault, and that undercutting of lesser magnitude (~0.060 inch) had occured in some areas of the forward compartment and of more severe magnitude (~0.500 inch) in an area on the aft compartment.

All machining on these compartments has been performed with numerical control, using tapes generated from selected thickness values from the design release. The latter release defines ablator thickness at some 50,000 points on the heat shield. With the tape generation program employed, only some 990 of these values were used as inputs to the computer, and the program faired between these points to generate the punched tape which guided the grinding wheel in the actual machining. Figure 47 shows the nosecap and forward compartments of AFRM 006 in the numerically controlled vertical turret lathe. The actual ablator thickness was checked during machining, but only at the locations of the 990 input thicknesses. These locations can be seen in figure 47. It has developed that the fairing between these points was erroneous in areas where the curvature was changing sharply, and the above noted undercutting was the result.

Disposition of the undercut regions of AFRM 006 is being studied, but major effort is under way to change the tape generation technique so as to prevent any recurrence of this problem on AFRM 009 or on the crew compartment of AFRM 006, which has not yet been finish machined. In the new technique, all 50,000 design thicknesses will be used as inputs to the tape generation program, so that no major fairing error can result. In addition, a computer check of the output tape will be employed to insure that it has indeed, produced the desired thicknesses. Many additional thickness check points will be used during machining to evaluate the thickness of the ablator and to insure that no undercutting can result. All of these techniques are currently being tried out in the mock-ups to insure their effectiveness before vehicle machining commences.

Curing of the ablator on the crew compartment of AFRM 006 produced some minor cracking in regions adjacent to the horizontal edges of some of the doors. This was traced to the fact that tooling pins used to hold the fiberglass edge-members in place during gunning were left in place during the cure. These restrained the ablator and apparently caused the cracking. These cracks are being repaired, and steps have been taken to insure that the pins will be removed prior to cure in all future vehicles.

The crew compartment of AFRM 006 was rough machined with the current numerical control tapes, but cannot be finish machined until tapes from the new program are completed and checked. Therefore, it is being radiographed in its present state, and defect repairs will be made before completion of the machining.

[redacted]

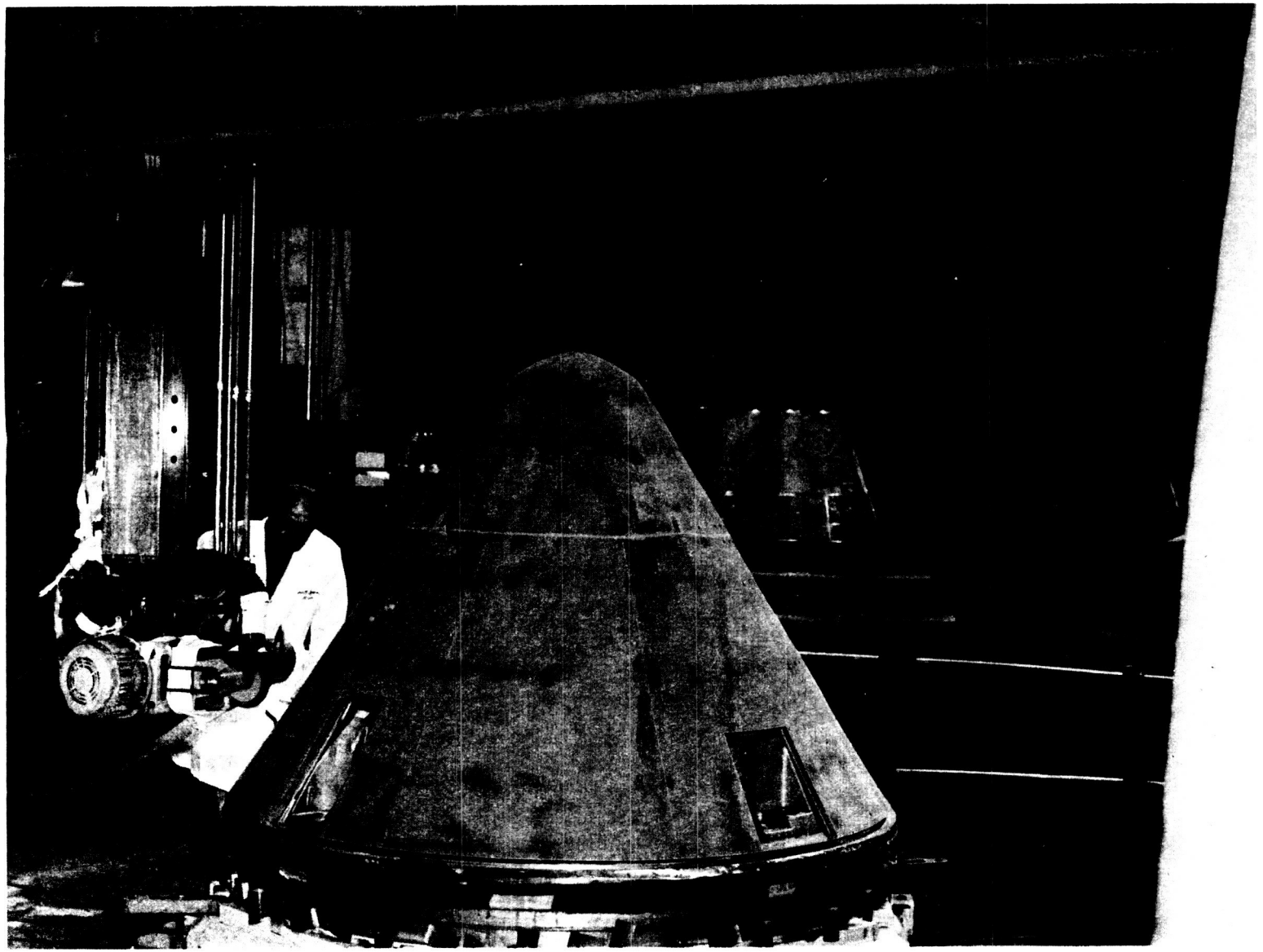

Figure 47 NOSECAP AND FORWARD COMPARTMENTS OF AFRM 006 IN PROCESS OF ABLATOR MACHINING
12103-M-1

[redacted]

Replacement of honeycomb in the areas of the ablator removal on the aft compartment of AFRM 006 was completed and gunning of these areas is in process. During cure of the honeycomb bond in the repair areas, many additional cracks opened in the ablator areas which were not repaired. In all cases, these cracks are associated with gross void areas, and it seems clear that they have resulted from weakening of the ablator by the presence of the voids. Disposition of these defects is being considered, but no actions will be taken until the gunning and cure of the repair regions are complete. As previously noted, severe undercutting in one region of this compartment occurred during rough machining. This also will be dispositioned after completion of the replacement repairs.

On removal of the doors from the crew compartment of AFRM 006 after cure of the ablator, it was discovered that delamination of the edgemembers on many of the doors had occurred. This appears to be the result of the large gaps (0.050 to 0.060 inch) which exist between the metal flanges of the doors and the openings in the substructure. It is believed that bolting in of the doors and closure of this gap produces sufficient stress to cause bond failure in the edgemember. Any measures to eliminate closure of this gap by shimming or other means require approval by NAA/S&ID, and this disposition is currently under consideration.

Examination of the edgemembers on the doors of the crew compartment of AFRM 009 shows that some bond delaminations have occurred on these doors as well, and presumably for the same reason. Since the doors require some repairs in any case, it has been decided to strip all the edgemembers and replace them after a suitable method has been devised to prevent recurrence of the delamination. In the meantime, gunning will proceed on the compartment itself.

Honeycomb machining was completed on the nosecap and forward compartments of AFRM 009, and the ablator was gunned without significant difficulty. Figure 48 shows the gunning in progress on the nosecap, and figure 49 shows the forward compartment. All green repairs were made during the gunning of these compartments, and they were cured without incident. Gunning quality, as measured by the number of voids detected in the green state X-rays, was markedly improved over previous gunned compartments.

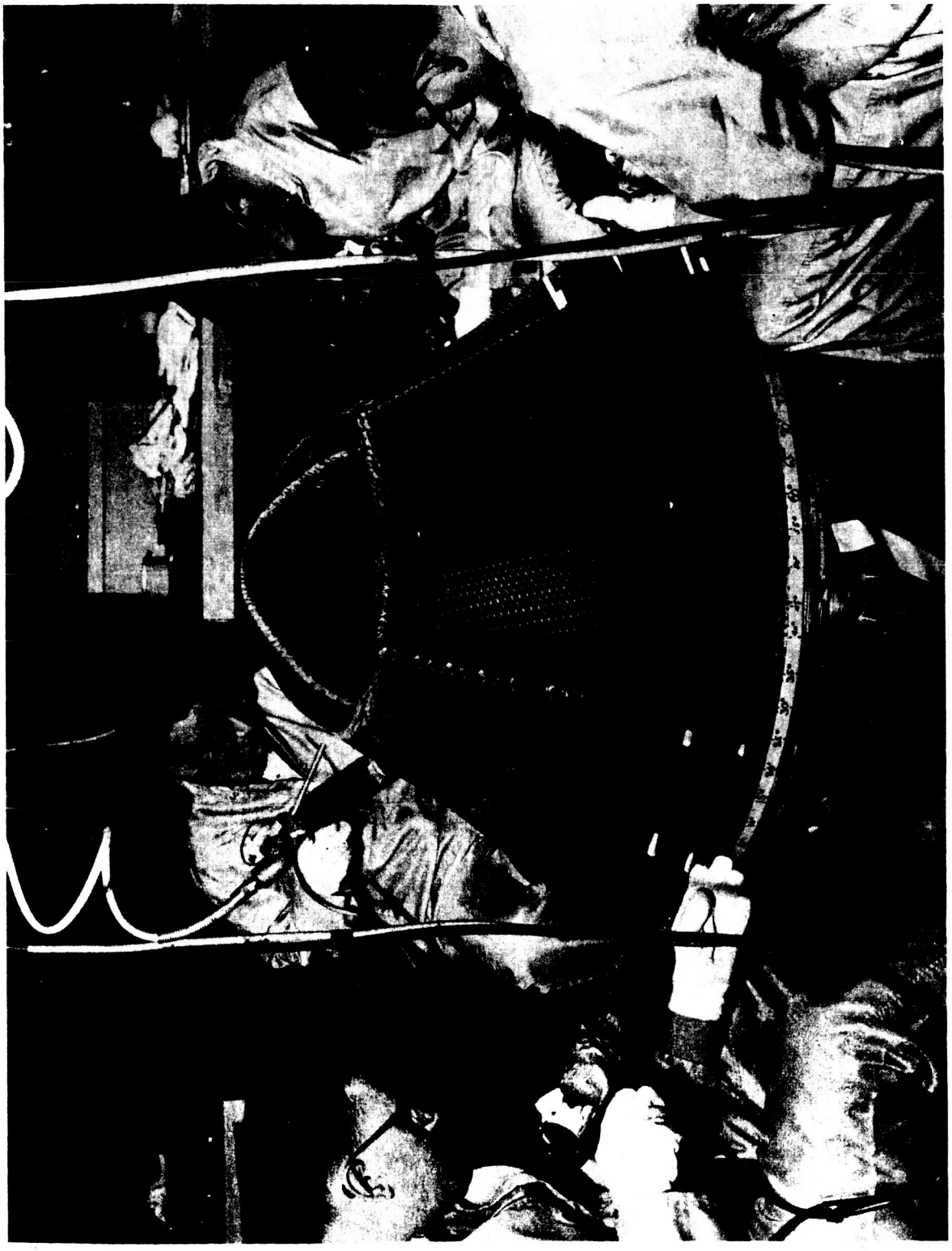

Figure 48 NOSECAP OF AFRM 009 IN PROCESS OF GUNNING OF 5026-39 ABLATOR
12604A

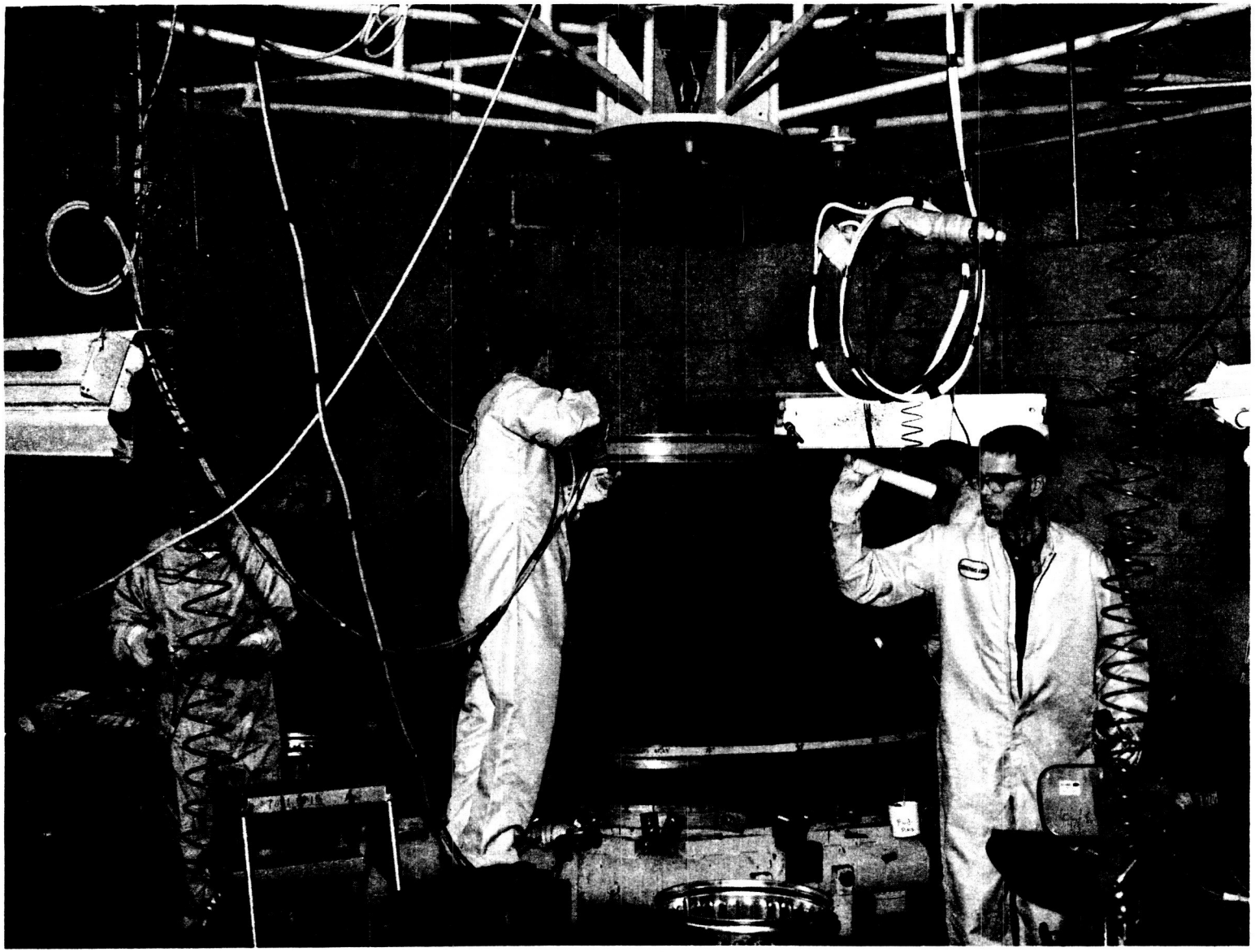

Figure 49 FORWARD COMPARTMENT OF AFRM 009 IN PROCESS OF GUNNING
5026-39 ABLATOR
12091U

[redacted]

III. QUALITY

Nose/Fwd Compartments ARFM 009 have been radiographically inspected several times during the gunning of the ablator. Each time radiography was completed, the compartments were returned to Manufacturing for rework. The curing of both compartments took place only after no voids were detected on the X-ray films.

Ultrasonic and visual inspections have been completed for bonds of the edge-members and honeycomb core to the Crew Compartment structure.

Final X-ray of Nose and Fwd ARFM 006 compartments is completed.

The Crew Compartment ARFM 006 has all ablator cured, and in-process X-rays are completed.

The Aft Compartment is being inspected after repairs of honeycomb core to the structure.

Fourteen SCN's were reviewed and approved by Quality Assurance personnel. Three specification revisions were approved and are listed below:

G70002A	Repair of A.C.M. Ablators
P70057C	Molded Edgemembers
M70114C	Fiberglas Edgemembers

QATP 2028 is being prepared. It will require that thickness of the ablator be measured at a larger number of points on Vehicle 009. This revision results from the low degree of assurance afforded by QATP 2021 on the heat shield of Vehicle 006; this in turn was caused by discrepancies between the machining tape program and the design requirements of IBM Run 401098. QATP 2028 will require that ablator thickness be measured at all manufacturing and design points and at a number of points in pertubation areas.

Radiographic Sensitivity charts have been drawn for the forward and nose compartments of the 006 heat shield. A similar chart is being drafted for the crew portion of the same heat shield. These charts will indicate for information purposes the radiographic sensitivity attainable at all points on the points on the heat shield.

[redacted]

[redacted]

DISTRIBUTION

Addressee	No. of Copies
NAA/S&ID (+ 1 reproducible)	25
R. H. Hugghins (Avco Rep. at NAA)	1
F. B. Matthews (NAA Rep. at Avco)	1
J. A. Wagner (NAA Rep. at Avco)	1
Apollo Central File (+ 1 reproducible)	5
Central File	1
Document Accounting	1
Research Library (+ 1 reproducible)	5

[redacted]

[redacted]

DISTRIBUTION

Addressee	No. of Copies	Addressee	No. of Copies
E. Belason	1	E. Offenhartz	1
C.F. Berninger	1	D. Rennington	1
Y.G. Biry	1	J. Phaneuf	1
F.W. Diederich	1	J.E. Richard	1
C.C. Kipps	1	O.K. Salmassy	1
K. Goodman	1	D.E. Stafford	1
M. Goriansky	1	A. Woodhull	1
A.J. Hanawalt	1	W. Wolz	1
H. Hoercher	1	W. Zeh	1
M.E. Ihnat	1		
E.J. Kaszynski	1		
E.D. Kenna	1		
R.S. Knower	1		
K.A. Kyger	1		
A.J. Lavigne	1		
A. Ogman	1		
T.W. Mix	1		
A.A. Rothstein	1		

Off-Site Avco Personnel

P.T. Andrews	1
R.L. Bentley	1
F. Brown	1
R. Bussy	1
C. Cohen	1
J. Collins	1
F. DeGiacomo	1
R.E. Demming	1
M. G. Friedman	1
M. Guidi	1
L. Hammond	1
C. Huffine	1
H. Hurwicz	1
J. Johnson	1
E. Kaminsky	1
J. Kossar	1
L. Levin	1
D. Moodie	1
D. Mosher	1
N. Mykytyn	1

[redacted]